Earth-Science Reviews 243 (2023) 104488

Contents lists available at ScienceDirect

Earth-Science Reviews

journal homepage: www.elsevier.com/locate/earscirev

The Northern Calcareous Alps revisited: Formation of a hyperextended margin and mantle exhumation in the Northern Calcareous Alps sector of the Neo-Tethys (Eastern Alps, Austria)

Philipp Strauss [a,b], Pablo Granado [a,*], Josep Anton Muñoz [a], Katharina Böhm [c], Ralf Schuster [d]

[a] Institut de Recerca Geomodels, Departament de Dinàmica de la Terra i de l'Oceà, Universitat de Barcelona, Martí i Franquès s/n 08028, Barcelona, Spain
[b] OMV Austria Exploration and Production GmbH, Trabrennstrasse 6-8, 1020 Vienna, Austria
[c] Department of Earth Sciences, Vrije Universiteit Amsterdam, De Boelelaan 1085, 1081HV Amsterdam, The Netherlands
[d] GeoSphere Austria, Neulinggasse 38, 1030 Vienna, Austria

ARTICLE INFO

Keywords:
Rifted margin
Neo-Tethys
Fold-and-thrust belt
Salt tectonics
Balanced crosssection
Thermal modelling

ABSTRACT

The Neo-Tethys margin evolution is preserved in the Northern Calcareous Alps (Eastern Alps), from Late Permian crustal stretching to Late Triassic oceanization. The Northern Calcareous Alps represent the salt-floored fold-and-thrust belt developed from the salt-influenced Triassic carbonate sedimentary cover of the ancestral European margin of the Neo-Tethys Ocean. A crustal scale model for the margin has been obtained by restoration of regional cross-sections of the Northern Calcareous Alps carbonate platforms. Lithospheric break-up was investigated from remnants of exhumed mantle found within an evaporitic melange, suggesting hyperextended crust underneath the distal Triassic platforms of the Northern Calcareous Alps preceding breakup. By modelling the thermal evolution of the margin in combination with excellent stratigraphic control, a detailed timeline has been established for the evolution of the Neo-Tethys margin, especially around the period of rapid mantle exhumation. Our study indicates that salt-floored carbonate shelfs can be used as a proxy to characterize the margins evolution, from crustal stretching to continental breakup. Diagnostic stratigraphic records are preserved in the carbonate platforms: pre- mantle exhumation carbonates are represented by aggrading isolated carbonate platforms first, followed by expanding and margin wide prograding carbonate shelfs once thermal subsidence dominates. In addition, a distinct clastic sequence is deposited as an immediate response to mantle exhumation, in between the pre- and post-mantle exhumation carbonate factory. Our study proposes a new refined model for the formation of the Neo-Tethys margin and provides new insights for the dynamic coupling of salt-controlled carbonate shelfs and the underlying lithosphere during continental breakup.

1. Introduction

The classical model for the evolution of continental rifts to rifted margins consists of pre-rift, *syn*-rift and post-rift stages (i.e., Hubbard, 1988; Prosser, 1993) formed under dominantly pure-shear (i.e., McKenzie, 1978), or simple shear (i.e., Wernicke, 1985). In the last decades, it has been shown that none of these seminal works is capable to harmonize the structural, subsidence, tectonostratigraphic and thermal records of rifted margins, particularly for their distal parts, as (i.e., Reston and Pérez-Gussinyé, 2007; Ranero and Perez-Gussinye, 2010; Tugend et al., 2014; Lescoutre et al., 2019; Péron-Pinvidic et al., 2019; Ribes et al., 2019a, 2019b; Chenin et al., 2022; Manatschal et al., 2011, 2022). Modern concepts on rift margin development conclude that rifting is a poly-phasic strain localisation process, with each of these phases developing sequentially under a dominant plate kinematic framework. In broad terms however, recent models also invoke a *syn*-tectonic phase (i.e., active extension of the lithosphere), and a post-tectonic phase dominated by thermal cooling (i.e., McKenzie, 1978; Lavier and Manatschal, 2006; Péron-Pinvidic and Manatschal, 2009; Péron-Pinvidic et al., 2019; Chenin et al., 2022; Manatschal et al., 2022; Pérez-Gussinyé et al., 2023). The diachroneity of the rifting processes is thus reflected on the stratigraphic record, since post-tectonic stratigraphy on the proximal domain of a margin, can be time-equivalent to *syn*-tectonic units in the developing necking and hyperextension domains (Péron-Pinvidic and Manatschal, 2009; Chenin et al., 2022). Such complex geological evolution in space and time, must not be confused

* Corresponding author.
E-mail address: pablomartinez_granado@ub.edu (P. Granado).

https://doi.org/10.1016/j.earscirev.2023.104488
Received 11 January 2023; Received in revised form 16 June 2023; Accepted 23 June 2023
Available online 28 June 2023

with multirift (or multistage rifting) once several successive extensional events take place under various plate kinematic directions, either or not overlapping in space (i.e., Alves et al., 2009; Tugend et al., 2014; Gouiza et al., 2017; Cadenas et al., 2020).

In polyphase rifting, each phase and its related rift domain are expressed by characteristic tectonic structures and related stratigraphic architectures, differing amounts of different accommodation space and depositional environments (Sutra et al., 2013; Ribes et al., 2019a, 2019b; Chenin et al., 2022) and thermal records (Manatschal et al., 2011; Clerc and Lagabrielle, 2014; Lescoutre et al., 2019). Current models of polyphase rifting include an initially distributed lithospheric stretching phase - as preserved on the proximal domain of rifted margins - followed by focused crustal thinning favoured by the presence of ductile crustal layers. When crustal sections become thinned and laterally extracted down to at least 10 km thick (thus reducing the crust to <30% of its original thickness), hyperextension is said to occur (see Sutra et al., 2013; Petri et al., 2019). Crustal thinning leads to the formation of a necking domain and a coupling point where the brittle upper crustal portions are mechanically linked with lower crust and uppermost mantle by faults and shear zones, preceding oceanic lithosphere accretion. The characteristic stratigraphic signature of these processes (i.e., Ribes et al., 2019a, 2019b, 2020; Chenin et al., 2022; Manatschal et al., 2022) and related subsidence and thermal history may vary significantly by the environmental conditions (i.e., clastic vs. carbonate dominated margins). In the common case of deformed salt-bearing rifted margins, the tectono-stratigraphic record of polyphase rifting evolution can be biased by the presence of a salt layer, mainly if it developed previously or during the rifting event (i.e., Rowan, 2014; Granado et al., 2016a; Strauss et al., 2021a, 2021b; Epin et al., 2021; this study).Decoupled extensional deformation due to the presence of salt horizons can strongly mislead in the interpretation of accommodation space creation and subsidence, as well as on the geodynamic interpretation of the depositional record (i.e., Strauss et al., 2021a, 2021b; Epin et al., 2021). Thus, the accommodation space for the sedimentary sequences can also be given by salt stretching and salt evacuation superimposed to crustal thinning, adding difficulties for the correlation between stratigraphic signature and rift domains (Chenin et al., 2022). Moreover, in salt-bearing rifted margins involved in orogenic systems the salt layer acts as a décollement level during the contractional deformation, decoupling the supra-salt succession from the basement and preventing a direct comparison between the location of the *syn*-tectonic packages and the nature of the basement underlying the basins (Granado et al., 2019). In such circumstances the reconstruction of the rifted margin and its structural evolution requires detailed restoration of the structural units

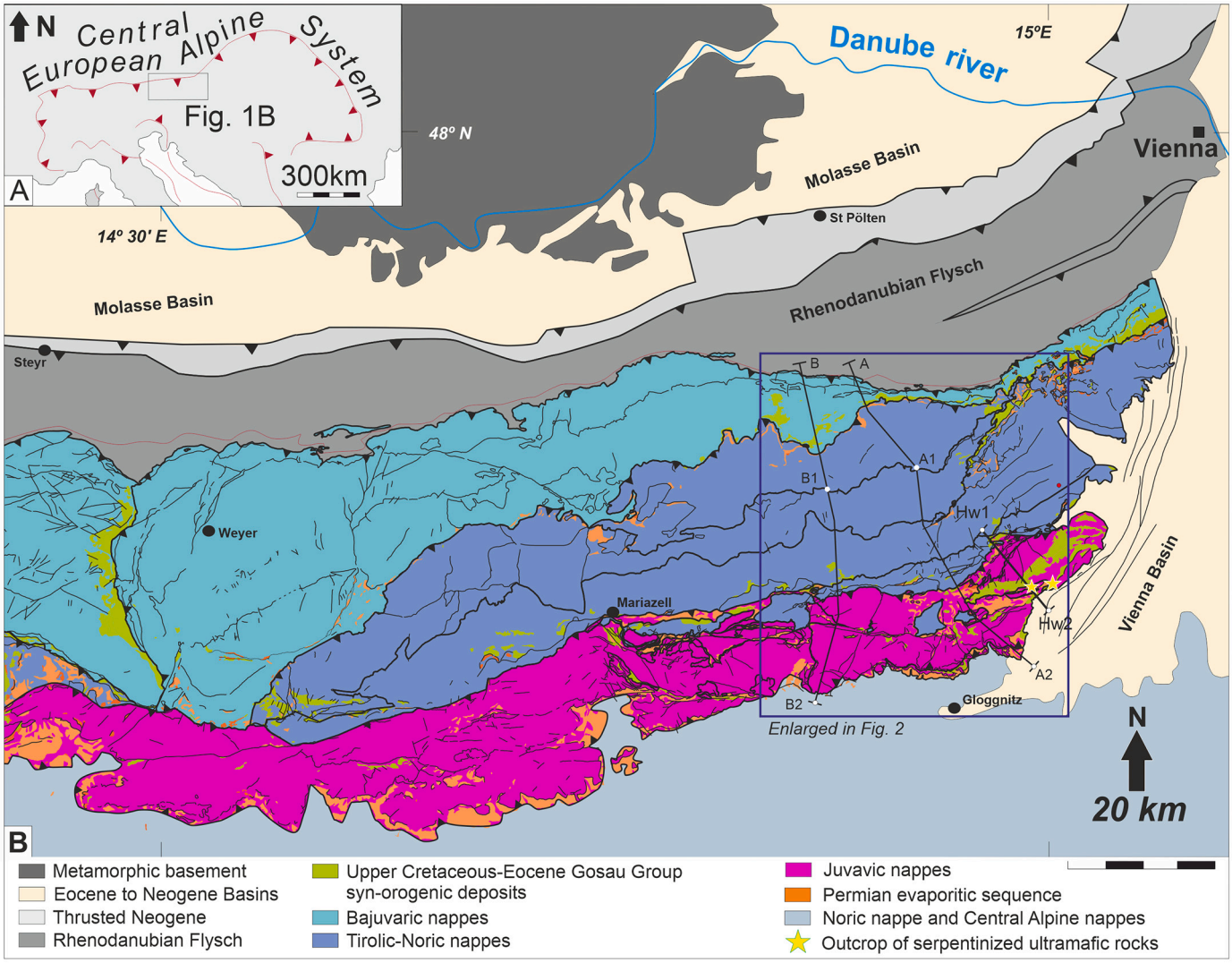

Fig. 1. Tectonic setting of the eastern Northern Calcareous Alps. a) Location of the tectonic map in respect to the Alpine thrust belt. b) Simplified geological map of the eastern Northern Calcareous Alps. Modified from GBA Geological Maps available on ArcGIS https://www.geologie.ac.at/en/services/web-services). The locations of 2 regional cross sections, labelled A and B, and a shorter section HW are shown.

at the time of deposition of the sedimentary units, and knowledge of: i) internal architecture and distribution of depocenters of the supra-salt basins, ii) salt-sediment interface relationships, iii) thermal data and thermal modelling to constrain the crustal thickness and iv) any other structural, sedimentological and petrological data to constrain the rifted margin evolution at a crustal scale.

The Northern Calcareous Alps fold-and-thrust belt of the Eastern Alps (Fig. 1) offers a unique opportunity to carry out such multidisciplinary analysis. The Alpine orogenic system has extensively preserved the Triassic calcareous cover of the former Neo-Tethys rifted margin as well as parts of its pre-salt basement. This is largely due to the presence of the extensive uppermost Permian to lowermost Triassic layered evaporitic sequence that acted as a regional décollement during orogenic convergence and allowed for a low taper tectonic wedge that prevented massive erosion of the rifted margin carbonate stratigraphic sequence. A protracted shallow water carbonate depositional record, only punctuated by a thin but regionally extensive siliciclastic input in middle Carnian times (Tollmann, 1976a, 1985; Mandl, 2000), provides key anchoring proxies for palaeowater depths estimations, which are one of the most problematic issues to constrain rifted margin horizontal widening and vertical movement.

Different rifting phases (i.e., multistage rift systems) have taken place in the Tethys domain after the orogenic collapse of the Variscan orogen at Carboniferous times (e.g. Manatschal et al., 2023). These phases shaped the south European margins and their African-Adriatic conjugate margins since late Permian-Triassic to Early Cretaceous times. The Tethyan rifting events progressed westward from the Neo-Tethys Oceanic domain to the Bay of Biscay connecting the Tethys and Atlantic realms. In the central and western Alps, the Alpine Tethys magma-poor rifted margin has been recently reconstructed and interpreted because of a polyphase rifting event during Early and Middle Jurassic (Chenin et al., 2022; Manatschal et al., 2022 and references therein). Further east, in the Northern Calcareous Alps this event has superimposed with a previous rifting event, late Permian to Triassic in age, that shaped the Neo-Tethys margin. Because of a smaller width of the Neo-Tethys Ocean and associated facies belts at its western end, and stronger compression and erosion in the Eastern Alps compared with the Inner Western Carpathians, fewer remnants of this paleogeographic domain are preserved in the Eastern Alps (Channel and Kozur, 1997). The Neo-Tethys margin thus, has not been reconstructed and properly characterised in the studied area, since there is not yet an established relationship between the Triassic stratigraphic record and different phases of the late Permian-Triassic rifting event, since timing of the different phases have not been fully defined (see Lein, 1987; Kozur, 1991).

In this work, we review previous works about the formation of the western Neo-Tethys rifted margin and expand our research on the formation and evolution of the Triassic margin, which is represented today in the Northern Calcareous Alps. We present two new balanced regional cross-sections in the eastern Northern Calcareous Alps and their sequential structural restoration. Sequential restorations have allowed reconstructing the margin-wide distribution of a Permian layered evaporitic sequence. The shelf carbonate factory developed atop and its transition into the deeper water facies deposited on the necking, hyperextended and exhumation domains. Additionally, 1D thermal modelling and petrological data from mantle rocks are included to support and further constrain the restoration results. We then propose an internally consistent model for the evolution of the Northern Calcareous Alps sector of the Neo-Tethys rifted margin. The methods applied herein offer tools for unravelling the evolution of other salt-bearing rifted margins systems.

2. Regional Geological setting

2.1. Organization of the Neo-Tethys rifted margin and the Northern Calcareous Alps

The formation of the Neo-Tethys margin started with the Permian rifting of Pangea (Kozur, 1991; Channell et al., 1992; Haas et al., 1995; Mandl, 2000; Schmid et al., 2008, 2020; Van Hinsbergen et al., 2020). Rifting of the lithosphere was encompassed by profuse intrusion of mantle-derived basaltic melts to the base of and into the overlying crust, causing intense magmatic activity and a well-constrained HT/LP metamorphic event (see Roda et al., 2018 for a recent review). Peak metamorphic conditions were reached at about 280–260 Ma at geothermal gradients up to 45 °C/km (Kunz et al., 2018; Habler and Thöni, 2001; Schuster et al., 2001). Subsequently, lithospheric cooling took place slowly (i.e., Petri et al., 2017) to a calculated steady state geotherm of about 25 °C/km by the end of the Triassic (ca. 200 Ma; Schuster and Stüwe, 2008). In this context, a thick uppermost Permian to lowermost Triassic layered evaporitic succession interbedded with clastics, carbonates and magmatic rocks was deposited on top the *syn*-tectonic Permian sediments and the rifted basement. A complex Triassic carbonate platform architecture was established, characterised by significant changes in thickness and a distinct facies distribution: isolated Middle Triassic carbonate platforms developed first flanked by salt diapirs and were covered afterwards by an Upper Triassic regional lagoonal shelf, constituted by thick depocenters, with elongated diapir shoulders lying directly onto the Permian-Triassic evaporites (Granado et al., 2019; Strauss et al., 2021a). The Upper Triassic shelf was fringed by reef build ups at the shelf break and passed laterally to the slope and deep-water setting constituted by Upper Triassic Hallstatt pelagic carbonates, and the Meliata oceanic sediments, respectively (Kozur, 1991; Mandl and Ondrejicková, 1993; Mandl, 2000; Gawlick and Missoni, 2015; Strauss et al., 2021a). Such facies distribution and morphostructural architecture argue in favour of a fully developed rifted margin by Late Triassic times, including a shelf, a shelf break and slope, and oceanic domain (Channel and Kozur, 1997).

From the latest Triassic to Early Cretaceous, the Neo-Tethys margin was rifted apart from Europe, as the Alpine Tethys (sensu Stampfli et al., 1998 and Schmid et al., 2004, 2008) developed to the northwest (in present day coordinates; see Channell et al., 1992; Channel and Kozur, 1997; Schmid et al., 2020). Opening of the Alpine Tethys thus established an Adriatic lithosphere derived from 'ancestral' Europe. By about Late Jurassic times, northwest-directed ophiolite obduction (in present-day coordinates) on the north-western Neo-Tethys rifted margin (i.e., south-eastern Adriatic margin) took place, while southeast-directed subduction of the Alpine Tethys beneath the northwestern margin of Adria occurred since Late Cretaceous times (Schmid et al., 2004). However, a regional N-NW-directed convergence was established in the Early Cretaceous when shortening within the northern part of Adria initiated (i.e., Faupl and Wagreich, 1994; Von Eynatte and Gaupp, 1999; Neubauer et al., 2000; Frisch and Gawlick, 2003) along an intracontinental subduction zone (Stüwe and Schuster, 2010). As a result, the Mesozoic cover of the Adriatic margin was completely detached from its pre-salt basement (i.e., Linzer et al., 1995, 1997; Granado et al., 2019), to become the hanging-wall of a nappe stack over the southeast-dipping Alpine Tethys subduction zone (i.e., Stüwe and Schuster, 2010). Continental collision between the Adriatic and European continental lithospheres took place by around Eocene times (Schmid et al., 2004; Granado et al., 2016b). As a result, the Northern Calcareous Alps fold-and-thrust belt was transported over a considerable distance from its autochthonous rifted Adriatic basement to their present position on top of the European continental margin and the Alpine Tethys suture zone (i.e., Schmid et al., 2008; Stüwe and Schuster, 2010; Granado et al., 2016b). A minimum of 70 km of N-NW-directed tectonic transport for the Northern Calcareous Alps fold-and-thrust belt can be estimated from available geological maps (see Schnabel et al., 2002).

The structure of the Northern Calcareous Alps consists of ENE-WSW–striking thrust sheets, which from North to South have been traditionally grouped into three major tectonic domains (i.e., Bajuvaricum, Tirolicum, Juvavicum; Hahn, 1912, 1913; Tollmann, 1985, 1987) represented by the Bajuvaric, Tirolic and Juvavic nappe systems (Schmid et al., 2004). All three nappe systems were detached from their autochthonous Adriatic continental crust during Alpine convergence. Therefore, and for simplicity, we remain in this study with the traditionally used terms Bajuvaric, Tirolic and Juvavic sensu Tollmann (1976a). The Meliata zone (Mandl and Ondrejicková, 1993) originated from oceanic crust of the Neo-Tethys Ocean. It consists of Triassic deep-water radiolaritic sediment, olistoliths and a Jurassic flyschoid matrix. (Mandl, 1984; Lein, 1987; Mandl, 1996). The Meliata zone is well-preserved in Slovakia, east of the studied area, whereas in the eastern Northern Calcareous Alps it is only poorly represented (Channel and Kozur, 1997; Mandl, 2000).

The stratigraphic record of each of these nappes defines an approximate north-to-south deepening depositional trend for the Neo-Tethys rifted margin (i.e., Mandl, 2000; Neubauer et al., 2000; Frisch and Gawlick, 2003; Gawlick and Missoni, 2015, 2019; Strauss et al., 2021a, 2021b; Fig. 1). In a very generalised view, each of these large nappe systems is characterised by a distinct association of Middle to Upper Triassic carbonate facies. The nappes of the proximal Bajuvaric nappe system show thinner (< 2 km thick) Middle to Upper Triassic carbonate successions, with a localized siliciclastic influence in middle Carnian times (i.e., the Lunz, Reingraben, Leckkogel and Raibl Fms). In contrast, the Tirolic nappe system is characterised by a thicker succession (i.e., in excess of 4 km thick, vertically stacked depocenters) deposited in a just slightly deeper lagoonal environment, with occasionally present middle Carnian siliciclastics. The transition from the Upper Triassic lagoonal environment to the open marine setting marks the differentiation between the Tirolic and the Juvavic nappe system. The Upper Triassic shelf break was established at the southern boundary of the Tirolic nappes. However, the relationship of these nappes and their corresponding stratigraphy shall not lead to direct correlations along the Northern Calcareous Alps in general, since originally unrelated stratigraphic successions have been grouped into the same nappe system by Alpine *out-of-sequence* thrusting (Faupl and Wagreich, 1994), as constrained by over-thrusting of unconformable Lower Cretaceous to Eocene synorogenic strata (see Geological maps series at scales 1:200.000 and 1:50.000 by the Austrian Geological Survey - https://www.geologie.ac.at; Fig. 1).

2.2. Triassic salt tectonics and Alpine overprinting: Key observations

Even though the Northern Calcareous Alps have been studied for many years, is not until recently that both structure and stratigraphic development are being harmonised and consolidated (Mandl, 2000). Detailed geological mapping, cross-section construction and sequential restorations (Granado et al., 2019, 2021) coupled with subsidence analysis (Strauss et al., 2021a, 2021b) have shown that parts of the Northern Calcareous Alps shelf developed as an *isolated minibasin province* (sensu Rowan and Vendeville, 2006), where thick isolated carbonate minibasins flanked by km-long salt walls developed in Middle to Late Triassic times. Those isolated carbonate platforms were formed upon the combination of salt-detached extension and salt evacuation over an uneven pre-salt basement topography inherited from rifting, initially assisted by an incipient, and then fully active, regional thermal subsidence (see Granado et al., 2019, 2021; Strauss et al., 2021a, 2021b for discussions).

Reactivation of the salt structures during the Alpine convergence resulted into large panels of overturned stratigraphy (i.e., Sulzbach nappe, in: Tollmann, 1985) and frequent steep mechanical contacts that can either repeat or omit significant parts of the stratigraphic sequence (i.e., Granado et al., 2019). In fact, both kinds of relationships can be found laterally along the same tectonic contact in the eastern Northern Calcareous Alps, particularly between the Reisalpen and the Sulzbach nappes (i.e., as shown in the maps from Schnabel et al., 2002). Such apparently subtractive contacts were initially interpreted as the result of gravitational tectonics (Tollmann, 1987), but in fact, developed as a result of the contraction and welding of previous linear salt structures (i.e., salt walls) in between carbonate platforms (Granado et al., 2019, 2021), as well as Alpine out-of-sequence thrust stacking (Schmid et al., 2008; this work).

Other parts of the fold-and-thrust belt conform to classical thrust contacts bringing older stratigraphy onto younger stratigraphy and constituting thrust sheets of significant lateral continuity (i.e., tens of kilometres; Fig. 2). However, all these thrust sheets are also characterised by significant changes in stratigraphic thickness and facies along strike (i.e., Tollmann, 1985, 1987; Mandl, 2000; Granado et al., 2019; Strauss et al., 2021a). Such changes are readily evident from the regional geological maps and are also reflected when constructing serial cross-sections. Marked changes in thickness and facies are best shown along the north-eastern terminations of the Reisalpen, the Unterberg and the Göller nappes (see Fig. 2a) Drastic variations in thickness occur along the Unterberg Nappe (Fig. 2b), which changes from 6 km thickness to one km thickness preserving its full stratigraphic content. Many of these features are spatially associated with the presence of the uppermost Permian to lowermost Triassic layered evaporitic sequence; (Spötl and Hasenhüttl, 1998; Leitner et al., 2017). In the Northern Calcareous Alps, syn-orogenic growth strata are also commonly found directly overlying or juxtaposed to these evaporites (Schnabel et al., 2002), including the non-evaporitic insoluble components of the Haselgebirge Fm, such as shales, sandstones, magmatic rocks and other exotic blocks (Mandl, 2000; Schorn et al., 2013) that will be referred to in the following sections.

2.3. General stratigraphy of the eastern part of the Northern Calcareous Alps

The sedimentary record of the Neo-Tethys margin (Fig. 3) begins with upper Permian *syn*-tectonic deposits formed by continental red beds, quartzites, conglomerates and some magmatic rocks belonging to the Alpine Verrucano Fm, Präbichl and Laas Fm Fms (Bosselini et al., 2003; Tollmann and Faupl, 1972; Cassinis et al., 1979; Tollmann, 1985; Krainer and Stingl, 1986; Neubauer, 1988; Krainer, 1993). A regionally thick and widely distributed layered evaporitic sequence was deposited during uppermost Permian to Lower Triassic times, containing chloride and sulphate salts as well as the associated clastic and carbonate deposits (Schauberger, 1986), including the main halite-bearing Haselgebirge Fm, the Werfen Fm and the carbonate to evaporitic Reichenhall Fm (Leitner et al., 2017, 2020). Such layered evaporitic sequence occasionally includes Permian basic volcanic rocks (Spötl and Hasenhüttl, 1998), whose enriched immobile trace element signature indicates an intraplate or rift-related basaltic volcanism (Leitner et al., 2017). The Haselgebirge Fm was covered by the Lower Triassic shallow marine siliciclastic Werfen Fm and the Reichenhall Fm. According to Leitner and Spötl (2017), the evaporites were sedimented in a late *syn*-rift to early post-rift setting (i.e., upon the transition between the old-fashioned *syn-rift* and *post-rift* megasequences; see Rowan, 2014). The geodynamic interpretation of these evaporites will be further discussed in this work. Evaporite thickness distribution varied in accordance with a pre-salt topography created by syn-tectonic thick-skinned basement faults. In the largest depocenters, the thickness of the layered evaporite may have reached >2 km, as indicated by subsidence analysis (see Strauss et al., 2021a, 2021b, and comment Schollnberger, 2021). The upper Permian to Lower Triassic layered evaporitic sequence is hereafter referred to as *salt*, for simplification.

The Middle Triassic shelf was characterised by pronounced temporal and spatial changes in carbonate facies and thickness, resulting into a diachronous carbonate platform (Brandner and Resch, 1981; Krystyn and Lein, 1996; Krystyn et al., 2008; Lein, 1987; Lein et al., 2012; Mandl,

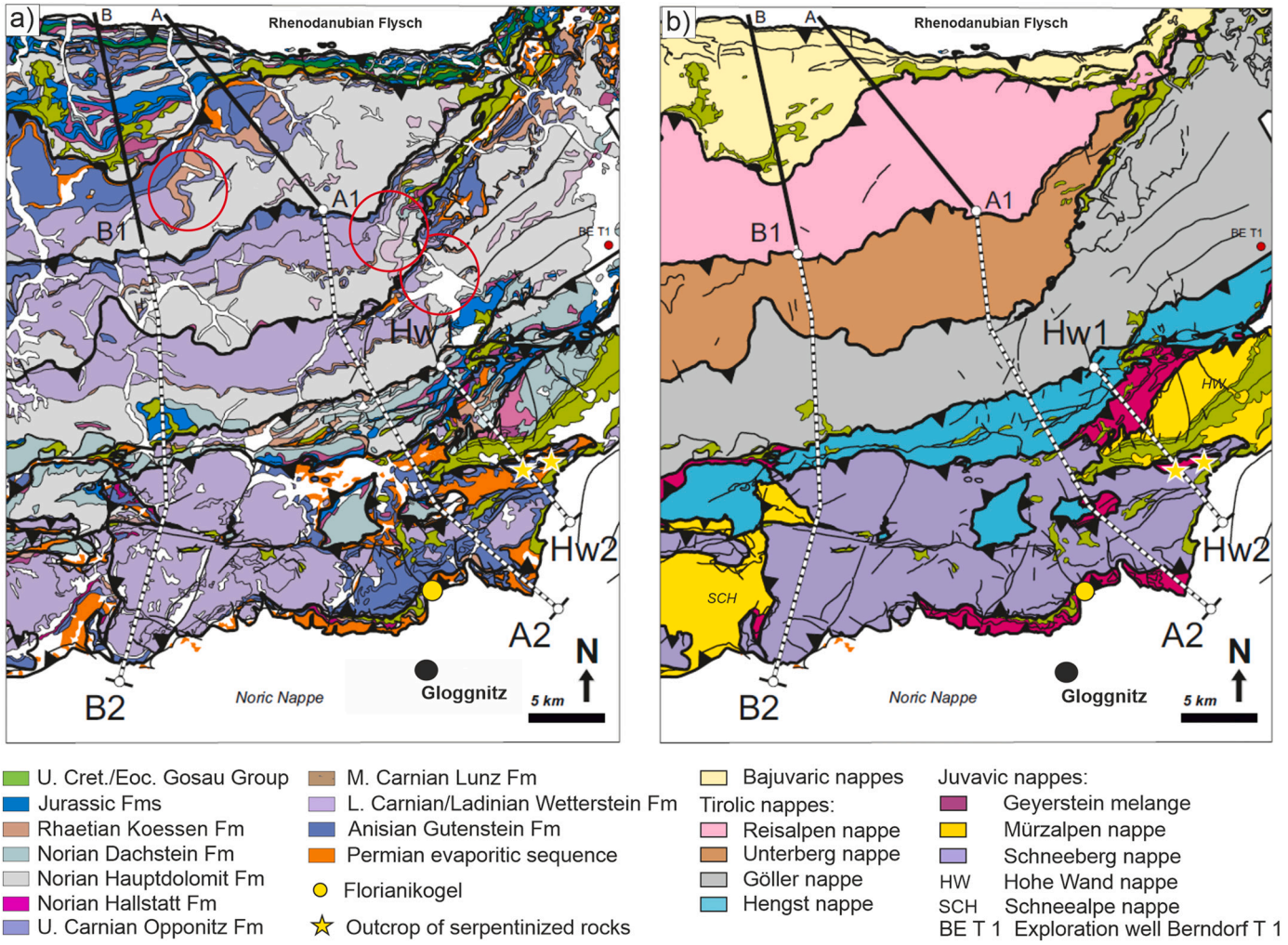

Fig. 2. Enlarged area of the geological map indicated in Fig. 1, along with the position of the two regional cross-sections A and B, and the supporting section Hw. Segments of these sections which were restored are highlighted with stippled lines, from A1 to A2 and B1 to B2 respectively. a) Simplified geological map of the study area based on the published 1:200.000 scale map https://www.geologie.ac.at/en/services/web-services. Middle Triassic facies changes from platform to basin are encircled. b) Main tectonic elements of the study area.

2000; Tollmann, 1976a). Sedimentary facies range from restricted shallow water basins (i.e., the Anisian Gutenstein Fm) to deeper water slope and basinal facies (i.e., the Ladinian Reifling and Partnach Fms, respectively; Schlager and Schöllnberger, 1974), to well-developed shallow water carbonate platforms in Anisian (i.e., Steinalm Fm), and Ladinian to early Carnian times (i.e., Wetterstein Fm). Each of these isolated shallow water Wetterstein carbonate platforms can reach >1500 m (i.e., true stratigraphic thickness), whereas some can reach as much as 2500 m (see Fig. 2a and geological maps e.g. Wachtel and Wessely, 1981; Summesberger, 1991, Schnabel et al., 2002). Coevally to the shallow water Triassic platform, Middle Triassic pelagic Hallstatt limestones (Krystyn, 1973; Mandl, 1996) were deposited in deeper basins on the distal sector of the margin (Mandl, 2000). In the Neo-Tethys oceanic realm, radiolarites were deposited and are now found in the Meliata zone at the Florianikogel (see Fig. 2b; also in Mandl, 1996).

By middle Carnian times, the topography of the Middle Triassic shelf of the Pangea segment from which the Northern Calcareous Alps derive (i.e., Northern Calcareous Alps shelf in the following) was covered and infilled by middle Carnian siliciclastic sediments (i.e., Lunz, Reingraben, Leckkogel and Raibl Fms), originally referred to as the Reingraben turnover (Schlager and Schöllnberger, 1974), or more recently, as the Carnian Pluvial Phase (Hornung and Brandner, 2005; Mueller et al., 2016; Aubrecht et al., 2017). Based on heavy minerals provenance, Aubrecht et al. (2017) tracked the source area for the siliciclastic material in the central European Bohemian Massif and as far north as the Fennoscandian shield. The growth of the isolated Middle Triassic carbonate platforms was terminated by the massive siliciclastic input and infilling of the inter-platform basins. Siliciclastic input resulted in a bathymetrically levelled fluvial to coastal and shallow marine shelf. Carbonate and evaporitic deposition resumed with the upper Carnian Opponitz Fm, followed by an aerially extensive Norian carbonate shelf represented by the lagoonal Hauptdolomit, the Dachsteinkalk and Dachstein-Riffkalk Fms (Tollmann, 1976b; Mandl, 2000). The Norian carbonate shelf displayed a minimum thickness of some 300 m in the northernmost proximal domains (i.e., the Frankenfels nappe of the Bajuvaric nappe system; Fig. 1), thickening southwards up to 2500 m in the central domains of the Northern Calcareous Alps (i.e., in the Tirolic nappes). The lagoonal shelf became fringed to the south, in present day coordinates, by the development of a rimmed reef (i.e., the Dachstein reef limestone) passing southwards to slope and basinal facies (i.e., Pötschen, Aflenz and Zlambach Fms) in the distal domain. Pelagic limestones of the Norian Hallstatt Fm (see Mandl, 2000 and references therein) represent the distal depositional environment, which today is preserved in the southernmost Juvavic tectonic slices (i.e., the Geyerstein mélange; Fig. 2b).

In the Triassic-Jurassic transition, the conditions for carbonate production became less favourable (i.e., Richoz et al., 2012). Mainly pelagic limestones with chert or condensed sections with abundant manganese

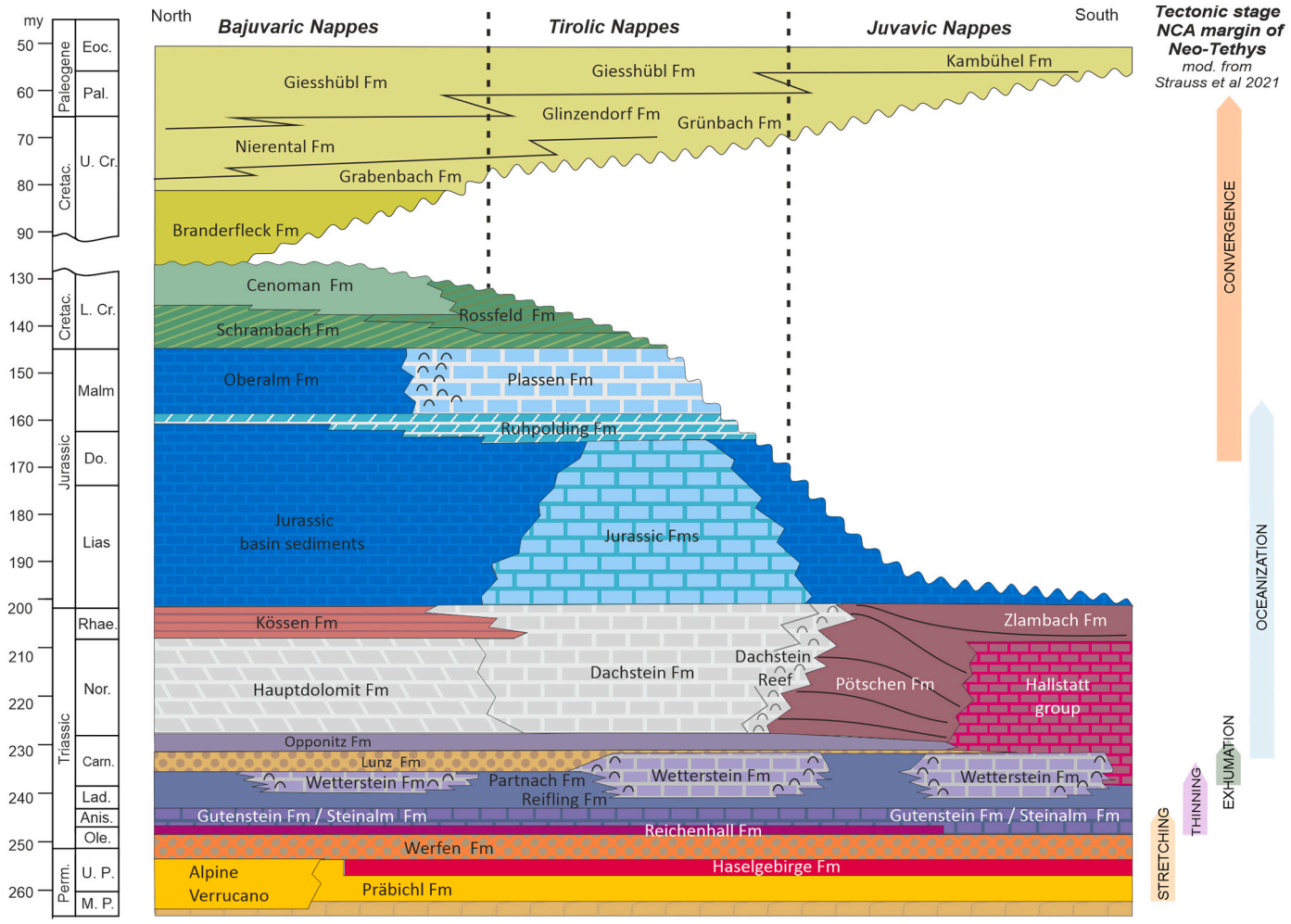

Fig. 3. General stratigraphy of the Northern Calcareous Alps. Modified from Leitner and Spötl (2017). The Tectonic stages of the Northern Calcareous Alps margin of Neo-Tethys are modified from Strauss et al., 2021a.

nodules are preserved from the Lower and Middle Jurassic across the Northern Calcareous Alps. The Upper Jurassic succession in the southern and central domains became influenced by convergence related to the closure of the Neo-Tethys realm (i.e., Eo-Alpine shortening, sensu Faupl and Wagreich, 2000), whereas the northern domain experienced the early phases of rifting that brought apart Europe from Adria and led to the opening of the Alpine Tethys Ocean (Schmid et al., 2004, 2008; Granado et al., 2019). By Early Cretaceous times the southern and central domains of the Northern Calcareous Alps shelf became involved in the fold-and-thrust belt. In the northern proximal domain (i.e., the Bajuvaric nappes) of the eastern Northern Calcareous Alps, Lower Cretaceous to lowermost Upper Cretaceous syn-orogenic sediments become progressively younger towards the north (i.e., Schrambach, Rossfeld, Tannheim and Losenstein Fms). Conversely, in the western Northern Calcareous Alps, Lower Cretaceous sediments are also found in the Tirolic nappes. Syn-orogenic sediments filled thrust-related foredeeps as these were incorporated as piggy-back basins during the foreland-ward propagation of thrust belt. Permian basaltic rocks associated with the evaporitic Haselgebirge Fm have also been found within the syn-orogenic Jurassic and Cretaceous growth strata, suggesting active salt extrusion coeval with orogenic shortening (Mandl, 2017; Santolaria et al., 2022). Due to the closure and subduction of the Alpine Tethys beneath Adria beginning earliest in Albian to Cenomanian times onwards, the Northern Calcareous Alps fold-and-thrust belt experienced further shortening and syn-orogenic sedimentation of the Gosau Group in nearly all areas (Wagreich and Faupl, 1994; Wagreich et al., 2008). The Gosau Group comprises a continental to shallow-marine lower interval (i.e., Lower Gosau Subgroup, Upper Turonian to Campanian; Wagreich and Decker, 2001) followed by deep water deposits (i.e., Upper Gosau Subgroup, mainly Campanian to Eocene in age; Wagreich and Faupl, 1994; Neuhuber et al., 2007; Wagreich, 1995, Wagreich et al., 2006; Krenmayr, 1999; Wagreich and Krenmayr, 2005).

3. Structural, stratigraphical and petrological constraints of the Northern Calcareous Alps sector of the Neo-Tethys

3.1. Cross sections and stratigraphic type-sections of the eastern Northern Calcareous Alps

Two new regional balanced cross-sections were produced to document the structural styles and the structural-stratigraphic relationships between thrust sheets in the studied area (Fig. 4). The two cross-sections are oriented approximately north-south (see Fig. 1 for location) and are representative of the traditionally described eastern Northern Calcareous Alps including the Bajuvaric, Tirolic and Juvavic nappe systems (i.e., Tollmann, 1976b; Linzer et al., 1995, 1997; Mandl, 2000). Input data to carry out these regional sections have been our own structural data (i.e., bedding, faults and geological contacts from mapping) collected in several field campaigns, published geological maps at scale 1:50,000 and 1:200,000 from the Geological Survey of Austria (GBA - https://www.geologie.ac.at), and a series of unpublished maps from former field campaigns. Stratigraphic tops from hydrocarbon exploration

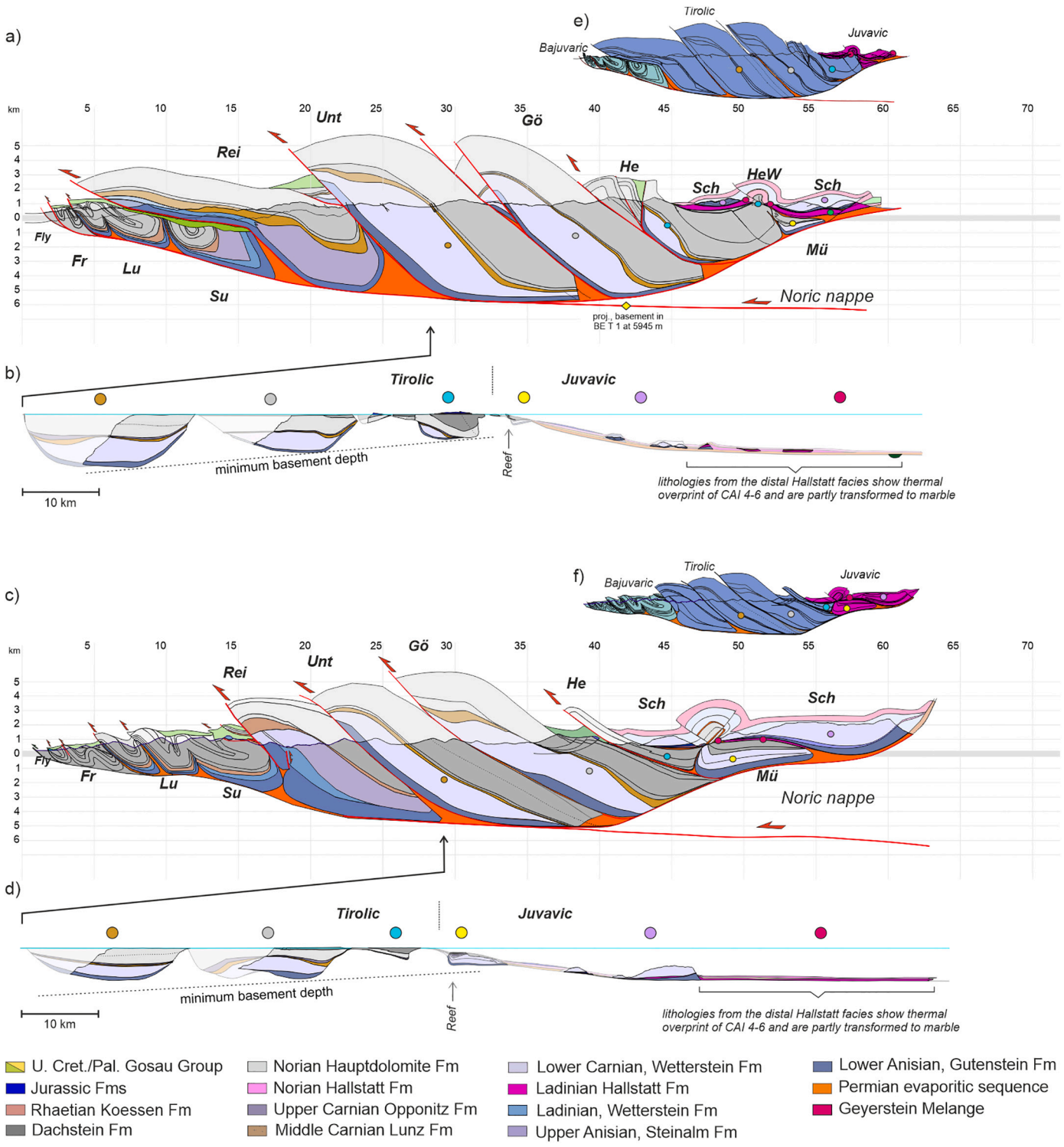

Fig. 4. Geological cross sections of the eastern Northern Calcareous Alps described in this study. The location of both sections is displayed on Fig. 2. Note the difference in thickness and structural wavelength between the major tectonic domains. a) and c) regional sections together with a display of the major nappe systems. b) and d) nappes restored to the top Norian level and distributed based on their stratigraphic content. Exploration well BE_T1 (projected 37 km from the east), drilled crystalline basement at 5945 m depth. Insert sections e) and f) illustrate the three major tectonic domains: Bajuvaric (light blue); Tirolic (grey); Juvavic (magenta) nappe systems. Fly = Flysch. Abbreviated nappes: Fr = Frankenfels, Lu = Lunz, Su = Sulzbach, Rei = Reisalpen, Unt = Unterberg, Gö = Göller, He = Hengst, Sch = Schneeberg, Mü = Mürzalpen. HeW = Hengst window. CAI: Conodont Alteration Index. (For interpretation of the references to colour in this figure legend, the reader is referred to the web version of this article.)

borehole data (i.e., well Berndorf T1, Wachtel and Wessely, 1981; Brix and Schultz, 1993; Zimmer and Wessely, 1996; Wessely, 2006) were also included. Using well-established structural restoration techniques (i.e., Hossack, 1979, 1995; Kupper and Hossack, 1981; Woodward et al., 1989; Stewart and Coward, 1995; Rowan and Ratliff, 2012), the two regional sections were validated during their construction. The sections were sequentially restored to the top of the Norian Hauptdolomit Fm, the top of the siliciclastic middle Carnian event (i.e., Lunz Fm and equivalents), to the top of the lower Carnian Wetterstein Fm carbonate platforms, and to the top of the Anisian carbonates (i.e., Gutenstein Fm). Based on the observed field relationships (i.e., even stratigraphic thickness, and sharp truncations against the Permian salt) the Anisian carbonates are considered to be a pre-kinematic layer deposited immediately above the salt before any movement related to salt evacuation or salt-detached extension (i.e., Granado et al., 2019).

Based on the cross-sections construction, a series of stratigraphic type sections are compiled (Fig. 11) for various thrust sheets involved in the Bajuvaric, Tirolic and Juvavic nappe system of the eastern Northern Calcareous Alps. The stratigraphic type-sections represent the characteristics from the central to the distal stratigraphic units of the Northern Calcareous Alps. The stratigraphic relationships with major faults bounding the present-day thrust sheets, the presence of salt along the faults and the salt-sediment relationships clearly indicate the existence of minibasins bounded by salt walls across the shelf of the rifted Neo-Tethyan margin as previously described by Granado et al. (2019); Fernández et al. (2021); Strauss et al., 2021a, 2021b and Santolaria et al. (2022). Salt-related minibasins in the eastern Northern Calcareous Alps appear often in a row, separated by former salt walls (now squeezed and thrust-welded; see Vidal-Royo et al., 2021) in a similar fashion to those described for the South Atlantic (i.e., Duval et al., 1992; Eichenseer et al., 1999; Rouby et al., 2002; Moore and Blanchard, 2017; Kukla et al., 2018; Ge et al., 2020). Similar geometries and temporal relationships have been produced by scaled physical analogue models (e.g., Warsitzka et al., 2021; Santolaria et al., 2022; Granado et al., 2023). The stratigraphy involved in a single thrust sheet is rather similar along strike but is characterised by strong changes in facies and thickness in an orthogonal direction (i.e., north-south, and parallel to the Alpine direction of tectonic transport; see Fig. 4). In a similar fashion, since these thrust sheets involve minibasins, facies and stratigraphic relationships also change abruptly at minibasin boundaries along the strike of the thrust sheet and control the shape and dimensions of the thrust sheets (Fig. 2a).

3.1.1. The Bajuvaric nappes

Both cross-sections show strong variations in structural wavelengths (Fig. 4), which directly relate to stratigraphic thickness involved in the fold-and-thrust system and the depth to the detachment: the frontal most and structurally lowest Bajuvaric units display breached detachment anticlines flanked by strongly deformed growth synclines filled with Lower to lowermost Upper Cretaceous syn-orogenic strata (i.e., Frankenfels, Lunz and Sulzbach thrust sheets; Fig. 4). The Frankenfels nappe is detached on the middle Carnian Opponitz Fm (Linzer et al., 1997); howeverAnisian and Ladinian units locally occur imbricated as well at the base of these thrust sheets (see Schnabel et al., 2002 and the GBA https://www.geologie.ac.at geological maps). The Lunz nappe immediately to the south shows significantly thicker stratigraphic units than those of the Frankenfels nappe and is generally considered to be detached on the Permian salt based on well data and cross-section construction constraints. These relationships suggest an irregularly distributed Permian salt pinch-out to the north, as well as the presence of thrust ramps along which the basal detachment climbed up from the southerly Permian salt to the middle Carnian evaporites of the Opponitz Fm to the north. Another fundamental characteristic of the Bajuvaric nappes resides on its southernmost structural element: the Sulzbach nappe. This nappe shows further increase in stratigraphic thickness (Fig. 4), including along-strike changes in sedimentary facies related to the growth of isolated Wetterstein Fm platforms and inter-platform basins (Fig. 2). However, the most important structural characteristic is that the he Sulzbach nappe represents a strongly overturned panel in the footwall of the Tirolic emergent thrust front (i.e., see sections A and B on Fig. 4).

3.1.2. The Tirolic nappes

The tectonic boundary between Bajuvaric and Tirolic nappe system is often highlighted by the first massive appearance of salt at surface and a significant change on the Triassic stratigraphic thickness which marks the position of the Tirolic thrust. Immediately to the south, the Tirolic nappes are characterised by the thickest stratigraphic succession involved in the imbricate stack of the Reisalpen, Unterberg and Göller nappes (Fig. 4). In the studied sections, the Tirolic thrust front is characterised by a typical thrust contact (i.e., older units on top of younger units) with a hanging wall flat on a footwall ramp position (Fig. 2). Conversely, the thrust contact between the Bajuvaric and Tirolic nappe system to the west of the studied area is represented by an apparent subtractive contact, with Norian Hauptdolomit Fm juxtaposed to Anisian successions; this contact is accompanied by the presence of a strongly deformed stripe of Permian evaporites (see regional map by Schnabel et al., 2002). At several locations, clastic sediments of the Upper Cretaceous to Paleogene Gosau Group are unconformably deposited on the overturned footwall below the frontal Tirolic thrust (Tollmann, 1976b; Schnabel et al., 2002; Fig. 4). The Gosau Group covers an erosional relief of intensely folded Bajuvaric units in the footwall to the Tirolic nappe. Since the Bajuvaric structures are characterised by Early to lowermost Upper Cretaceous growth synclines, the presence of unconformable Gosau Group sediments truncating previously developed folds and related thrusts in the footwall of the Tirolic thrust is a clear indication of the *out-of-sequence* character of the Tirolic nappe system (Fig. 4).

Comparing stratigraphic thicknesses, the Tirolic nappes are about three to four times thicker than the frontal Bajuvaric nappes. From north to south, four nappes are represented in the A and B cross sections of Fig. 4: the Reisalpen, Unterberg, Göller and Hengst nappes. The Hengst nappe is the smallest nappe of the Tirolic nappe system and shows a noticeable change in the Upper Triassic stratigraphy: from the Hengst Nappe northwards, the Norian stage is represented by the lagoonal Hauptdolomit Fm whereas in the Hengst nappe (and the nappes further south) this stage is dominated by the sub-tidal Dachsteinkalk Fm. The stratigraphy of the Hengst nappe displays an asymmetric development however, since its southern part exclusively consists of Upper Triassic units, i.e., thin Lunz, Opponitz and Dachsteinkalk Fms deposited directly on Permian salt.

A major stratigraphic difference of the Bajuvaric and Tirolic nappes is the massive development of the upper Ladinian to lower Carnian Wetterstein Fm carbonate platforms. Whereas in the Bajuvaric nappes Middle Triassic carbonate platforms are rare and occur only occasionally in the overturned Sulzbach nappe (Granado et al., 2019), in the Weyerer Arc (Schnabel et al., 2002), or below the Urmannsau tectonic window (Schnabel et al., 2002; Wessely, 2006) in the Tirolic nappes the Wetterstein Fm platforms are massively developed and reach thicknesses of some 2.5 km for the Unterberg nappe. The Wetterstein carbonate platforms in the Unterberg nappe reaches a lateral extent in excess of 20 km (see Schnabel et al., 2002). Based on this, the Unterberg nappe represents the Middle Triassic depocenter of the eastern Northern Calcareous Alps. Due to their comparatively larger stratigraphic thickness the Tirolic nappes usually occur imbricated and back-tilted conforming a rather coherent unit and are not as tightly folded as the Bajuvaric tectonic elements, as essentially pointed out by Mandl (2000). Minor folding is observable along the thrust contacts, where the original stratigraphy was thin, as for example at the northern limit of the Hengst nappe, where a thin Upper Triassic and Jurassic succession occurs imbricated.

3.1.3. The Juvavic nappes

The Juvavic nappes are characterised by a series of thrust-stacked structural units, each of which is constituted by distinct stratigraphic sequences and lithologies. Based on these differences, the Juvavic nappes will be grouped and described below. Stratigraphic thinning of individual units (see Figs. 4 and 5) in combination with the presence of Permian-Triassic salt results in a more complex deformation style of the Juvavic structural elements, in a sense, similar to that of the Bajuvaric, with tight folds involving overturned limbs, but significantly different to that of the stiffer and thicker Tirolic nappes (i.e. Mandl, 2000). Two detailed cross sections were created and shown on Fig. 5 to display in higher resolution the architecture of the Juvavic nappes,. Immediately visible is the strong contrast in thickness of the Juvavic nappe system in the hanging wall (i.e., the Hohe Wand nappe, and the Schneeberg nappe) and the Hengst nappe of the Tirolic nappe system in the footwall: the Hengst Nappe alone is thicker than the whole Juvavic nappe system. Secondly, all Upper Triassic carbonates of the Juvavic nappe system that were beyond the shelf break of the Dachstein reef were deposited in slope to deep-water settings.

A close observation of the tectonic contacts and the relative ages between them is necessary to fully understand the structural development of the fold-and-thrust belt, but also to constrain the depositional site of the different sedimentary facies on the correct paleogeographic depositional site of the Juvavic facies belts, in particular those containing serpentinized ultramafic rocks (see following sections). These tectonic contacts are displayed on a very generalised cross section in Fig. 6a. Three major steps on the shortening can be derived from the contacts inside the Juvavic nappe-stack itself and of Juvavic-Tirolic contacts on the geological maps (see Fig. 6b). The oldest set of thrusts are those which bring distal Juvavic units (i.e., Hallstatt facies and allochthonous salt) in contact with the Upper Triassic platform carbonates of the Hengst nappe, the Hohe Wand nappe and the Schneeberg nappe (contacts 2,4 and 8 in Fig. 6). This thrusting happened during Oxfordian times (Mandl, 2016) and the distal Hallstatt units are associated with large amounts of salt and serpentinized ultramafic rocks. Further shortening during Late Jurassic and Early Cretaceous times emplaced the minibasin which formed along the shelf break (i.e., Hohe Wand nappe) and other, more distal minibasins (i.e., Schneeberg nappe) over the Hallstatt facies transported earlier (contacts 5 and 11). This out-of-sequence movement brought the Hallstatt facies in the footwall position of the Hohe Wand nappe and Schneeberg nappe, a situation which is observed for example north of the Hohe Wand (Fig. 6).

A third group of contacts is of Upper Cretaceous age (i.e., contacts 6, 7 and 10 in Fig. 6), but those are erosional surfaces covered with sediments belonging to the Gosau Group The fourth group of contacts record internal shortening of the Juvavic units, documented by syn-orogenic Upper Cretaceous thrusting (contacts 3, 9 and 11). Post Palaeocene thrusting is shown by Hohe Wand nappe thrusts over the overturned erosional contact number 6 (see also Plöchinger, 1961), whereas back-thrusting over the Gosau Group units at the southern limit of the Northern Calcareous Alps has also been mapped (contact 13 in Fig. 6).

3.1.3.1. The Lower Juvavic nappes. The northernmost and lower structural units of the Juvavic nappe system show distal Hallstatt facies and

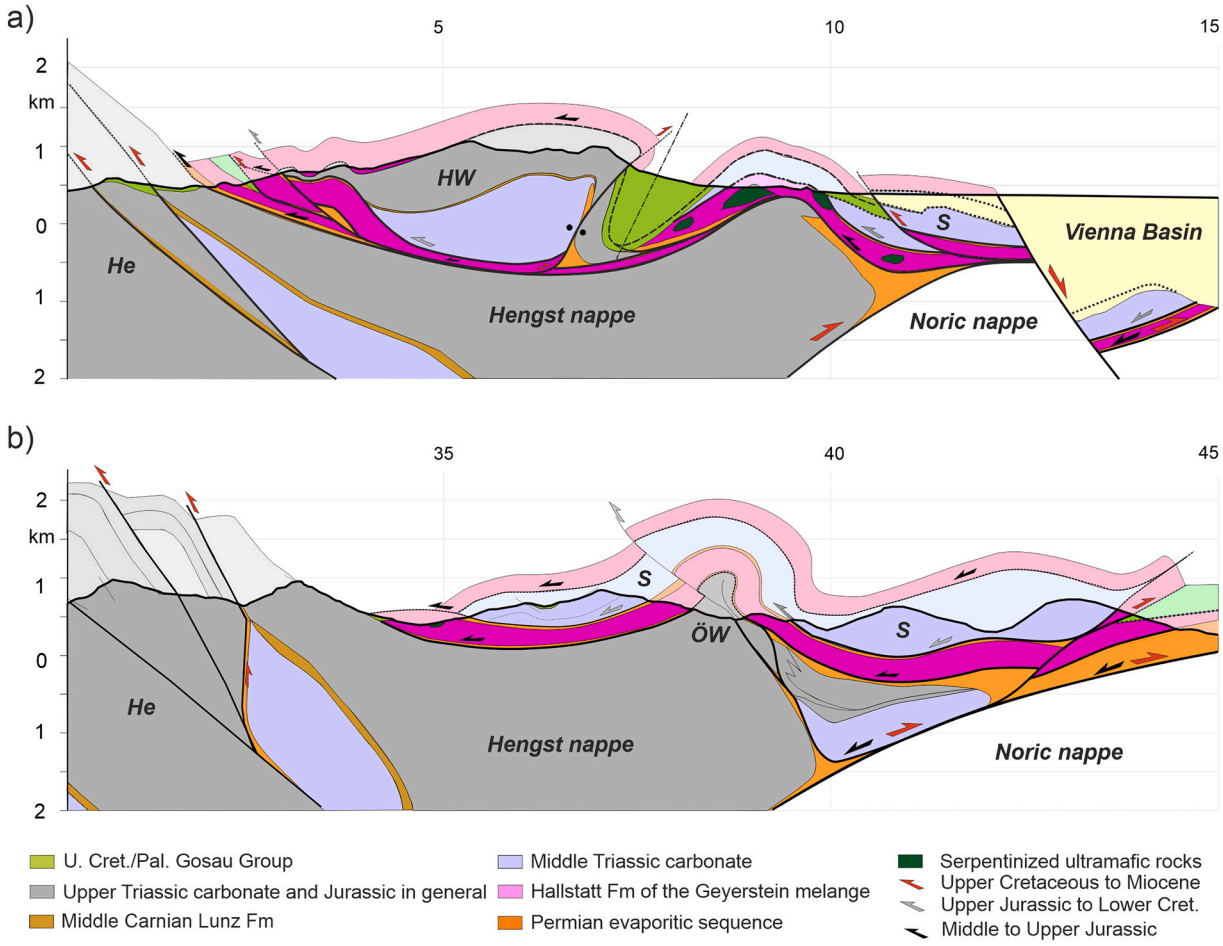

Fig. 5. Detailed sections displaying the relationships between the Juvavic nappes. a) displays the situation at the outcrops of ultramafic rocks. This section is referred to as section "Hw" in Fig. 1. b) is a close-up of regional section shown in 4c, focusing on the Ödenhof tectonic window (ÖW), which allows to restore the thrust relationships of the Juvavic nappes. The colouring of the arrows indicates different thrust ages. HW = Hohe Wand nappe, He = Hengst nappe, S = Schneeberg nappe.

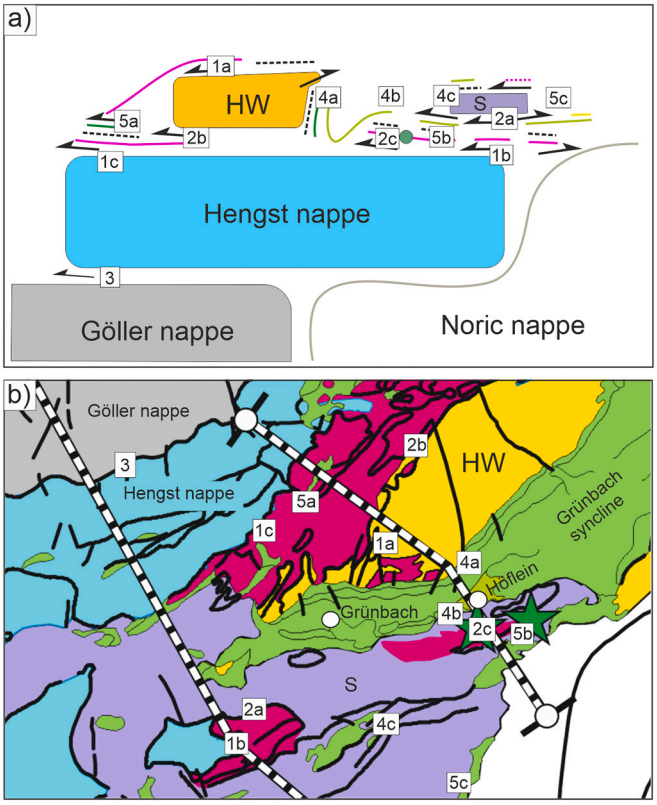

Fig. 6. Location of observed critical thrust contacts on the geological map. a) this diagram is a strongly simplified version of the detailed section 5a. b) close-up of the tectonic map displayed in Fig. 2b. The colours in 6a correspond to those in 6b. HW: Hohe Wand; S: Schneeberg. The Upper Cretaceous to Eocene Gosau Group is displayed in green. (For interpretation of the references to colour in this figure legend, the reader is referred to the web version of this article.)

the out-of-sequence thrusted Upper Triassic reef facies of the shelf break (Figs. 6 and 7). Further noticeable is the southwards decrease in stratigraphic thicknesses of all stratigraphic units in the Lower Juvavic nappes in comparison to the Tirolic nappes (Figs. 4, 6 and 7), especially of those belonging to the Upper Triassic. Such stratigraphic thicknesses decrease correlates with a change in sedimentary facies, from thick shallow marine carbonates to thin deep marine, pelagic and condensed Ladinian to Jurassic units (i.e., dominantly, the *so-defined* Hallstatt Fm sensu Tollmann, 1976a, 1976b, Mandl, 1984 and Lein, 1987).

In the northernmost imbricate the Triassic stratigraphic succession is thin and the middle Carnian Raibl Fm directly overlies the Haselgebirge Fm (Figs. 5, 6 and 7). To the south, the Dachstein Fm becomes thicker and further south it is bounded by their equivalent reef and slope facies in the Mürzalpen nappe. This transition is also observed further east in the Hohe Wand nappe (Kristan, 1958), but in a different structural position as explained below, as it is at present thrusted above the Middle Juvavic nappes (Figs. 5, 6 and 7).

3.1.3.2. The Middle Juvavic nappes: the Geyerstein mélange. Above the Lower Juvavic nappes, the Middle Juvavic nappes and Juvavic thrust slices contain facies associations related to slope and deep marine settings (Kozur and Mostler, 1991; Mandl, 1996), which in the southern structural units are mixed with magmatic and metamorphic components (Figs. 5, 6 and 7). This structural unit has been defined according to its distinct lithological composition. It includes Permian-Triassic salt and related siliciclastics, metamorphic components from the Tirolic nappe system (i.e., greenschists next to the Ödenhof window (Tollmann, 1976b), slices of slightly metamorphosed Triassic carbonates in close association with strongly serpentinized ultramafic rocks. The "Geyerstein Schuppenzone" sensu Tollmann (1976b) includes slices of the Meliata zone (Kozur and Mostler, 1991). Since this tectonic element consists of several subunits with their own chaotically arranged stratigraphic succession (i.e., a *block-in-matrix* texture, sensu Raymond, 1984) we propose to summarise all those different units into one tectonized zone, and name it after the biggest fragment "Geyerstein mélange" (see also Mandl, 1996). Additionally, slices of Upper Cretaceous to Early Paleogene syn-orogenic sediments belonging to the Gosau Group appear along thrust contacts (i.e., syn Upper Cretaceous thrusting contacts 3, 9 and 11; see Fig. 6) of the Geyerstein mélange.

In the study area, the Geyerstein mélange crops out in the vicinity of the village of Höflein (Figs. 2,4,5 and 6) carrying exotic rocks which include: deep water MiddleTriassic and Jurassic radiolarites, marbles, basic volcanic rocks and several serpentinite bodies (their petrology is described in the following chapter 3.2). The mélange mapped in the Grünbach area by Plöchinger (1961) is embedded within a weakly metamorphosed, inhomogeneous carbonate-dominated fault-breccia formed by the tectonized leached remnants of Permian-Triassic evaporites and Middle Triassic carbonates (i.e., *rauhwacken*; see Warren, 2006, page 486 for clarifications about the meaning of the term and genesis). Carbonate rocks derive from the Werfen, Reichenhall, Gutenstein and Wetterstein Fms, whereas gypsum may be attributed to the Haselgebirge or Reichenhall Fms, and sandstones and slates to the Werfen Fm. Serpentinite is present as millimetre to decimetre sized components within a breccia (again mapped as *rauhwacke*), but also several larger bodies have been mapped. The biggest of these serpentinite bodies is located north of the village of Höflein (red star in Fig. 2) and can be traced for >300 m with a thickness up to 40 m (Böhm, 2012). The occurrence of serpentinite involved in the evaporitic mélange is of key tectonic significance, and hence, is treated in more detail in the following section.

3.1.3.3. Emplacement of the Geyerstein mélange. Following the analysis of the structural contacts displayed in Fig. 6 the original positions of the Juvavic nappes and the Geyerstein mélange can be obtained after a conceptual sequential restoration (see Fig. 8). The lithologies found in the mélange were deposited off the shelf break marked by the Upper Triassic Dachstein reef (Fig. 8a), and clearly derive from a distal position belonging to the Hallstatt facies. The distal sediments of the Neo-Tethys rifted margin became part in the developing orogenic wedge already in Middle Jurassic times (see i.e., Gawlick and Missoni, 2019), and a mélange consisting of Hallstatt facies sediments and primarily Permian-Triassic salt (i.e., the future Geyerstein mélange) was thrusted over the Upper Triassic platform carbonates in around Callovian-Oxfordian times together with the Meliata zone (i.e., Mandl, 2016; see Fig. 8b). Out-of-sequence thrusting of the Schneeberg nappe in Oxfordian-Kimmeridgian times brought the Geyerstein mélange and Meliata zone in a structural position between Triassic platform carbonates (Fig. 8c). This relationship is today best displayed in the Ödenhof window (Fig. 5b, and also Fig. 2 in Mandl, 1996), where Upper Triassic platform carbonates are exposed in the centre of the tectonic window, followed structurally upwards by the Geyerstein mélange and the Schneeberg nappe. Further thrusting in Kimmeridgian to Upper Jurassic times included the Hohe Wand nappe into the orogenic wedge and placed the tectonic assembly of Juvavic nappes on top of the Tirolic Hengst nappe (Fig. 8d). Erosion in Upper Jurassic and Lower Cretaceous times exposed the Triassic platform carbonates (Fig. 8e), the erosional unconformity being at the base of the Upper Cretaceous Gosau Group (Fig. 8f).

This complex emplacement history also offers an explanation to the observed metamorphic record. The Noric nappe, the overlying Tirolic and Juvavic nappes and the Meliata zone experienced a Cretaceous greenschist and a very low-grade metamorphic overprint, respectively (Kralik et al., 1987; Frank and Schlager, 2006). Such metamorphic imprint is contemporaneous or post-dates the thrusting of the Triassic carbonate platforms. Therefore, the metamorphic age in the slightly

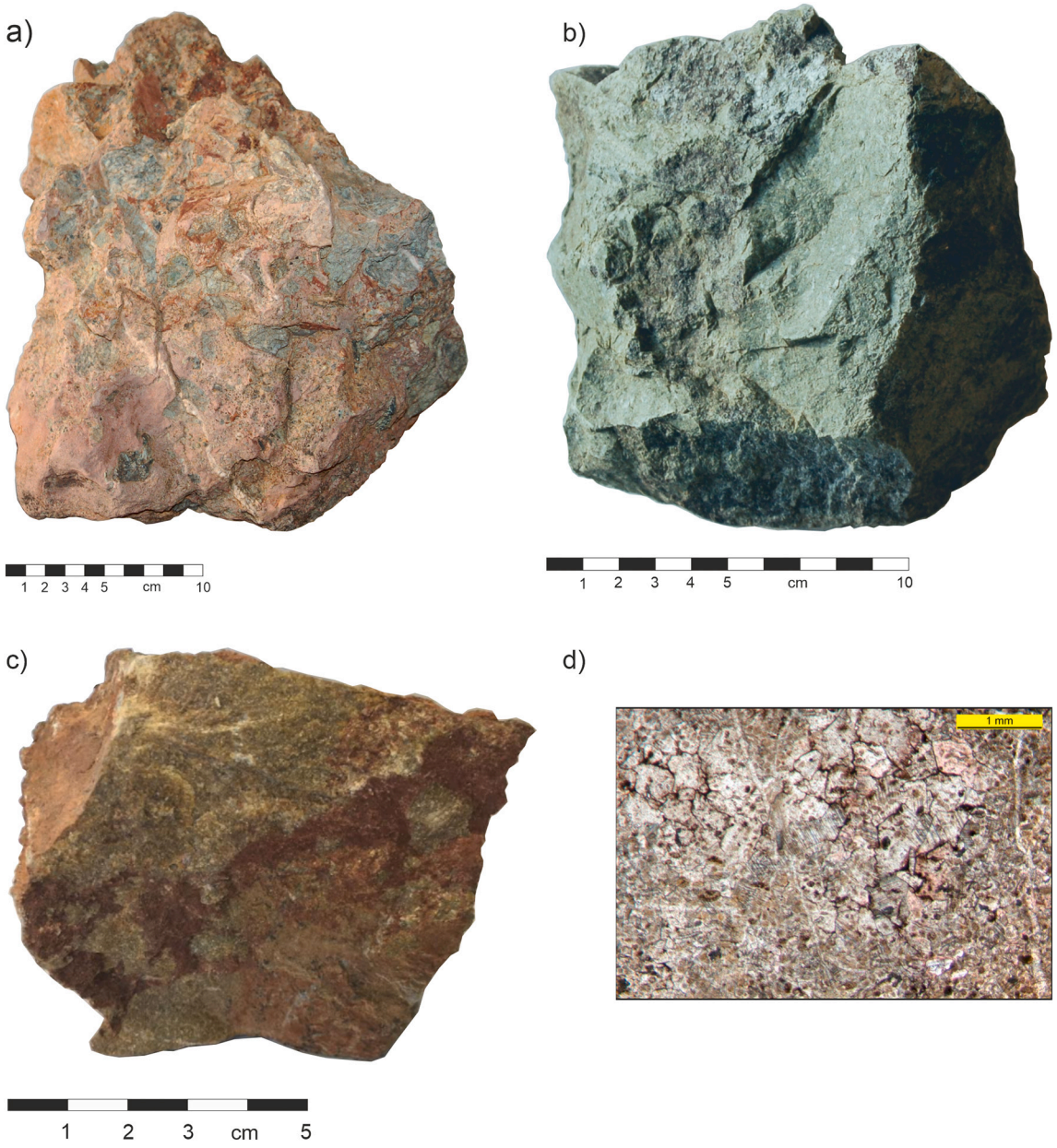

Fig. 7. Lithologies from the Geyerstein mélange: a) Sedimentary mélange including serpentinized ultramafic rocks and red carbonate. b) Serpentinized ultramafic rock. c) Marble from the vicinity of ultramafic rocks outcrop. d) thin section of the marble from the Geyerstein mélange. (For interpretation of the references to colour in this figure legend, the reader is referred to the web version of this article.)

higher-temperature thrust slices of carbonate rocks and Werfen Fm has to be Triassic to Jurassic in age.

3.1.3.4. The Upper Juvavic nappes: the Schneeberg nappe. At present, the Schneeberg nappe and its klippen form the structurally highest tectonic unit in the eastern Northern Calcareous Alps. Since the Schneeberg nappe was located paleogeographically south of the Upper Triassic shelf break, the stratigraphy at present day ranges only from the upper Permian to the Carnian. Upper Ladinian to lower Carnian Wetterstein Fm platform carbonates are the dominant lithology (see also Fig. 4) forming vast and deeply karstified plateaus. Based on the restoration of paleogeographic positions of Juvavic units we must assume that the Upper Triassic sediments of the Schneeberg nappe would have been formed by deeper water Hallstatt facies, but the current erosional level has totally removed the higher sections of original stratigraphy, as well as stacked Hallstatt nappes (Fig. 8e) in the hanging wall.

3.2. Petrology of the ultramafic rocks in the Geyerstein mélange

Strongly serpentinized ultramafic rocks are found in the Grünbach area (Fig. 2b for location);these are greenish in colour and are locally deformed by ductile deformation features such as schistosity and shear bands, as well as brittle structures like cataclastic breccias and slickensides, and veins filled by carbonate minerals. Larger bodies consist of dark greenish domains which preserve primary textures of an ultramafic protolith. By optical microscopy observations, textures of parental ultramafic rocks are recognizable, even if the primary mineral assemblage of olivine, orthopyroxene, clinopyroxene and chrome spinel has been completely altered. An inequigranular texture with abundant, up to 5 mm large, pyroxene with nicely visible cleavage planes and 0.3–0.4 mm olivine is preserved. The secondary mineral assemblage consists of serpentine minerals with minor chlorite, talc, magnetite, hydrogrossular and calcite. Olivine is replaced by typical mesh-textured chrysotile. The

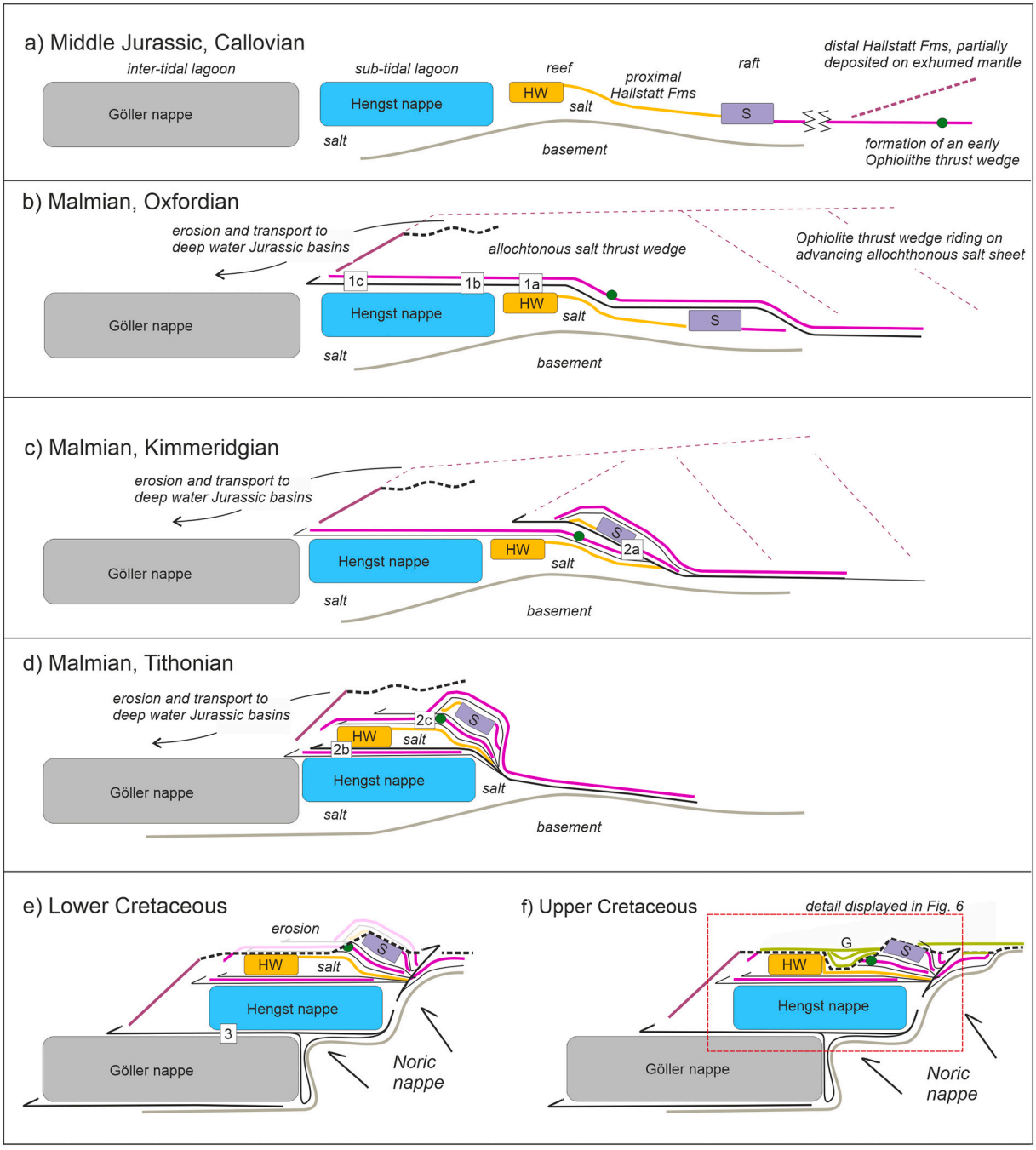

Fig. 8. Evolutionary model of the southern Tirolic and Juvavic units of the Northern Calcareous Alps focusing on the structural development of the Juvavic nappes and the Geyerstein mélange a-f) The green circle marks the position of the ultramafic rocks found in the study area. c) thrusting moves the Schneeberg nappe over the originally more distal Juvavic units. f) The Gosau basin of Grünbach, "G", is formed by the evacuation of salt from the thrust stack. (For interpretation of the references to colour in this figure legend, the reader is referred to the web version of this article.)

rims of the mesh consist of two-axial positive chrysotile-γ and in between chrysotile-α is present. Serpentine minerals also replaced the former pyroxene, but deformed twin lamellae are still visible. In a few samples, relics of clinopyroxene are easily recognized by their conspicuous first and second order interference colours. Chrome spinel is mostly replaced by magnetite and serpentine minerals. According to XRF-analyses, clino-chrysotile is the most abundant serpentine mineral, which together with ortho-chrysotile and lizardite are present in all investigated samples; traces of antigorite were found in half of the samples. Chlorite, carbonate minerals and talc are more frequent in the highly deformed rock types and hydrogrossular is rare.

The major, minor and rare earth element composition of nine serpentinite samples (all samples were collected at the location indicated in Fig. 2 and its close proximity) were determined by ICP-MS (Table 1). The concentrations of SiO_2 vary in a range between 30.9 and 40.3 wt% and the X_{Mg} value is close to 0.93. Al_2O_3 and CaO concentrations are low and range between 1.5 and 3.5 wt% and 0.1–1.0 wt % respectively. Chondrite-normalized REE patterns are depleted especially for the LREE and no negative Eu anomaly can be seen (Fig. 10a). Relative to C1 Chondrite (Sun and McDonough, 1989) the samples show depletion in Cs and Sr (large-ion lithophile elements) and enrichment in Nb and Zr (high field strength elements), while the La/Yb is in the range of 0.05–0.50.

Using whole rock geochemical data of nine samples with well-

Table 1
Chemistry of the serpentinite samples taken from the tectonic mélange near Höflein (see Fig. 2 for location) in the Geyerstein mélange.

Sample:	WRB11/03b	WRB11/13b	WRB12/01b	WRB12/05b	WRB12/06b	WRB12/08b	WRB12/09b	WRB12/17b	WRB12/18b
Rock type:	harzburgite	harzburgite	harzburgite	harzburgite	harzburgite	harzburgite	harzburgite	harzburgite	harzburgite
olivine (wt%)	0,732	0,722	0,638	0,736	0,714	0,716	0,737	0,703	0,741
orthopyroxen (wt%)	0,241	0,222	0,291	0,257	0,268	0,267	0,263	0,278	0,254
clinopyroxen (wt%)	0,011	0,035	0,039	0,002	0,001	0,000	0,000	0,000	0,002
spinell (wt%)	0,016	0,020	0,032	0,005	0,017	0,017	0,000	0,019	0,002
major elements (wt%)									
SiO_2	39,75	39,59	40,30	39,77	40,05	38,50	37,04	34,79	30,87
TiO_2	0,06	0,08	0,07	0,06	0,06	0,04	0,03	0,06	0,02
$Al2O_3$	2,39	3,52	2,86	2,41	2,19	1,97	2,05	2,24	1,53
Fe_2O_3T	4,91	3,49	5,93	3,58	5,28	5,50	2,98	4,41	3,15
MnO	0,12	0,07	0,12	0,10	0,13	0,08	0,07	0,06	0,08
MgO	41,17	40,95	39,02	41,28	40,99	39,40	38,41	35,48	32,00
CaO	0,40	0,98	0,99	0,28	0,20	0,09	0,20	0,11	0,21
P_2O_5	0,01	0,01	0,01	0,01	0,01	0,01	0,01	0,01	0,00
Cr_2O_3	0,60	0,71	0,62	0,61	0,63	0,56	0,58	0,52	0,43
NiO	0,25	0,25	0,25	0,23	0,26	0,23	0,23	0,22	0,19
LOI									
Total	89,66	89,65	90,16	88,33	89,79	86,37	81,60	77,91	68,48
X_{Mg}	0,94	0,95	0,92	0,95	0,93	0,93	0,96	0,93	0,95
trace elements (ppm)									
Cs	0,01	0,02	0,01	0,01	0,01	0,01	0,01	0,01	0,00
Ba	1,94	1,31	5,59	2,05	3,02	2,38	1,98	3,00	2,82
Th	10,169	0,1554	0,0710	0,0421	0,0335	0,0146	0,0266	0,0114	0,0004
U	0,011	0,035	0,025	0,000	0,096	0,001	0,004	0,040	0,000
Pb	1,34	2,04	0,75	0,69	0,68	0,94	1,84	1,13	0,59
Li	1,59	6,81	12,91	1,53	3,12	1,51	1,44	1,65	0,58
Nb	0,56	0,45	0,43	0,42	0,42	0,40	0,80	0,46	0,48
Ce	0,13	0,24	0,12	0,00	0,15	0,00	0,00	0,11	0,00
Sr	0,85	1,86	1,45	1,09	1,32	2,38	2,45	2,36	1,47
Zr	7,31	6,27	5,79	5,46	5,39	5,17	5,20	4,90	4,74
Tb	0,01	0,02	0,01	0,01	0,01	0,01	0,00	0,02	0,00
Y	1,70	2,66	2,08	1,64	1,13	1,09	1,13	2,05	0,83
Cr	2502	2987	2584	2544	2656	2335	2442	2188	1803
Ni	1973	1939	1984	1844	2008	1792	1846	1717	1499
Zn	25,09	33,80	36,77	20,35	30,61	40,03	26,90	48,19	34,41
Ta	0,02	0,01	0,01	0,00	0,00	0,00	0,00	0,01	0,00
B	7,58	11,53	8,50	8,59	7,39	7,85	7,15	7,10	5,16
Sc	13,91	16,11	14,33	14,72	13,51	11,48	12,39	12,74	9,41
V	51,7	46,2	58,4	44,3	50,9	37,7	31,3	53,3	30,1
Co	92	85	103	81	70	94	100	80	69
Cu	0,92	2,01	2,37	0,92	9,18	1,06	1,26	6,01	0,62
Ga	1,76	2,27	2,30	1,77	1,69	1,51	1,35	1,78	1,17
Hf	0,176	0,081	0,055	0,027	0,011	0,007	0,020	0,021	0,000
La	0,026	0,201	0,037	0,071	0,062	0,020	0,009	0,086	0,015
Ce	0,134	0,236	0,121	0,000	0,145	0,000	0,000	0,105	0,000
Pr	0,000	0,054	0,000	0,000	0,000	0,000	0,000	0,021	0,000
Nd	0,026	0,266	0,000	0,062	0,054	0,035	0,000	0,147	0,018
Sm	0,003	0,057	0,020	0,000	0,000	0,000	0,000	0,000	0,000
Eu	0,020	0,046	0,033	0,016	0,017	0,023	0,004	0,043	0,010
Tb	0,011	0,024	0,015	0,011	0,007	0,006	0,004	0,017	0,003
Gd	0,039	0,092	0,057	0,023	0,019	0,000	0,000	0,000	0,000
Dy	0,094	0,171	0,120	0,104	0,068	0,061	0,050	0,123	0,033
Ho	0,054	0,087	0,068	0,059	0,039	0,034	0,035	0,065	0,020
Er	0,184	0,261	0,212	0,181	0,128	0,107	0,116	0,188	0,080
Tm	0,024	0,037	0,028	0,028	0,019	0,017	0,014	0,025	0,010
Yb	0,172	0,243	0,203	0,179	0,135	0,111	0,109	0,177	0,083
Lu	0,027	0,043	0,032	0,029	0,019	0,016	0,019	0,027	0,012

preserved primary textures (Table 1) and a reference data set from Albania (i.e. Onuzi et al., 2021), the primary modal proportions of olivine, orthopyroxene and clinopyroxene were recalculated by an interactive method. The reference data set includes typical chemical whole rock compositions of lherzolite, harzburgite and dunite samples as well as their mineral phases. For the calculation, the oxide values (in wt%) of SiO_2, TiO_2, Al_2O_3, FeO, MnO, NiO, MgO, CaO were considered. The values of the investigated samples were compared to average oxide values (in wt%) of the whole rocks and minerals of the reference material. According to the difference between the sample and the weighted averaged reference values proportion, parts of olivine, orthopyroxene, clinopyroxene and spinel were empirically calculated with the integral least square method. The defined target value was the sum of differences, which should be as small as possible. Proportions of primary minerals in the sample were assigned as modifiable values, with the condition that the sum of the values has to be 100%. During the process, it became apparent that the method works best with the harzburgite reference material.

The calculated primary mineral compositions of the samples were plotted in the ternary diagram for ultramafic rocks (Fig. 10b). The results indicate harzburgites as precursor rocks of the investigated serpentinite samples. Olivine was the most abundant mineral with 64–74

wt% followed by 22–29 wt% orthopyroxene, <4 wt% clinopyroxene and spinel. These values argue for a harzburgite composition as lherzolites are typically characterised by higher Al_2O_3 and CaO contents (Melcher et al., 2002). Higher CaO values of two samples might be an indication for secondary calcification, however, as CaO is correlated to Al_2O_3 it will be due to a higher modal proportion of clinopyroxene in these samples. Also, the REE-patterns follow that of harzburgite with a typical depletion trend, following their refractory origin from lherzolite. In the classification diagrams of Deschamps et al. (2013) the investigated serpentinite samples plot mostly in the field of subducted serpentinite and close to depleted mantle (Fig. 10c, d, e, f). Accordingly, they are also slightly enriched in Pb with respect to depleted mantle (Fig. 10g). The significance of strongly serpentinized harzburgitic rocks within the Geyerstein mélange will be discussed further in the context of the Neo-Tethys evolution.

3.3. Age constraints, bathymetry and thermal history of the Northern Calcareous Alps

3.3.1. Age constraints of the Northern Calcareous Alps stratigraphy

Chrono- and lithostratigraphy are well established in the Northern Calcareous Alps and generalised stratigraphic tables were published by Tollmann (1976a), Mandl (2000), Piller et al. (2004) and Wessely (2006). Detailed work concerning individual stratigraphic units of the Northern Calcareous Alps was published as well for the upper Permian and Lower Triassic (Leitner et al., 2017), for the Ladinian and lower Carnian Wetterstein Fms (Brandner and Resch, 1981; Lein et al., 2012; Moser and Tanzberger, 2015), the middle Carnian Lunz Fm (Mueller et al., 2016), for the Norian and Rhaetian stages (Richoz et al., 2012; Galbrun et al., 2020; Rizzi et al., 2020) and the Jurassic (Gawlick et al., 2009). We adhere to those works for our calculations.

3.3.2. Paleo-bathymetry of sediments in the Northern Calcareous Alps

Detailed knowledge of the paleo-bathymetry allows establishing regional *datum* levels (see Fig. 11). Establishing these is of paramount importance for basin scale correlation and of great use for sequential restoration of the geological cross-sections. Based on sedimentary facies, estimates of paleo-water depth are well constrained for the uppermost Permian to lowermost Triassic, and as well as for Middle and Late Triassic successions in the Northern Calcareous Alps, since all units belonging to these series/stages were deposited on a shallow water marine environment (see Tollmann, 1976a; Mandl, 1984; Krystyn and Lein, 1996; Leitner et al., 2011, 2017; Lein et al., 2012; Strauss et al., 2021a, 2021b). Some uncertainty is arguable as to paleo-bathymetry at the Upper Triassic and Jurassic distal domain of the rifted margin, since pelagic carbonates of the Hallstatt have been interpreted as deposited on the distal slope and on the oceanic basin, respectively (Krystyn, 1973; Kozur, 1991; Channel and Kozur, 1997; Mandl, 2000; Gawlick and Missoni, 2015, 2019).

3.3.3. Thermal constraints relevant to our study

3.3.3.1. Supra-salt cover and Permian evaporites. In the Northern Calcareous Alps, the thermal record has been documented by the colour alteration index (CAI) of conodonts found in Anisian units (i.e., directly sitting above the salt) in the Bajuvaric, Tirolic and Juvavic nappes (Gawlick and Königshof, 1993; Gawlick et al., 1994). For the most parts in the Northern Calcareous Alps conodonts show CAI values of 1 to 2, which is considered to be equivalent to 80–140 °C. Such temperature are related to the sedimentary overburden, thrust stacking and syn-orogenic sedimentation, as in many other foreland fold-and-thrust belts (i.e., Hardebol et al., 2009). However, the southernmost and structurally higher Juvavic units have recorded temperatures as high as ~300–400 °C according to CAI values of 5–6 (i.e., Rantitsch et al., 2020). In addition, the occurrence of marbles derived from the Anisian Gutenstein and Steinalm Fms at the base of Schneeberg nappe (Figs. 2b, 4 to 7) and within the Geyerstein mélange (Fig. 6b) are consistent with temperatures in excess of ~300 °C. The same authors, have reported CAI values of 5–6.5 for Anisian to Norian levels, along with Raman spectroscopy of carbonaceous material in the Juvavic Mürzalpen nappe (i.e., in an equivalent structural position to the Hohe Wand and Schneeberg nappes of Fig. 2b) indicating temperatures in the range of 280–310 °C.

Leitner et al. (2017, 2020, and references therein) described large amounts of replacement cements of halite, anhydrite or polyhalite (i.e., a hydrated sulphate of potassium, calcium and magnesium with formula $K_2Ca_2Mg(SO_4)_4{\cdot}2H_2O$) in sandstones within the Permian salt; their petrographic studies suggest closure of the intergranular pore spaces under an overburden estimate of about ~500 ± 100 m. Polyhalite crystallization at the base of the Juvavic depositional areas occurred at ~235–230 Ma (i.e., mid-upper Carnian times) as dated by $^{40}Ar/^{39}Ar$ method (Leitner et al., 2020). This provides a crystallization age only ~15–20 Ma after deposition of the Permian evaporites. Crystallization of polyhalite can occur as fluids are driven out from mudstones and/or generated by the gypsum-to-anhydrite conversion at temperatures above 90 °C (Ostroff, 1964; Warren, 2006). Since, Leitner et al. (2014) describe temperatures for the recrystallization in the salt of ca. 250–300 °C a high geothermal gradient and related heat flow are expected for the Carnian stage.

3.3.3.2. Thermal constraints from the pre-salt basement. Aside of the well-recognized Variscan and Alpine metamorphism (i.e., Dallmeyer et al., 1998) the Austroalpine unit was affected by a regional HT-LP Permian metamorphic event that lasted through the Triassic (i.e., Thöni and Miller, 2000; Habler and Thöni, 2001; Schuster and Stüwe, 2008; Knoll et al., 2023). The Permian-Triassic HT-LP event is documented not only the Austroalpine realm but also in neighbouring crustal blocks, including the Southalpine unit, the Transdanubian Range, the Tisza Superunit, the Carpathian realm and the Subpenninic and Middle Penninic units (e.g. Rebay and Spalla, 2001; Kunz et al., 2018; Ondrejka et al., 2021). The widely accepted interpretation for this event is lithospheric thinning associated with rifting (or back-arc extension) accompanied by significant magmatic underplating and partial melting of the crust, protracting through the Middle Triassic (i.e., Roda et al., 2018; Putiš et al., 2019b; Villaseñor et al., 2021; Huang et al., 2022). In the Austroalpine and Southalpine realm, the Permian-Triassic event shows obvious similarities with respect to the observed magmatic rocks, the timing of magmatism and metamorphism, the P-T conditions, and metamorphic assemblages. The available data allow to determine a generalised P-T-t path for the Variscan to Permian-Triassic metamorphic history. Magmatic and metamorphic crystallization ages argue for the thermal peak of this event at 270 ± 30 Ma, with data scatter explained by a slightly different time of the thermal peak at different crustal levels and different localities (Schuster et al., 2001; Knoll et al., 2023). Calculated geothermal field gradients on the retrograde part of the Variscan P-T path are about 35 °C/km but increased to 45 °C/km by heating during decompression at about 270 Ma because of lithospheric thinning and melting of the mantle lithosphere (Schuster and Stüwe, 2008).

4. Reconstruction of the Triassic Neo-Tethys rifted margin

4.1. Restoration of the regional cross-sections to their pre-shortening configuration

In this work we have aimed at reconstructing the Neo-Tethys rifted continental margin. Our reconstruction is based on the structural restoration the two regional sections (Fig. 4a, c). We have firstly removed the Alpine contractional deformation (Fig. 4b, d). We have taken special care in reconstructing the eroded sections at the tips of the imbricated thrust sheets to obtain geologically reasonable pre-

shortening geometries. To carry this out, we have interpreted the geological map patterns to reconstruct the missing parts of the sections removed by erosion. Afterwards, each structural unit has been restored to its original depositional geometry and attitude. By interpreting the facies distribution, we have then repositioned each structural unit to its respective palaeogeographical position (i.e., Schmid et al., 2008; McPhee et al., 2018).

After this first step, we have established 3 main regional markers for correlation across the Northern Calcareous Alps (Fig. 9), namely the top Norian (i.e., top of the Hauptdolomit and Dachstein Fms), the top upper Carnian (i.e., top Opponitz Fm), and the top of the Lower Triassic (i.e., top salt or base of the pre-kinematic Anisian Gutenstein Fm). These three marker levels are basin-wide lithostratigraphic and chronostratigraphic horizons (Strauss et al., 2021a, 2021b). The concept of regional elevation (i.e., a given datum level) is of paramount importance for structural and stratigraphic restoration studies (i.e., Hossack, 1979, 1995; Kupper and Hossack, 1981; Woodward et al., 1989; Stewart and Coward, 1995; Rowan and Ratliff, 2012; Epin et al., 2021). In this first restoration step major differences in stratigraphic thickness between the structural units are readily illustrated (Fig. 9a); these are taken as a first indication for a basement topography underlying the supra-salt stratigraphy. This first step reveals a carbonate depocenter in the Tirolic nappes and a possible basement outer high underneath the restored position of the Juvavic nappes (Figs. 4b, c; see Fig. 8). A cautionary note is that vertical stacking of minibasin depocenters by dominant vertical subsidence has been considered as the main driver for downbuilding and salt evacuation concomitant with thermal subsidence for the Hauptdolomit Fm, but a certain component of salt-detached extension occurred as well (Granado et al., 2019; Strauss et al., 2021a, 2021b). It is assumed that movement of salt out of the section can be neglected for simplification (Hossack, 1995). We use the datum-restored stratigraphic thicknesses as a proxy for the original salt thickness distribution, and the geometry of the underlying pre-salt rifted basement, in a similar fashion as that described for the North Sea (Jackson et al., 2018; Joffe et al., 2023), or the Barents

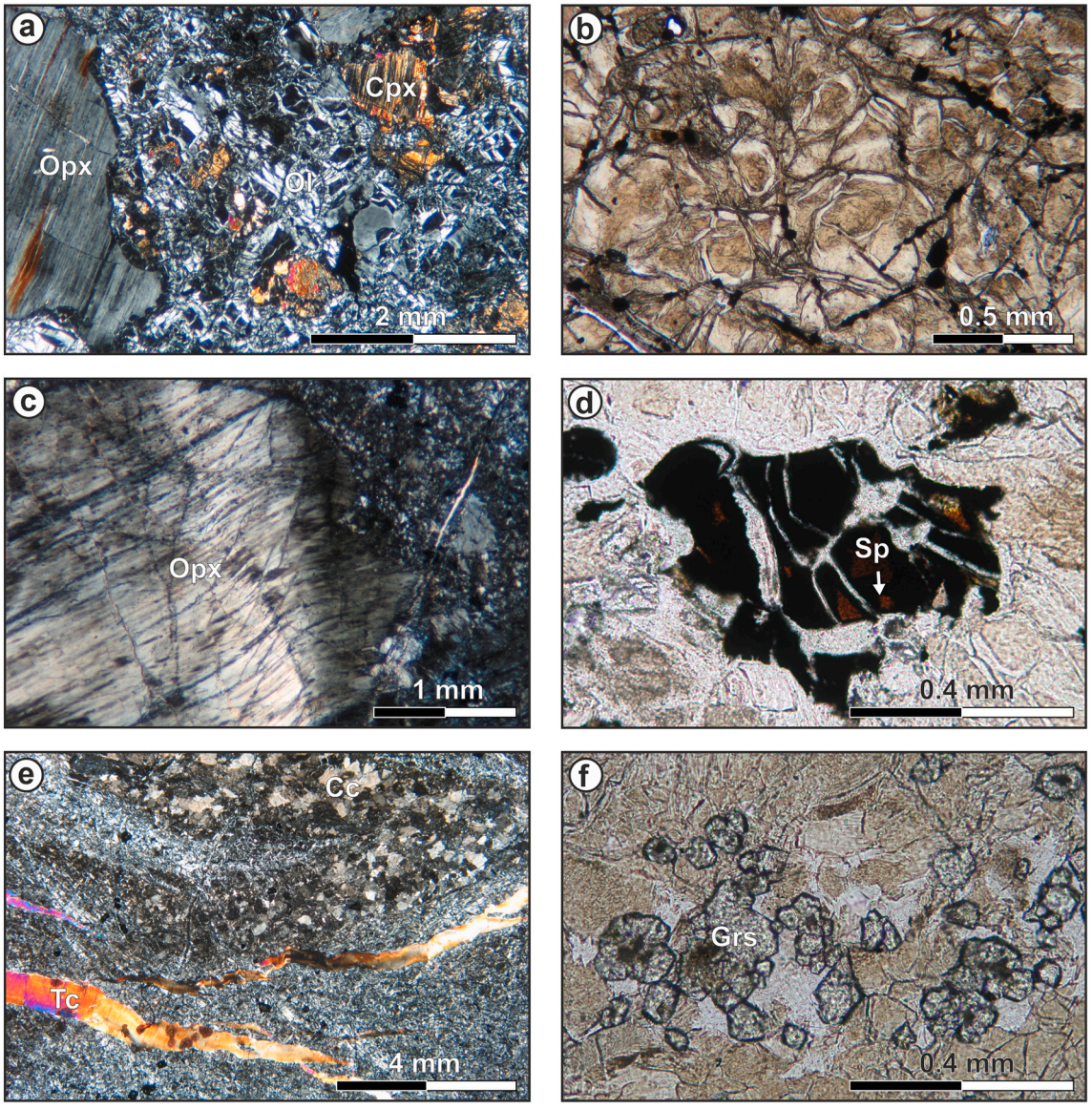

Fig. 9. Thin section photographs in crossed polars of serpentinites from Höflein: a) Typical mineral assemblage of an ultramafic rock (ol + cpx + opx) with serpentine minerals pseudomorphing olivine (Ol) and orthopyroxene (Opx), and partly preserved clinopyroxene (Cpx). b) Growth of chrysotile out of olivine results in a mesh texture. c) A pseudomorph of orthopyroxene (Opx) with twin-lamellae, bended by tectonic stress. d) Chrome spinel (Sp) is just partially preserved and mostly transformed to magnetite and serpentine minerals. e) Many samples are altered, as indicated by large amounts of chlorite, talc (Tc) and carbonate (Cc) minerals. f) Hydrogrossular (Grs) originated from Al-rich spinel.

Sea (Hassaan et al., 2021). In the following, we explain the rationale, procedures and results of each of these steps to reconstruct the rifted margin of the Northern Calcareous Alps sector of the Neo-Tethys.

4.2. Sequential restoration of the rifted margin

4.2.1. Rationale for sequential restoration

The main uncertainty for such margin-wide restoration is the geometry of the *syn*-tectonic basement faults responsible for lithospheric extension below the thick Permian-Triassic salt. To carry out these restorations we have considered and integrated previous regional studies (i.e., Kozur, 1991; Kozur and Mostler, 1991; Channell et al., 1992; Channel and Kozur, 1997; Mock et al., 1998; Schuster et al., 2001; Faryad et al., 2005; Froitzheim et al., 2008; Schuster and Stüwe, 2008; Gawlick and Missoni, 2015, 2019; Leitner et al., 2017, 2020; Putiš et al., 2011, 2019a, 2019b; Schollnberger, 2021; Ondrejka et al., 2021; Villaseñor et al., 2021). In addition, previously published models for the rifted margin of the Northern Calcareous Alps by Granado et al. (2019), and Strauss et al. (2021a) postulate a supra-salt carbonate stratigraphy developed to its maximum degree by salt evacuation by differential sedimentary loading promoted by carbonate aggradation (i.e., downbuilding), assisted by salt-detached extension promoted by a sea-wards slope provided by the regional thermal subsidence. In the initial stages, downbuilding seems to have been the leading driver, but as the regional basinwards slope increased, salt-detached extension may have gained in importance relative to downbuilding. This is evidenced by the widening of salt walls flanking the carbonate minibasins, as well as the formation of associated diapir shoulders since about Norian times (e.g., Granado et al., 2019; Santolaria et al., 2022; Granado et al., 2023). These works have demonstrated that the accommodation space needed to account for the Middle Triassic carbonate platforms can be explained by a combination of salt evacuation by downbuilding and salt-detached extension.

Consequently, subsidence in the studied area could be solely explained without synchronous crustal thinning by basement faults underneath the Tirolic nappes. In addition, the uppermost Anisian and Ladinian radiolarite facies in the Juvavic and the Meliata units witness for crustal thinning before and during Middle Triassic times, but localized south of the Tirolic. In a more distal position than the most southerly Wetterstein Fm platforms, deep water sediments were deposited since the upper most Anisian and Ladinian as represented by the Hallstatt Fm limestones, and Ladinian radiolites of the Florianikogel (i.e., Kozur and Mostler, 1991; Mandl, 2000; Gawlick and Missoni, 2015, 2019; Fig. 2) and located today in the Geyerstein mélange (Figs. 5-8). A well-developed shelf, shelf break and slope towards deep waters had already begun in the Ladinian at least. Such underlying tectonic elements must have located originally south of the Schneeberg nappe Wetterstein Fm platform. The restoration of the supra-salt stratigraphy to a series of datum levels of regional tectonic significance (Fig. 11) has been used as a proxy to obtain the pre-salt basement topography of the proximal domain of the margin (i.e., the shelf segment of the Northern Calcareous Alps), and its infilling by Permian-Triassic salt. Fig. 12 depicts the reconstructed rifted margin through time, including the pre-salt rifted basement below the minibasins. Facies distribution in time and across the margin have been integrated with the thermal constraints commented in previous sections.

4.2.2. Sequential restoration

Following the regional stages described the two regional cross sections presented in this study have been restored (Fig. 12) in four major steps. The evolutionary stages are: sedimentation of a carbonate pre-kinematic layer on the salt; salt evacuation (primarily by downbuilding); crustal hyperextension and mantle exhumation; salt-detached extension upon prevailing thermal subsidence in oceanic accretion. The geometry of the basement is kept similar between the sections since no evidence for a hard-linked (i.e., coupled) development of pre-salt basement and supra-salt stratigraphy is observed in the Northern Calcareous Alps.

4.2.2.1. Restoration to the Norian (top of Hauptdolomit Fm): salt-detached stage. The dominating feature of the stratigraphic record during the Norian stage are the strong variations in sedimentary thickness of lagoonal carbonates (Fig. 12a, e). Thicknesses range from some ~500 m in the Bajuvaric to up to 2500 m of lagoonal carbonates in the central Tirolic minibasins, decreasing towards the south to some 800 m in the proximal Juvavic minibasins. In the Hengst minibasin (i.e., turquoise minibasin in Figs. 11, 12a, e) the thickness of shallow water Norian carbonates remained comparable thin, on top of a large inflated salt structure. Beside the lagoonal carbonates, the lower Juvavic minibasins of the Mürzalpen nappe (i.e. yellow minibasin, Figs. 11, 12a, e) also carry the Norian reef that indicates the transition to the deeper marine Hallstatt facies of the distal Juvavic minibasins. Since the Middle Triassic platforms were located south of the Upper Triassic reef belt (i.e., Mandl, 2000), he Schneeberg nappe (i.e., purple minibasin in Figs. 11 and 12a, e) must have had Upper Triassic deep-water sediments (Hallstatt facies) deposited on top of the Middle Triassic shallow marine carbonates but those were more likely eroded during nappe stacking). The restoration of both cross sections at Top Norian times shows a marine shelf, which is clearly divided in two major realms: a shallow water lagoon bounded to the open sea by a reef, and a deep water open marine area to the south (Fig. 12a and e). Greater thicknesses of Upper Triassic lagoon facies are observed in the central sector of the margin and on the flanks of the minibasins. The lagoon close to the outer high was affected mostly by salt-detached extension starting during middle Carnian times. Between the Göller nappe and Hengst nappe inflated salt is covered by a thin stratigraphic roof, whereas the Hengst nappe itself shows a strong asymmetry with nearly all stratigraphy formed by Dachstein Fm (Fig. 11a). Laterally, the termination of the Hengst minibasin is observable in section B and Fig. 12e. Displacement by salt-detached extension decreased significantly towards north as the outer high prevented the rafting of the thick minibasins of the central Tirolian sector further south. The Juvavic minibasins, which were at sea level in Middle Triassic times, became deep water environments by rafting into deeper waters, in a similar fashion to the South Atlantic salt basins (Duval et al., 1992; Eichenseer et al., 1999; Moore and Blanchard, 2017; Kukla et al., 2018; Ge et al., 2020).

4.2.2.2. Restoration to the middle Carnian (top of Lunz Fm): mantle exhumation stage. The upper Carnian Opponitz Fm represents a shelf-wide transgression following the siliciclastic middle Carnian Lunz Fm (Fig. 12b and f). The so far clastic-free carbonate shelf sedimentation is interrupted in middle Carnian times by a massive terrigenous input from the north, known as the middle Carnian Reingraben clastic event (i.e., Schlager and Schöllnberger, 1974). The top of the Lunz Fm is taken as the regional datum which corresponds to the margin-wide change from isolated Wetterstein carbonate platforms to the vast Upper Triassic Hauptdolomit lagoon covering the entire proximal domain of the rifted margin. In some minibasins of the proximal Tirolic realm the Lunz and the Opponitz Fms filled up the remaining space of the deeper water basins in between the Wetterstein platforms. Both formations provide a thin cover for the Wetterstein platforms, emerged during the middle Carnian (Fig. 11b). Since both formations are thin on top of all Wetterstein platforms (< 50 m) the Lunz and the Opponitz Fms record a phase devoid of any significant subsidence, or even emersion (Moser and Tanzberger, 2015). This is also supported by previous subsidence analysis from the Gamsstein minibasin (Strauss et al., 2021a, 2021b), located further west. This regional level can also be used as a proxy for a restoration of the Wetterstein reefs back to sea level, which allows the comparison of platform development between adjacent minibasins. In respect to stratigraphic thickness, the same overall trend as for the Upper Triassic can be observed, which is the appearance of thinner Wetterstein Fm in the Bajuvaric, thickest in the centre of the Tirolic and

generally thinner again towards the Juvavic in the south. South of the outer high, further lithospheric extension affected the already deep-water basin (i.e., Hallstatt pelagic facies, and Meliata radiolarites). The Reingraben event is represented as the Raibl beds in the southern areas of the central sectors and in the distal sectors of the margin; thicker deposits of this formation are preserved, however, in the Geyerstein mélange.

The slope generated upon the lithospheric thinning caused the minibasins of the outer high, or directly south of it, to glide downslope into deeper water environments of the hyperextended and exhumed mantle domains. All minibasins which moved by salt-detached extension beyond the outer high into deeper waters by the end of the Carnian, did not develop any further carbonate platform in latter Triassic times, because they rafted down below the photic zone.

4.2.2.3. Restoration to the lower Carnian (top Wetterstein platforms). Growth of the Wetterstein platforms occurred at sea-level and was terminated simultaneously by the mentioned input of the siliciclastic Lunz Fm in middle Carnian times (Fig. 12c, g). The Wetterstein platforms grew to very different thicknesses over the same time span across the eastern Northern Calcareous Alps. A reasonable explanation for this relates to the different depositional thicknesses of the underlying Permian-Triassic salt. Therefore the aggradational growth potential of the carbonate producers was not necessarily the limiting factor (Strauss et al., 2021a). but the available accommodation space by salt evacuation and salt-detached extension; if the Wetterstein platforms did not outgrow the available accommodation space, they were terminated by the clastic input of the Lunz Fm.

Restoring the eastern Northern Calcareous Alps shelf to the top of the Wetterstein platforms shows that their maximum thickness was reached in the central sector of the margin (i.e., Unterberg in the Tirolic), being thinner in the southern sector of the Tirolic (i.e., Hengst nappe), to reach greater thickness again in the southern Juvavic to the south. In both restored sections this observation can be made, thus highlighting changes in basement topography, and the presence of an outer high. The carbonate minibasins reached a thickness of up to 2500 m in the depocenter of the Northern Calcareous Alps shelf, whereas the platforms which grew on the outer high reached only some 500 m and had equivalent smaller horizontal extensions. At least one Wetterstein Fm platform developed south of the outer high, reaching some 1000 m in (preserved) thickness.

4.2.2.4. Restoration to the Early Triassic (top salt, or base of pre-kinematic Anisian Gutenstein Fm). On a regional perspective, the Gutenstein Fm. was deposited on top of the Permian-Triassic layered evaporitic sequence, thus configuring a margin-wide carbonate overburden for the salt. Since the top of the layered evaporitic sequence represents the post-tectonic sediments in the rift proximal domain (as suggested by Leitner and Spötl, 2017), thick-skinned extension in the Permian to lower most Triassic rift basin was no longer taking place during the sedimentation of the Middle and Upper Triassic carbonate platforms above. The rift basins formed on the crystalline basement during the *stretching* and *thinning* phases on the proximal domain (based on the data provided by Schuster et al. (2001), Petri et al. (2017), Mandl, 2000; Leitner et al. (2017) and Villaseñor et al. (2021) were then overfilled by salt and associated siliciclastic and carbonate sediments, with very minor magmatic additions. Both the Werfen and the Reichenhall Fms were deposited in shallow water conditions across the future proximal domain of the margin, which is of great significance for the onset of the Middle Triassic carbonate factory, starting with the pre-kinematic Anisian Gutenstein Fm (Fig. 12e, h). Since basement-involved faults were inactive during the Middle Triassic in proximal domain the restored stratigraphic panel at Anisian times provides an proxy for the pre-salt rifted basement topography, as well as for the thickness distribution of the salt (Fig. 11c).

4.3. Lithospheric thickness evolution from thermal modelling

We further inquire into the lithospheric thickness evolution and related thermal impact on the studied region by carrying out a thermal modelling in PetroMod®. For such, we apply regional constraints detailed in the preceding sections, and those obtained from our own work.

4.3.1. Rationale for thermal modelling

Knowledge of depth of the lithosphere-asthenosphere-boundary and the Moho are crucial to restore the geometry of any given rifted margin. The thermal overprint of sedimentary rocks is a measure for the thermal gradient, and ultimately for the depth of the Moho and the lithosphere-asthenosphere-boundary (i.e., Allen and Allen, 2005; Hantschel and Kauerauf, 2009). 1D thermal models for selected critical positions (locations are indicated in Fig. 12a) of the margin obtained from cross-section restoration can yield potential thickness of the continental crust and its changes in thickness over time. The timing for the onset of post-tectonic thermal cooling phase is one critical input parameter to the thermal modelling, aside of the maximum temperature recorded during the *syn*-tectonic stretching and thinning phases. The temperature which the sediments were exposed to, as recorded by the CAI of conodonts, or the transformation of limestone to marble, is a result of the heat flow in the lithosphere. A thermal gradient results from the depth of the lithosphere-asthenosphere-boundary and is defined by the recorded thermal overprint in the sediments and the petrological composition of the continental crust (i.e., from the concentration of heat-producing radioactive elements). Thermal models show that the syn-tectonic phase leading to mantle exhumation must happen rapidly (i.e., see Lescoutre et al., 2019). The high heat conductivity of the mantle and the absence of heat-producing radioactive minerals results in high cooling rates for the exhuming mantle, which could prevent the transformation of carbonates to marble if the exhumation process is too slow. Since we have reported the presence of marble from Anisian protoliths within the Geyerstein mélange, there is only a limited time-gap for exhumation to have happened in the study area. A sensitivity analysis of key parameters as lithospheric thickness and exhumation rate was done for multiple parameter combinations, which is included in the supplementary materials.

Key point for the setup of our thermal model is therefore, constraining the approximate age for the exhumation of the mantle south of the eastern Northern Calcareous Alps, as well as the timing of syn-tectonic extension of the crust. The exhumation of lower crustal rocks and eventually the sub-continental lithospheric mantle defines the transition from a syn-tectonic phase (i.e., stretching and thinning phases) to a post-tectonic one characterised by decaying thermal subsidence. Such evolution must be fundamentally reflected in the change in the carbonate factory and the platform architecture (from isolated to margin-wide), being as well affected by the presence of a regional salt horizon (i.e., Epin et al., 2021; Chenin et al., 2022). Based on our reconstruction and sequential restorations, regional and thermal constraints, the subcontinental lithospheric mantle was most likely exhumed at middle Carnian times, thus coincident with the deposition of the siliciclastic Lunz Fm Previous subsidence analysis (i.e., Strauss et al., 2021a) and related discussion (i.e., Schollnberger, 2021; Strauss et al., 2021b) concluded that after a phase of emersion and the deposition of the siliciclastic Lunz Fm in middle Carnian, the margin entered undoubtedly into a stage dominated by cooling, and salt-detached extension. Such dramatic change is marked by the re-establishment of the carbonate factory at upper Carnian times (i.e., ~232 Ma) with the platform-wide transgressive Opponitz Fm and the organization of a homogeneous, slowly subsiding carbonate platform on top (i.e., the Norian Hauptdolomit and Dachstein Fms). This platform i) clearly follows along a typical Atlantic-type cooling curve (see Quirk et al., 2013), and ii) widening of the salt-walls by salt-detached extension (Granado et al., 2019; Strauss et al., 2021a), as observed in many modern salt-

bearing rifted margins with salt tectonics (Duval et al., 1992; Eichenseer et al., 1999; Moore and Blanchard, 2017; Kukla et al., 2018; Ge et al., 2020).

4.3.2. Thermal modelling of the eastern Northern Calcareous Alps rifted margin

The crustal and lithospheric mantle thicknesses were evaluated by 1D modelling and adjusted within geologically reasonable limits to match the boundary conditions imposed by thermal constraints. The thermal evolution of the supra-salt stratigraphy on the margin on the selected positions is displayed in Fig. 13, which go along the depositional history. Two stratigraphic columns (location shown in Fig. 12a) each representing a nappe of the Northern Calcareous Alps from the restored cross section (Fig. 12) were modelled in PetroMod®. The input parameters to the PetroMod® model are listed below in Table 2. The thickness for the sediments are not listed in the table since this was varied between the positions.

The thermal alteration of the supra-salt stratigraphy gives direct evidence for changes of the lithospheric thickness. The amount and rate of thinning of crust and the lithospheric mantle was iteratively modified until: 1) the maximum temperature observed in the stratigraphic column at a given position of interest was reached, and 2) the onset of thermal subsidence resulting from the thermal model matched the observations from the eastern Northern Calcareous Alps stratigraphic record, where the thermal subsidence begins with the margin-wide transgression. The duration for the mantle exhumation process was found to be around 10 Ma., with a thermal maximum around 234 Ma. Mantle exhumation lasted enough for the Anisian carbonates in the Schneeberg nappe to be transformed to marbles. The results of his thermal modelling provide additional input to the reconstructed history for the rifted margin based on regional evidence and our sequential restorations.

5. Discussion

In our work, we have aimed at deciphering the formation and deformation of the Northern Calcareous Alps sector of the western Neo-Tethys margin. We have produced two regional balanced cross-sections in the eastern Northern Calcareous Alps (Fig. 4a, c). First, we have restored the shortening associated to the Alpine convergence (Figs. 4-8). We have investigated the petrology of mantle rocks and marble in an evaporitic mélange (i.e., the Geyerstein mélange) located in the internal thrust stack (Figs. 5-8), and sequentially restored the rifted margin (Figs. 10-12). With such procedure we have been able to provide a geologically coherent reconstruction for the rift to rifted margin transition of the eastern Northern Calcareous Alps sector of the Neo-Tethys. Then, we have carried out 1D thermal models for the proximal and necking domains of the reconstructed rifted margin (Figs. 13 and 14) to validate our reconstruction with the most likely lithospheric thickness found in the models and obtain timing constraints coherent with the available thermal records. In the following, all these data are integrated to discuss and propose an evolutionary model for the formation of the Northern Calcareous Alps since the onset of rifting in Permian times and the formation of the Neo-Tethys rifted margin in the Triassic (Fig. 15).

5.1. Thermal modelling, mantle petrology and timing of mantle exhumation

Thermal modelling of the Neo-Tethys rifted margin based on the sequential restoration and thermal constraints have allowed obtaining the time-integrated evolution of key physical parameters across the modelled rifted margin, including heat flow, temperature, depth to the lithosphere-asthenosphere boundary, and depth to the Moho (Fig. 14). The peak temperature to which the overlaying stratigraphy is exposed to when the mantle is fully exhumed is defined by the duration of mantle exhumation process and the pre-rift crustal thickness. The modelling has been carried out across different rift domains for the Bajuvaric, the Tirolic and the north and south Juvavic positions of the reconstructed rifted margin, allowing to define and describe the different rifting phases accordingly.

In the Bajuvaric and Tirolic nappes the observed thermal markers (section 3.3.3) are best achieved with an initial crustal thickness of ca. 35 km. This is also in agreement with the European Moho depth of Grad et al. (2009). A post-stretching crustal thickness of some 30 km for the Bajuvaric and 25 km for the Tirolic nappes (Fig. 14d) fits best to the used thermal markers. In the distal Juvavic nappes, which would represent the necking to hyperextended domain, the best match to the thermal markers was achieved with a post-thinning crustal thickness of only 1,5 km (almost fully necked crust). This extreme thinning and associated

Table 2
Input values for thermal modelling in PetroMod®. In general, the parameters suggested in PetroMod® were chosen (see Kukla et al., 2018 and Sekiguchi (1984).

Themal Cond Multi-Point Model & Lithology	Pre-Rift thickness in the model	Therm Cond at 20 °C	Therm Cond at 100 °C	Therm Cond at max. Temp.	Anisotropy Factor Thermal Cond	Thermal Expansion Coeff [1e-6/K]
	[m]	[W/m/K]	[W/m/K]	°C		
Upper crust (continental, granite)						
Granite (150 Ma old)	30,000	2.6	2.4	320	1.15	33
Lower crust (continental, diorite)						
Diorite	5000	2.7	2.47	320	1	33
Upper mantle (lithosphere)						
Peridotite (typical)	85,000	4	3.42	320	1	33
Sediments						
Limestone (ooid grainstone)		3	2.69	320	1.19	33
Limestone (micrite)		3	2.69	320	1.19	33
Limestone (shaly)		2.3	2.18	320	1.7	33
Dolomite (typical)		4.2	3.57	320	1.06	33
Sandstone (typical)		3.95	3.38	320	1.15	33
Sandstone (clay rich)		3.35	2.95	320	1.2	33
Shale (organic lean, silty)		1.77	1.79	320	1.8	33
Anhydrite		6.3	5.11	320	1.05	33
Gypsum		1.5	1.59	320	1.15	33
Halite		6.5	5.25	320	1.01	33
Polyhalite		1	1.22	320	1	33
Salt		6.5	5.25	320	1.01	33
Halite		6.5	5.25	320	1.01	33
Sylvinite		1	1.22	320	1.02	33

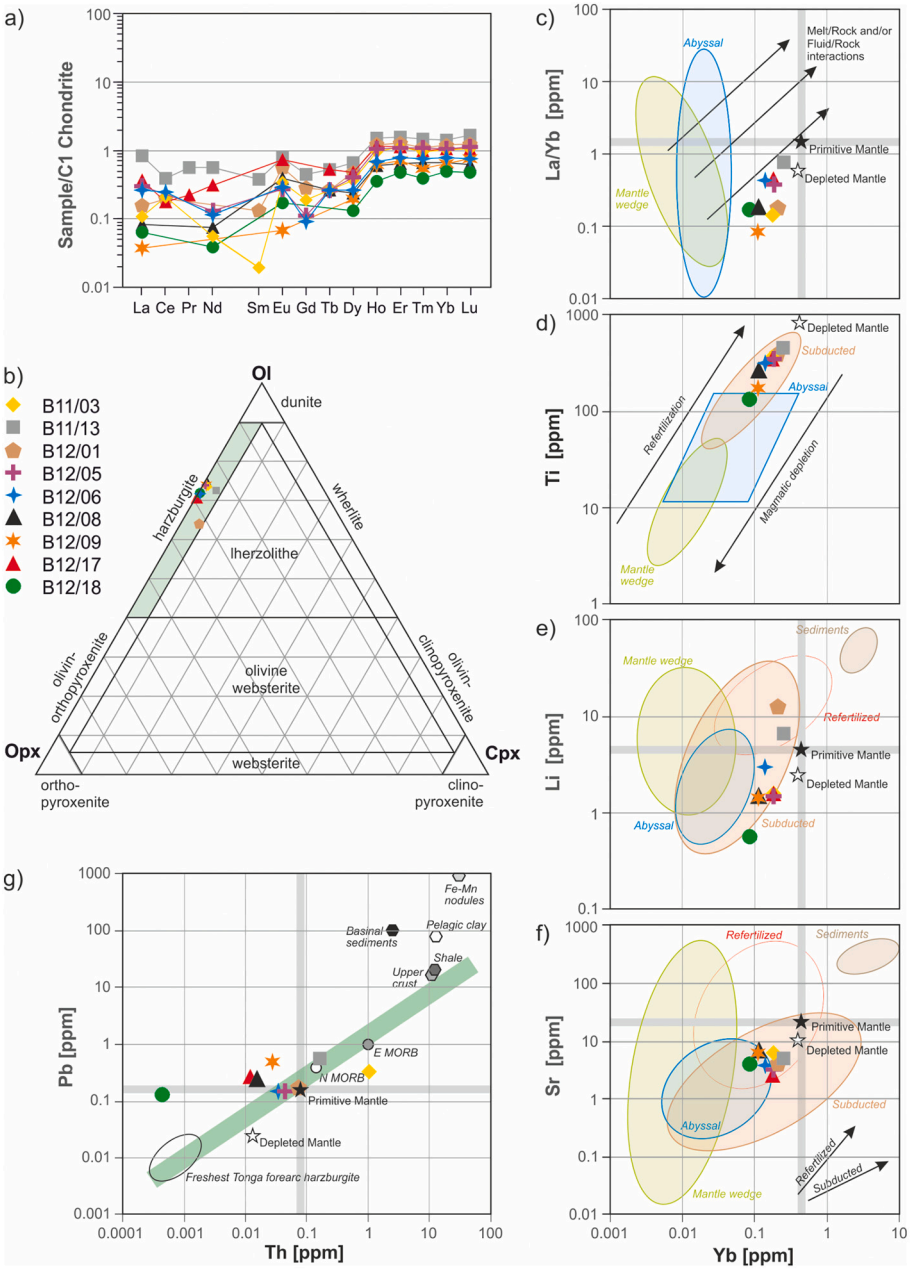

Fig. 10. a) C1 Chondrite-normalized diagrams for rare earth elements (REE). b) b) Ternary diagram for ultramafic rocks, showing that all studied samples fall within the harzburgite compositional field. c), d), e), f) Classification diagrams after Deschamps et al. (2013) indicating a subducted serpentinite signature and characteristics close to depleted mantle. g) Classification diagram after Deschamps et al. (2013) showing a slight enrichment in Pb with respect to depleted mantle.

temperatures would allow for the formation of polyhalite (~200 °C at 235 Ma) as reported in Leitner et al. (2017) for this sector of the margin (in a more westerly position, though). The most southern preserved supra-salt stratigraphy received enough heat (>300 °C) during the process of mantle exhumation so that carbonates at the base of the Triassic succession were transformed to marble (i.e., the Schneeberg nappe and carbonate of the distal Hallstatt facies of Juvavic nappes; Fig. 14b). In that position, the crust must have completely thinned out for the Moho itself to become the interface with the supra-salt stratigraphy (Fig. 15d). The exhumation of the mantle is documented in the thermal model by the heat flow increase due to the rise of the lithosphere-asthenosphere-boundary (Fig. 14a). Modelling suggests a period not much longer than 10 Ma from full stretching to full exhumation (Fig. 14b), or the cooling would have progressed too much that no marbles would have formed at all. Such fast cooling rates agree with results from present day margins in magma-poor rifted margins (e.g., Theunissen and Huismans, 2022).

Initial stretching of the continental lithosphere matches the time frame associated with the deposition of the Alpine Verrucano and Präbichl and Laas Fms, followed by the deposition of the Haselgebirge, Werfen and Reichenhall layered evaporites (~265–247 Ma). Lithospheric stretching is reflected on the elevation of the lithosphere-asthenosphere-boundary and the Moho across the Bajuvaric, Tirolic and Juvavic realms, with slight elevation of the heat flow and temperatures. With the onset of the Anisian (~247–242 Ma) a regional carbonate layer was deposited (i.e., the pre-kinematic Gutenstein Fm), marking the start of a quiescent stage in the proximal domain of the margin, but with fast increasing heat flow and rising temperatures related to crustal thinning outboard on the Juvavic. Upon Ladinian times (~242 Ma), thinning of the crust was focused on the Juvavic reaching

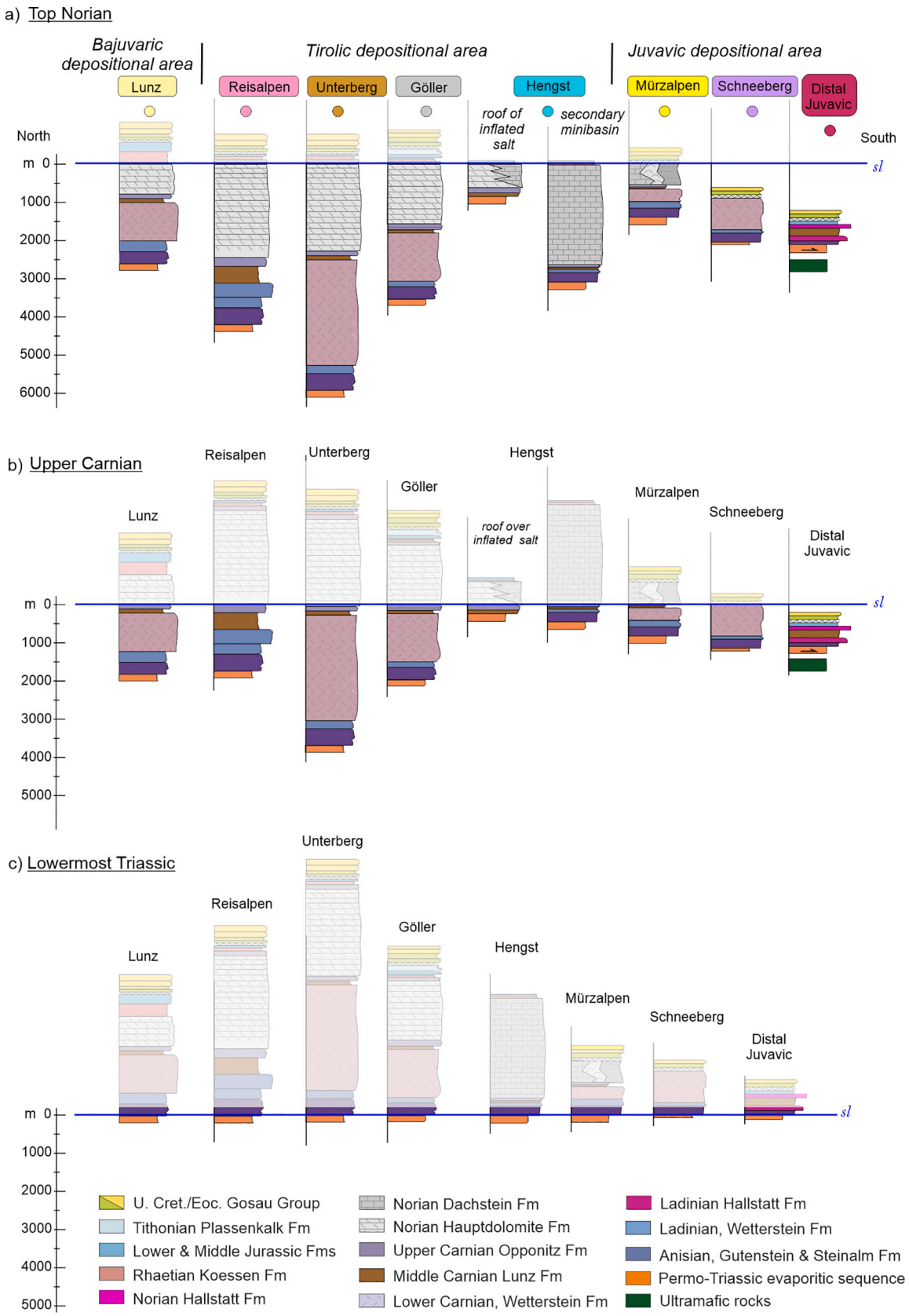

Fig. 11. Depocenters of each minibasin along the geological cross section are summarized in a stratigraphic column. To display the stratigraphic distribution and correlation across the basin, three regional datum levels have been used: a) Top Norian (Hauptdolomit Fm); b) Top upper Carnian (Opponitz Fm); c) Top of the Permian-Triassic salt. See further explanations on the text. The labels on the top (eg Lunz) refers to the nappes of the Northern Calcareous Alps, the colour reflects the colour of the nappes in Fig. 2b. sl stands for sea level.

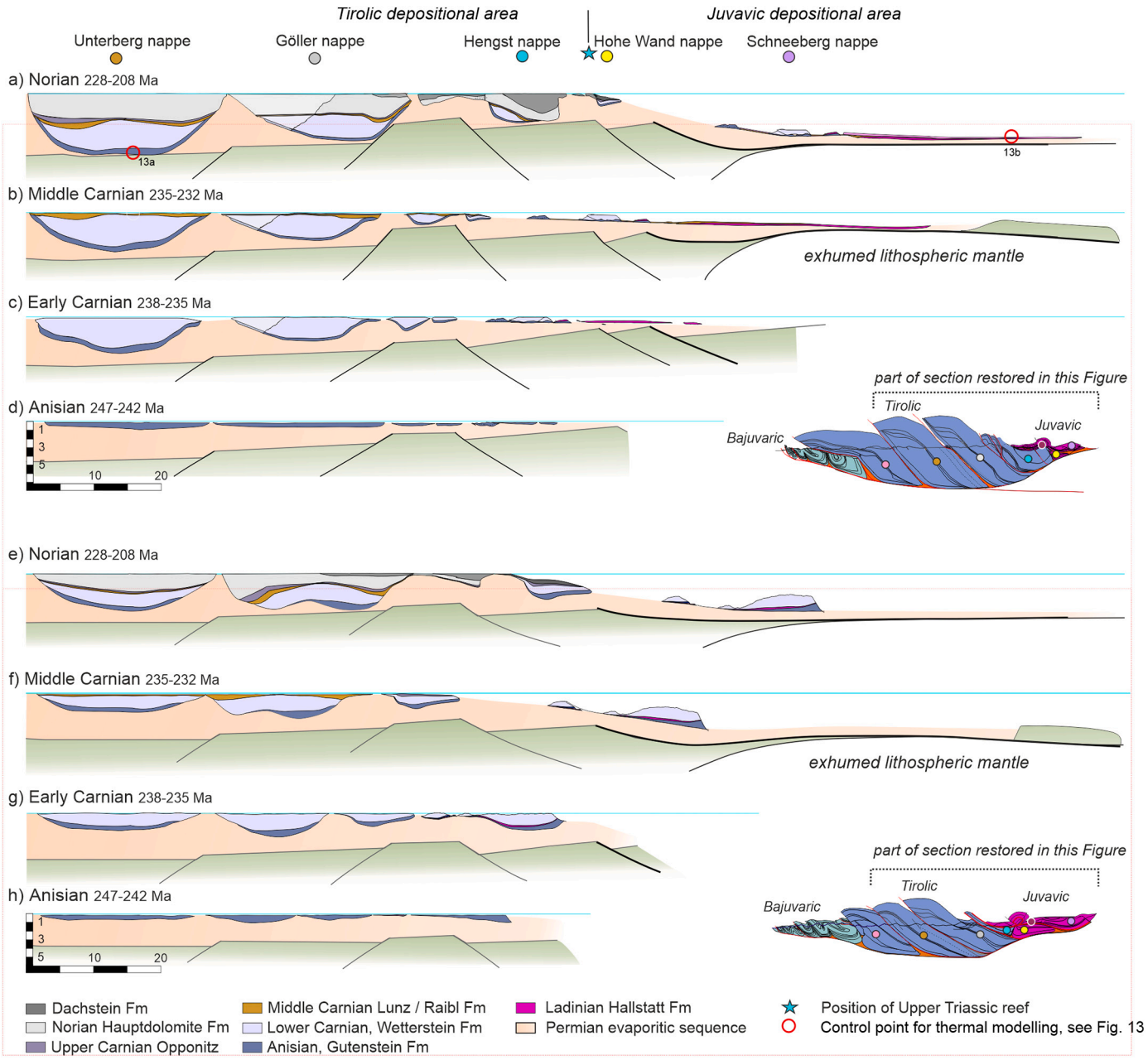

Fig. 12. Restoration of regional cross sections A and B in Fig. 4 to the four major evolutionary stages of the carbonate platforms of the Neo-Tethys margin. Coloured dots refer to minibasins using the same colour as in map in Fig. 2b. Numbers on section a), i.e., 11a indicate sample positions for geothermal modelling in Section 4.3. of this study. Note the oceanward gliding of the Mürzalpen and Schneeberg minibasins, leading to the general widening of minibasins trough time, and to the individualization of future nappes.

hyperextension, and eventually leading to the exhumation of the sub-continental lithospheric mantle at about middle Carnian (~235 Ma) time. This can be observed in the elevation of the lithosphere-asthenosphere-boundary and the Moho for the Juvavic realm, followed by the rising of the heat flow and as slight time-delay on the sudden rise of temperatures (Fig. 14c, d). Such exhumation rate is in line with values reported for the Pyrenean rifted margin evolution in a study by Lescoutre et al. (2019) and by studies on the Atlantic rifted margins by Huismans and Beaumont (2011) where mantle exhumation happens in some 12 Ma. Based on the thermal modelling carried out full crustal break-up and mantle exhumation cannot have taken place during the Permian, but later. Such fast exhumation rate is also supported by the sensitivity analysis carried out regarding the influence of initial lithospheric thickness and different exhumation rates. The initial lithospheric thickness has little relevance on the resulting temperatures of post-salt stratigraphy compared to the timing of the exhumation (see supplementary materials), hence 1D models are sufficient to do a first-order approximation of lithospheric thickness and the timing of mantle exhumation.

The Neo-Tethyan oceanic basin thus must have formed southwards of the original Permian and Triassic depocenter, since the restored units with the largest thrust-related transport (i.e., Geyerstein mélange, the pelagic Hallstatt facies, the Florianikogel radiolarites) where deposited outboard of the restored position of the Juvavic nappes. The thermal overprint recorded by the Anisian marble and the thermal modelling argues for fast hypertension of the continental crust, and its association with salt, for its rafting down the necking and hyperextended domains towards the mantle exhumation area. The Juvavic Schneeberg nappe,

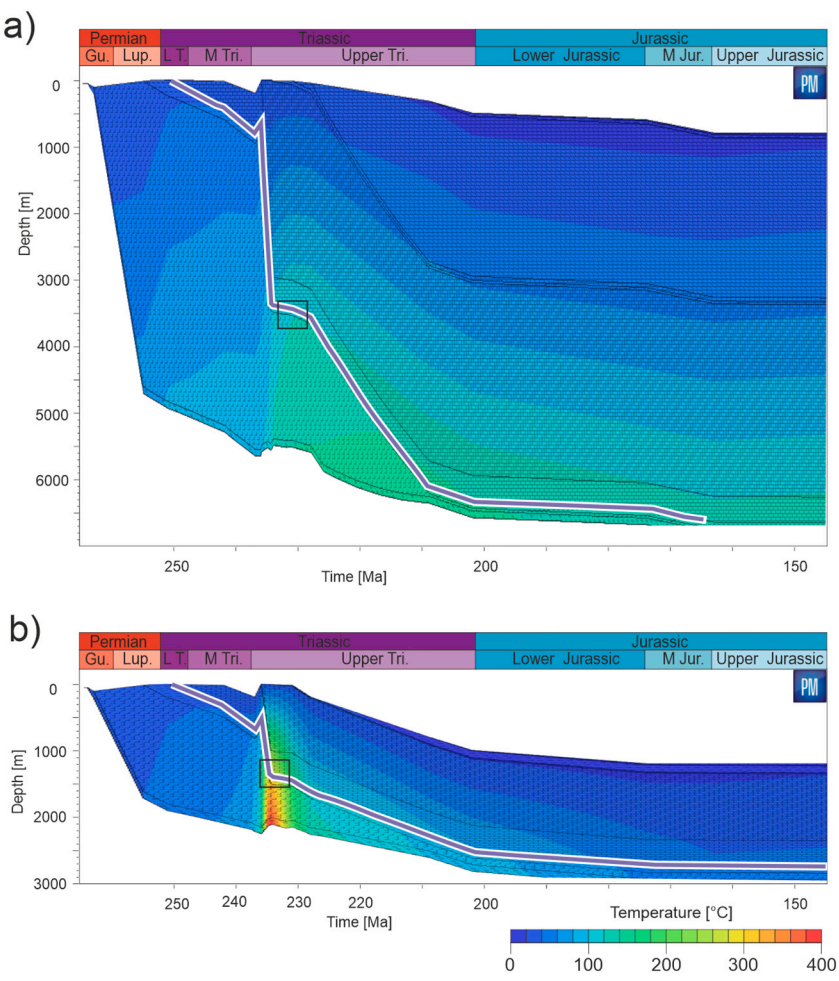

Fig. 13. 1D thermal models of two minibasins representing the major structural domains of the Northern Calcareous Alps. All the sections have a distinct common thermal peak at 234 Ma. The purple line marks the base of the Gutenstein Fm a) Base of the Anisian Gutenstein Fm exposed to some 140 °C in Tirolic units b) Base of the Anisian Gutenstein was exposed to ~340 °C, reaching conditions suitable for marble formation in distal Juvavic units. The locations of thermal profiles a) and b) are indicated on Fig. 12a. (For interpretation of the references to colour in this figure legend, the reader is referred to the web version of this article.)

therefore formed upon the incorporation of the salt-detached shallow water carbonate rafts in such large transport thrust (i.e. Figs. 4, 5, 8, 12), as reported on many other orogenic systems (Tavani et al., 2021).

The petrological analysis of the serpentinite presented in here identified a harzburgitic protolith (Figs. 7, 9, and 10). According to the trace element signatures, the rocks may have experienced a complex evolution including depletion and subduction. The almost complete serpentinization of the ultramafic protolith argues for a water rich environment whereas the dominance of chrysotile and lizardite indicate relatively low temperatures during serpentinization, since at higher temperatures (>300 °C) chrysotile and talc would be replaced by antigorite (Lafay et al., 2013). Thus, prior to their exhumation the studied mantle rocks may have been part of the subcontinental mantle of Adria and characterised by an inherited signature. This corresponds to a Type 1 mantle according to Picazo et al. (2016). According to studies on mantle rocks from Western and Central Europe the inherited signature may be due to the Variscan collisional event (Puziewicz et al., 2020) and/or the Permian extensional event (Manatschal et al., 2023, and references therein). The determined mineralogical composition suggests serpentinization during the exhumation of the sub-lithospheric mantle as the most likely scenario.

Other exotic basic rocks like basaltic metavolcanics (diabase), gabbros and diorites were described from the Grünbach area (Plöchinger, 1961) at the eastern margin of the Northern Calcareous Alps, via the southern side of Mt. Veitsch, the Johnsbach area further west of the studied section (Tollmann, 1976b; Kreuss, 2014; Mandl, 2016), as well as at Salzkammergut (Schorn et al., 2013) within the Permian-Triassic evaporitic sequence. To the east of the Northern Calcareous Alps, equivalents of the Meliata zone (Kozur, 1991; Channel and Kozur, 1997) and the Geyerstein mélange occur in the Western Carpathians. In the Aggtelek-Rudabánya Mountains the equivalents of the latter include serpentinized ultrabasic and basic rocks. They appear in the same tectonic position below the Aggtelek nappe of the Siliza unit (Less et al., 2004; Fodor et al., 2023), which is an equivalent to the Juvavic nappe system. Such widespread occurrence of mafic and ultramafic rocks argues in favour of a regional scale process of mantle exhumation and formation of oceanic crust.

5.2. *From rift to rifted margin: Polyphase or multirift?*

Polyphase rifts develop as a strain localisation process organized in several phases, each of which leads to different domains across rifted margins (i.e., proximal, necking, hyperextended, exhumation and oceanic) domains. Polyphase models dictate that these phases develop in sequence during a unique rift event, under the same plate kinematic framework, leading to the migration of extension towards the locus of future breakup (i.e., Lavier and Manatschal, 2006; Reston and Pérez-Gussinyé, 2007; Péron-Pinvidic and Manatschal, 2009; Ranero and Perez-Gussinye, 2010; Pérez-Gussinyé et al., 2023). Conversely, during multirift rifting, several successive extensional events take place under various plate kinematic directions, while the different extensional phases may or may not overlap in space (i.e., vertically stacked vs. laterally-shifted crustal thinning and related basin depocentres). Since each rift domain is characterised by its own stratigraphic and thermal records, we discuss in the following whether the studied area developed as a result of a multirift process (i.e., Permian breakup of Pangea, and Triassic rifting) or polyphase rifting (i.e., a continuum from Pangea breakup into a Triassic rifted margin).

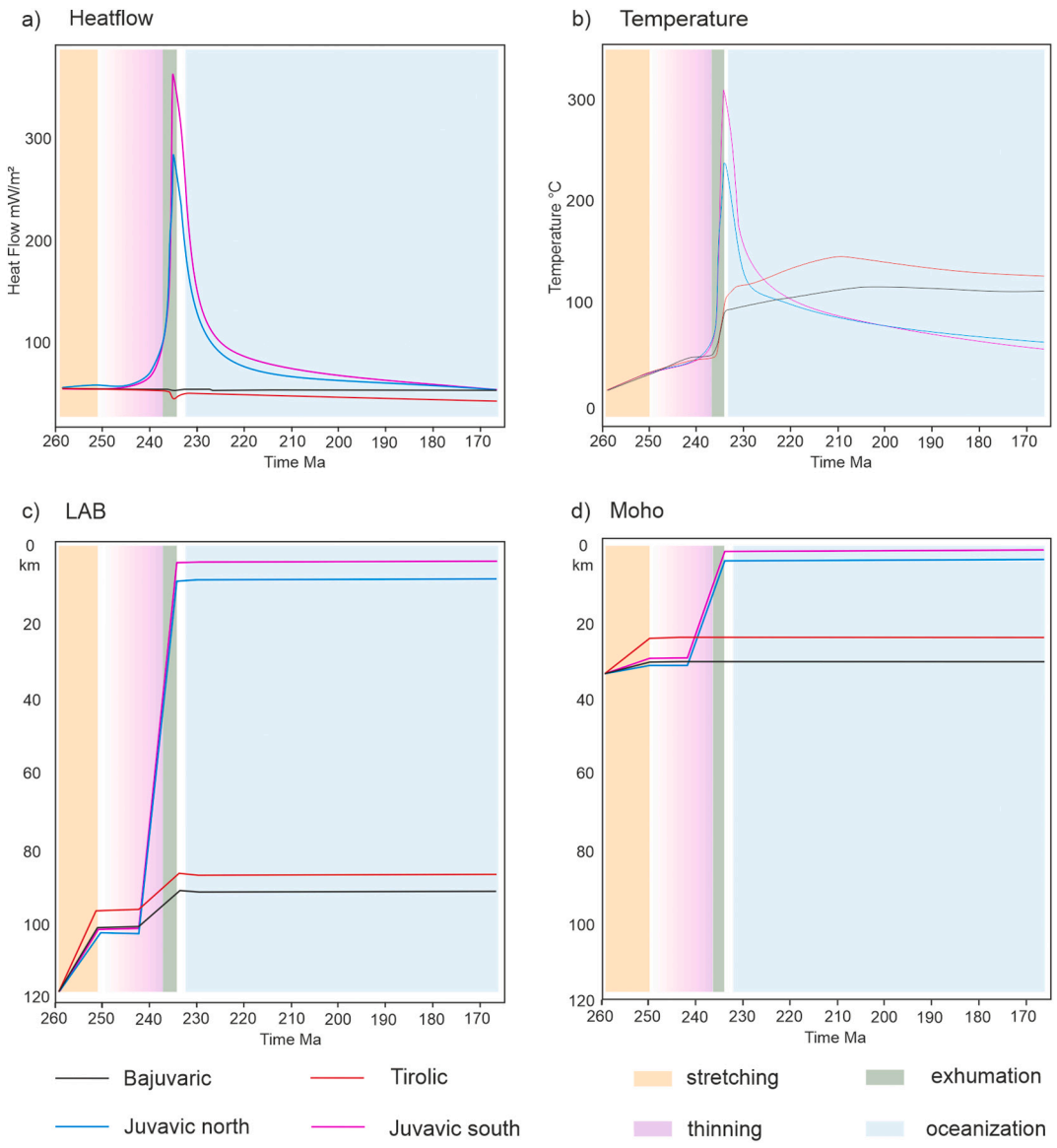

Fig. 14. Thermal evolution of the supra-salt stratigraphy of four minibasins and the derived lithospheric thicknesses along the Neo-Tethys margin. The plots show the thermal evolution for four selected minibasins, representing each of the main realms of the Northern Calcareous Alps. Figure a and b showing heat flow and temperature for the base of the supra-salt stratigraphy. c and d show the depth of LAB and depth of Moho for the minibasins to provide the heat necessary for the observed thermal imprints.

Different rifting phases have been described in the Tethyan domain after the orogenic collapse of the Variscan orogen since Permian times (i.e., Kozur, 1991; Haas et al., 1995; Channel and Kozur, 1997; Schmid et al., 2020; Van Hinsbergen et al., 2020). These rift phases shaped the southern European margins and their African/Adriatic conjugated margins since late Permian-Triassic to Early Cretaceous times. These rifting events progressed westward from the Neo-Tethys Meliata-Vardar-Pindos oceanic domains to the Bay of Biscay (i.e., Stampfli et al., 1998; Stampfli and Borel, 2002), thus connecting the Tethys and Atlantic realms (see discussion by Tavani et al., 2018). In the Central and Western Alps of Europe, the Alpine Tethys magma-poor rifted margin has been recently reconstructed and interpreted as a result of a polyphase rifting event during Early and Middle Jurassic (Chenin et al., 2022; Manatschal et al., 2022, 2023, and references therein).

In the Northern Calcareous Alps, the Alpine Tethys multirift seems to have been somewhat superimposed to a previous rifting event, late Permian to Triassic in age, that shaped the Neo-Tethys margin (Channell et al., 1992; Channel and Kozur, 1997; Granado et al., 2019). The late Permian to Triassic rifting event has been partly documented and dated by the recognition of HT regional metamorphism (Habler and Thöni, 2001; Schuster et al., 2001; Schuster and Stüwe, 2008), and widespread magmatism (Neubauer et al., 2000; Roda et al., 2018; Putiš et al., 2019b; Villaseñor et al., 2021), and deposition of fault-bound siliciclastic depocenters of the Alpine Verrucano, Präbichl, Laas Fm Fms (i.e., Leitner et al., 2017, and references therein). In the inner Western Carpathians of Slovakia (i.e., east of the Austrian Northern Calcareous Alps) the presence of Ladinian to Norian pillow lavas and their deep-water radiolarite sedimentary cover argue in favour of a well-established oceanic basin by -at least- Middle Triassic times already (Kozur, 1991; Haas et al., 1995; Channel and Kozur, 1997; Gawlick and Missoni, 2015; Putiš et al., 2019a). The geochemistry of these basalts, and other intrusive bodies, provide equivocal affinities however, compatible with N-MORB, but also with a back-arc spreading setting (i.e., Stampfli et al., 1998; Mock et al., 1998; Stampfli and Borel, 2002; Faryad et al., 2005; Froitzheim et al., 2008; Putiš et al., 2019b; Huang et al., 2022). Probably, due to a westward narrowing of the Neo-Tethys Ocean and its

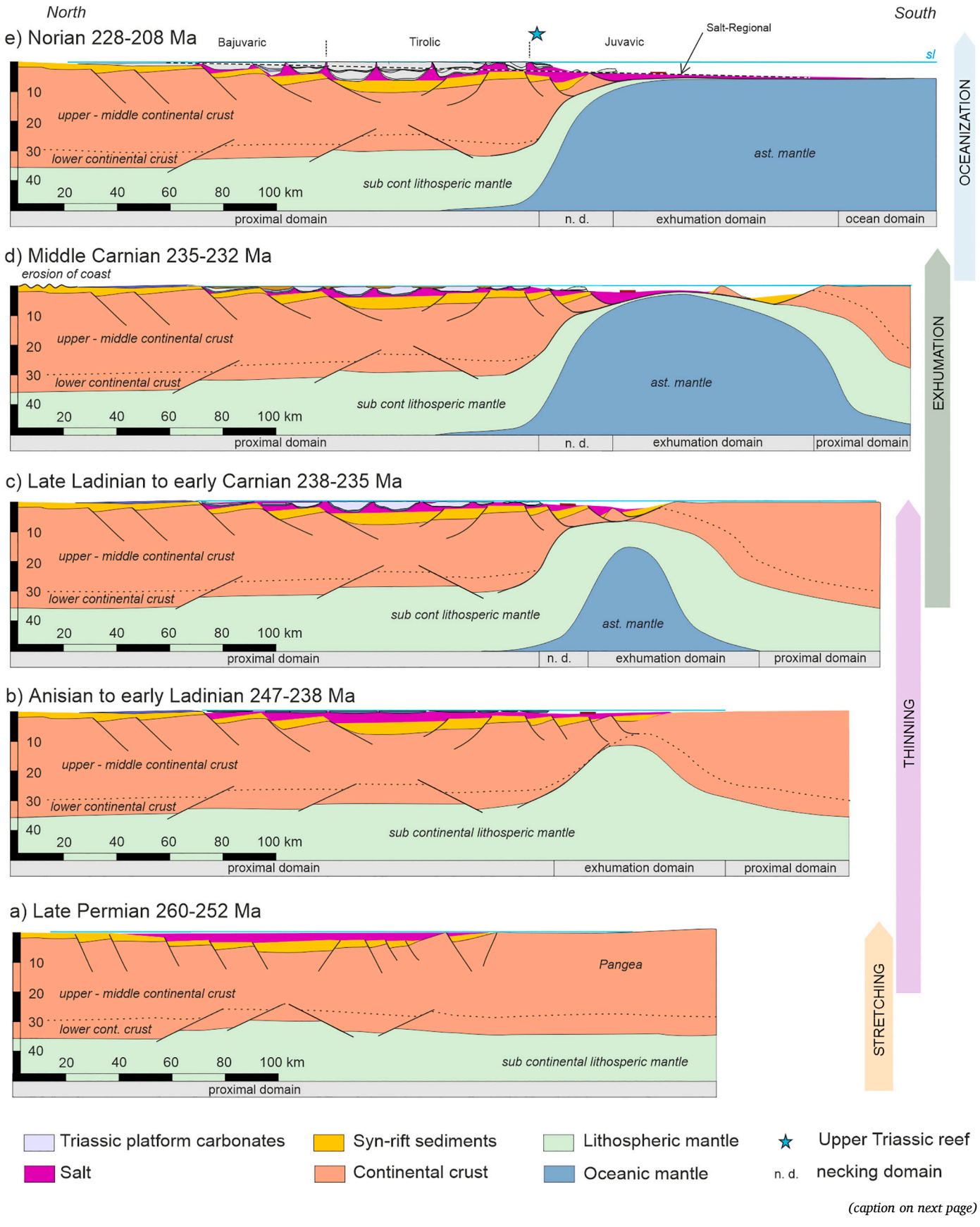

(caption on next page)

Fig. 15. Evolution of the Neo-Tethys margin in the easternmost Alps. a) Upper Permian, diffuse stretching of the crust, and deposition of *syn*-rift sediments. b) Uppermost Permian to Anisian, deposition of the layered evaporitic sequence and the pre-kinematic Gutenstein Fm across the Permian rift. Beginning of ductile crustal thinning and increase of bathymetry in the southern sector of the Northern Calcareous Alps margin. c) Lower Carnian, growth of major carbonate minibasins on top of the Permian salt depocenter downbuilding, minor salt-detached extension favoured by localization of outboard hyperextension and formation of a slope; increased heat flow leads to formation of polyhalite. d) Middle Carnian mantle exhumation, portions of the stratigraphy of the Northern Calcareous Alps base are transformed to marble. Deposition of Lunz Fm presumably due to a slight lithospheric uplift and related hinterland erosion. Removal of continental crust triggers salt-detached extension dominating over downbuilding, with minibasin rafting into deeper waters. e) Thermal subsidence of the margin and gliding of the supra-salt stratigraphy. Deposition of the vast Hauptdolomit and Dachstein Fms limited to the south by a reef marking the boundary between the proximal and necking domains of the margin.

associated rifted margin facies belts, and because of stronger compression and erosion in the Eastern Alps compared with the Inner Western Carpathians, fewer remnants of this deep-water and oceanic paleogeographic domains have been preserved in the Eastern Alps (Kozur, 1991; Channell et al., 1992; Channel and Kozur, 1997).

In our view, the formation of the Neo-Tethys Ocean started with the Permian breakup of Pangea and the formation of large rift basins formed by crustal stretching by basement-involved extensional faults (Fig. 15a). Permian fault-bound basins were first infilled by siliciclastic and volcaniclastic sediments (i.e., Alpine Verrucano, Präbichl, Laas Fm Fms), and then were covered by a layered evaporitic sequence with minor volcanic additions. Leitner and Spötl (2017) classified this uppermost Permian to lowermost Triassic layered evaporitic sequence as late *syn*-rift to early post-rift following the nomenclature proposed by Rowan (2014). In fact, since polyphase rifting models propose a diachroneity on the rifting processes across developing margins the evaporites can be considered as post-tectonic in the proximal domain of the margin, but syn-tectonic on its distal sectors, deposited upon active stretching and/or thinning of the continental lithosphere (Fig. 15a, b). This proposal allows to coherently explain the distribution of the stratigraphic facies, as well as the deformation reported in this work across the margin. The evaporites completely overfilled the Permian fault-bound, syn-tectonic basins in the Tirolic realm, levelling the rifted basement topography under continental to shallow water marine conditions. The distribution of the evaporites was uneven, and thus controlled by the inherited topography of the rifted basement.

Our restoration for the Middle-Upper Triassic carbonate stratigraphy at key chronostratigraphic levels (Figs. 11 and 12) shows an irregular, rifted-basement topography. Such architecture largely pre-defined the accommodation space for the isolated carbonate minibasins forming the Northern Calcareous Alps, their thickness and distribution, assisted by salt evacuation and minor salt-detached extension (Granado et al., 2019). In more detail, in the eastern portion of the Northern Calcareous Alps, the restored northernmost Bajuvaric and the Juvavic nappes to the south are characterised by significantly thinner carbonate platforms, while the thickest (i.e., up to 5 km thick) carbonate depocenters were located in the restored Tirolic realm, in the central sector of the restored Triassic shelf (i.e., compare Fig. 4 to restored sections in Fig. 13). Such stratigraphic architecture argues in favour of the Permian to Early Triassic rifted basement with a central depocenter, bound to the north and south by thicker crustal blocks. The Wetterstein isolated carbonate platforms acquired large thickness (i.e., in excess of 2.5 km in the Tirolic nappes, about 1.5 km in the southern Bajuvaric nappes) in very little time (i.e., ~1.4 Ma, according to Strauss et al. (2021a), and the established chrono- and lithostratigraphy of the Northern Calcareous Alps (i.e., Tollmann, 1976a; Mandl, 2000; Piller et al., 2004; Wessely, 2006). Such short time span is inconsistent with the timeframes needed for lithospheric stretching and thinning, which generally take at least an order of magnitude longer (i.e., tens of Ma.; Ziegler and Cloetingh, 2004). When the throw of pre-salt thick-skinned faults is less than the salt thickness, faulting is not the dominant factor in localizing salt movement, and most of the salt features have no real connection (i.e., coupling) to underlying faults (i.e., Erratt, 1993; Koyi et al., 1993; Stewart, 2007; Karlo et al., 2014). One may thus argue that waning extensional faulting could have been synchronous to the formation of the Wetterstein platforms. However, recent numerical modelling of thick-skinned extension involving salt layers and coeval salt evacuation by downbuilding driven by sediment loading have shown that the resulting geometries of carbonate minibasins are largely dependent on the rate of thick-skinned extensional faulting, besides salt rheology (i.e., Granado et al., 2021). The slower the fault kinematics the larger the salt evacuation related to downbuilding, leading to more symmetrical syncline minibasins. Conversely, on fast extending thick-skinned fault systems, the less influence of salt evacuation is reflected on the minibasin geometries, forming asymmetric sediment wedges thickening into the active fault planes. The fast rates of carbonate aggradation (~1.5 km thickness in <1.4 Ma) in the rather symmetrical Wetterstein carbonate platforms are at odds with those geometries developed by fast fault kinematics according to above mentioned numerical models results. To summarise, the formation of the upper Ladinian to lower Carnian isolated carbonate platforms seems not to be linked to active thick-skinned basement-involved faults (i.e., syn-rift, or syn-tectonic basement faults), as recently proposed by Fernández et al. (2021), or at least sub-salt thick-skinned extension was not the main driver. The isolated carbonate platforms of the Wetterstein Fm developed on the proximal domain must be largely post-tectonic, but were deposited synchronous to outboard hyperextension in the distal domain (Fig. 15c), preceding immediate mantle exhumation in middle Carnian times (Fig. 15d). As stated on previous sections one key supporting observation for the proposed model lies on the sedimentary record of radiolarites and siliceous shales deposited since upper Anisian-Ladinian times (Kozur, 1991; Mandl and Ondrejičková, 1991; Mandl and Ondrejicková, 1993; Channel and Kozur, 1997; Gawlick and Missoni, 2015, 2019) south of the position of the isolated carbonate platforms. This again argues in favour a domain of severely thinned lithosphere outboard of the formerly stretched proximal domain where the Wetterstein platforms deposition was largely assisted by salt evacuation.

In other words, the model presented implies the presence of a necking domain and an associated regional slope (i.e., Sutra et al., 2013) where such kind of deep-water sediments can accumulate (Chenin et al., 2022), south of the restored position of the Juvavic nappes, and slightly before the development of the Wetterstein platforms (upper Ladinian to lower Carnian). This leaves a short time span (i.e., ~5 Ma) from the sedimentation of the deep-water facies over and beyond the margin necking zone, and the formation of the shallow water Wetterstein platforms. For that same matter, these isolated platforms would have formed inboard of that necking zone, over the inherited upper Permian to Lower Triassic depocenter, on the proximal domain of the Triassic margin. Such thinned lithosphere allowed for a continental slope over the lithospheric necking area (i.e., Sutra et al., 2013; Chenin et al., 2022) over which salt-detached extension of the Triassic carbonate succession took place (Fig. 15d, e).

For us, the very short time span of events is a major evidence for a continuous polyphase rift assisted by salt tectonics, where extension was focused since Middle Triassic times (~Anisian-Ladinian) to the south of the Juvavic nappes, shifted from the original Permian to lowermost Triassic depocenter. Such rifting was a continuous polyphasic event of lithospheric extension, under the same plate kinematic setting. We have not found any regional or local geological evidence, or infer it from the thermal (this study), subsidence (Strauss et al., 2021a, 2021b) or numerical (Granado et al., 2021) or analogue modelling (Santolaria et al., 2022; Granado et al., 2023 for invoking two different rifting events

related to differing plate kinematic scenarios. We thus favour a polyphase rift rather than a multirift setting for the Northern Calcareous Alps sector of the Neo-Tethys rifted margin.

5.3. The stratigraphic record of polyphase rifting in the presence of thick salt

Salt deposition in latest Permian to earliest Triassic times could have been controlled by waning of lithosphere stretching and thinning underneath the Permian siliciclastic depocenters, while strain localization shifted outboard of the Juvavic, where necking of the crust made possible the sedimentation of deep-water sediments since late Anisian times, preceding mantle exhumation by about middle Carnian times. The presence of such a regional slope associated to crustal necking (Sutra et al., 2013) presents a fundamental argument for understanding the onset of salt tectonics in the Triassic rifted margin. The initiation of the thick isolated Wetterstein platforms must therefore have been coeval to the outboard thinning of the lithosphere in a necking zone south of the Juvavic realm, hence laterally shifted from the Tirolic carbonate depocenters. The slope associated with such crustal thinning controlled the onset of salt evacuation, triggered by a combination of differential sedimentary loading by carbonate aggradation, and salt-detached extension. As the slope increase, aided by thermal subsidence, salt-detached extension gained further importance to downbuilding (Granado et al., 2023).

Upon lithospheric thinning and mantle exhumation, the additional heat input results in transient isostatic uplift of the margin. Such uplift is described to be rather small as it is usually outrun by ongoing thinning of the crust (Quirk et al., 2013). The resulting net-subsidence of the margin would hence be stagnating, eventually a minor uplift in the range of tens of metres would be observable. The tectonic subsidence analysis and the distribution of the Lunz Fm in the Northern Calcareous Alps shows similarities to those studied by Cannat et al. (2009) and Jeanniot et al. (2016) in the Iberian-Newfoundland magma-poor rifted margins. The observed reduced tectonic subsidence, or actually a minor uplift of the Triassic margin in middle Carnian times has been already reported previously (i.e., Schlager and Schöllnberger, 1974; Bechstädt and Dohler-Hirner, 1983; Mutti and Weissert, 1995; Moser and Tanzberger, 2015; Strauss et al., 2021a), and its timing is coincident with that of the mantle exhumation proposed in this study. The direct consequence of such an uplift would be erosion of the coastal depositional environments (Fig. 15d) of the Lower to Middle Triassic European shoreline (see Aigner and Bachmann, 1992) and the fluvial deposits in the Central Europe hinterland, in fact matching the source areas proposed for the Lunz Fm (i.e., Behrens, 1972; Aubrecht et al., 2017; Kohút et al., 2017). Such relationships were already discussed as well by Hornung and Brandner (2005). The consequence of such uplift and erosion would have been the redistribution of clastic sediments from the shoreface to the carbonate platforms and the inter-platform basins. We therefore propose a direct link between thermal uplift of the ancestral European lithosphere induced by lithospheric break-up, erosion of the hinterland and subsequent mantle exhumation, leading to the clastic input of the middle Carnian Lunz Fm. Similar siliciclastic formations deposited on carbonate-dominated rifted margins have been linked to the exhumation and uplift of basement during crustal/lithospheric necking, such as the late Early Jurassic Grès Singuliers in the French Alps (i.e., Ribes et al., 2020), or the late Albian to middle Cenomanian Utrillas sandstones at the time of mantle exhumation, such as in the Basque-Cantabrian basin (i.e., Jammes et al., 2009; DeFelipe et al., 2017; Roca et al., 2021). The Lunz Fm marks in our view the time of mantle exhumation (Fig. 15d).

The transgressive upper Carnian Opponitz Fm re-establish the carbonate factory over the Lunz Fm signalling the transition from exhumation to the onset of thermal cooling in the distal domains. Above, a margin-wide dolomitic lagoon was formed (Fig. 15e), whose thickness and subsidence history falls on an exponentially decaying curve, typical of thermal subsidence (Strauss et al., 2021a), and thus coeval with oceanization. The large quantities of accessible Mg^{2+} to establish the vast Norian Hauptdolomit lagoon also argue in favour for an active spreading ridge at that time, and the serpentinization of the mantle peridotites (Quesnel et al., 2019).

6. Conclusions

This study documents the formation of a magma poor hyperextended segment on the Northern Calcareous Alps sector of the western Neo-Tethys margin. Our study reveals mantle exhumation as a result of polyphase rifting following the orogenic collapse of the Variscan orogen, and the westward propagation of the Neo-Tethys towards the Alpine and Atlantic realms. Restoration of the supra-salt Middle to Late Triassic carbonate stratigraphy and the occurrence of serpentinized harzburgites embedded in a strongly tectonized evaporitic mélange reveal the architectural evolution of the rifted margin involved in the European Alpine orogenic system.

Sequential restorations and thermal modelling allow to conclude that the uppermost Permian to lowermost Triassic layered evaporitic sequence was deposited during the post-tectonic phase of the proximal domain of the margin, but probably was deposited coeval to active hyperextension in the distal domain. The Middle Triassic isolated carbonate platforms were formed over the evaporite-filled upper Permian to Lower Triassic depocenter, on the proximal domain of the rifted margin, and can thus be considered as post-tectonic, not related to major sub-salt crustal stretching and thinning. Sequential restoration of regional cross sections showed growth of the carbonate platforms largely controlled by accommodation space provided by salt evacuation and minor salt-detached extension. Thickness and sedimentary facies of carbonate platforms and interpreted basement topography implies the existence of an outer basement high, corresponding to the southern limit of the Upper Triassic reef belt and the position of the shelf break at the time. Marbles derived from shallow water carbonate protoliths and serpentinized harzburgites indicate exhumation of an inherited, depleted subcontinental lithospheric mantle during the late stages of the formation of the Neo-Tethys rifted margin around middle Carnian times. Mantle was exhumed distal from of the Upper Triassic shelf break, and subsequently sheared off and incorporated in the thrust system during Late Jurassic to Early Cretaceous Alpine convergence. Lack of massive volcanism, and the occurrence of exhumed mantle associated with extreme crustal thinning indicates that the Northern Calcareous Alps most likely developed on a magma-poor hyperextended rifted margin. Thinning of the lithosphere caused thermal uplift of the margin and its hinterland, triggering the erosion, sourcing and distribution of an ephemeral clastic system in middle Carnian times (i.e., Lunz Fm). This marks a change from dominantly aggrading isolated carbonate platforms downbuilding on salt (i.e., late Ladinian to early Carnian Wetterstein Fm) to laterally expanding salt-detached platforms (i.e., Norian Hauptdolomit Fm). The siliciclastic input can be considered as a timestamp for mantle exhumation, as observed in other rifted margins settings. In salt-bearing rifted margins dominated by carbonate production, the change from vertical aggradation to lateral expansion could as well be taken as a proxy for the timing of mantle exhumation and onset of regional subsidence driven by thermal cooling and subsequent oceanization.

Supplementary data to this article can be found online at https://doi.org/10.1016/j.earscirev.2023.104488.

Declaration of Competing Interest

The authors declare the following financial interests/personal relationships which may be considered as potential competing interests: Pablo Granado reports financial support was provided by Spain Ministry of Science and Innovation.

Data availability

Data will be made available on request.

Acknowledgements

This work is a contribution of the Institut de Recerca Geomodels (Universitat de Barcelona). We acknowledge the financial support of the research project Structure and Deformation of Salt-bearing Rifted Margins (SABREM), PID2020-117598GB-I00, funded by MCIN/ AEI /10.13039/501100011033. We further acknowledge the support of OMV E&P GmbH. Friedrich Koller is thanked for supporting the description of the petrology of the mafic rocks. Michael Wagreich is thanked for discussing stratigraphic details of the Gosau Group, while Klaus Pelz is thanked for numerous discussions on regional tectonics. We acknowledge discussions with Gianreto Manatschal to establishing comparisons with the Alpine Tethys and Atlantic-type margins. Comments by Prof. Neubauer (Univ. Salzburg) and an anonymous reviewer largely contributed to the improvement of this work.

References

Aigner, T., Bachmann, G.H., 1992. Sequence stratigraphic framework of the German Triassic. Sediment. Geol. 80, 115–135.

Allen, P.A., Allen, J.R., 2005. Basin Analysis. Principles and Applications, 2nd ed. Blackwell, Oxford, UK.

Alves, T.M., Moita, C., Cunha, T., Ullnaess, M., Myklebust, R., Monteiro, J.H., Manuppella, G., 2009. Diachronous evolution of Late Jurassic–Cretaceous continental rifting in the northeast Atlantic (west Iberian margin). Tectonics 28. https://doi.org/10.1029/2008TC002337. TC4003.

Aubrecht, R., Sýkora, M., Uher, P., Li, X.-H., Yang, Y.-H., Putiš, M., Plašienka, D., 2017. Provenance of the Lunz Formation (Carnian) in the Western Carpathians, Slovakia: Heavy mineral study and in situ LA–ICP–MS U–Pb detrital zircon dating. Palaeogeogr. Palaeoclimatol. Palaeoecol. 471, 233–253. https://doi.org/10.1016/j.palaeo.2017.02.004.

Bechstädt, T., Dohler-Hirner, B., 1983. Lead-zinc deposits of Bleiberg-Kreuth. In: Scholle, P.A., Bebout, D.G., Moore, C.H. (Eds.), Carbonate Depositional Environments, Amer Assoc Petrol Geol Mem, 33, pp. 55–63.

Behrens, M., 1972. Schwermineralverteilungen und Sedimentstrukturen in den Lunzer Schichten (Kam, Trias, Österreich). Jahrb. Geol. Bundesanst. 116, 51–83.

Böhm, K., 2012. Serpentinite des Meliatikums am Alpenostrand. Bachelor of Science (BSc) thesis. Universität aus Wien, 50 pp.

Bosselini, A., Gianolla, P., Stefani, M., 2003. Geology of the Dolomites. Episodes 26 (3).

Brandner, R., Resch, W., 1981. Reef development in the Middle Triassic (Ladinian and Cordevolian) of the Northern Limestone Alps near Innsbruck, Austria. SEPM Spec. Publ. 30, 203–231, 27 Abb., Tulsa.

Brix, F., Schultz, O., 1993. Erdöl und erdgas in Österreich. Naturhistorisches Musen Wien. 1993.ISBN 3-85028-236-8, 688pp.

Cadenas, P., Manatschal, G., Fernández-Viejo, G., 2020. Unravelling the architecture and evolution of the inverted multi-stage North Iberian-Bay of Biscay rift. Gondwana Res. 88, 67–87. https://doi.org/10.1016/j.gr.2020.06.026.

Cannat, M., Manatschal, G., Sauter, D., Péron-Pinvidic, G., 2009. Assessing the conditions of continental breakup at magma-poor rifted margins: what can we learn from slow spreading mid-ocean ridges? Compt. Rendus Geosci. 341, 406–427. https://doi.org/10.1016/j.crte.2009.01.005.

Cassinis, G., Elter, G., Rau, A., Tongiergi, M., 1979. Verrucano: a tectofacies of the Alpine-Mediterranean Southern Europe. Mem. Soc. Geol. Ital. 20, 135–149.

Channel, J.E.T., Kozur, H.W., 1997. How many oceans? Meliata, Vardar and Pindos oceans in Mesozoic Alpine paleogeography. Geology 25 (2), 183–186.

Channell, J.E.T., Brandner, R., Spieler, A., Stoner, J.S., 1992. Paleomagnetism and paleogeography of the Northern Calcareous Alps (Austria). Tectonics 11, 792–810.

Chenin, P., Manatschal, G., Ghienne, J.-F., Chao, P., 2022. The syn-rift tectono-stratigraphic record of rifted margins (Part II): a new model to break through the proximal/distal interpretation frontier. Basin Res. 34, 489–532. https://doi.org/10.1111/bre.12628.

Clerc, C., Lagabrielle, Y., 2014. Thermal control on the modes of crustal thinning leading to mantle exhumation: insights from the Cretaceous Pyrenean hot paleomargins. Tectonics 33, 1340–1359. https://doi.org/10.1002/2013TC003471.

Dallmeyer, R.D., Handler, R., Neubauer, F., Fritz, H., 1998. Sequence of thrusting within a thick- skinned tectonic wedge: evidence from 40Ar/39Ar and Rb-Sr ages from the Austroalpine Nappe complex of the Eastern Alps. J. Geol. 106, 71–86. https://doi.org/10.1086/516008.

DeFelipe, I., Pedreira, D., Pulgar, J.A., Iriarte, E., Mendia, M., 2017. Mantle exhumation and metamorphism in the Basque-Cantabrian Basin (N Spain): stable and clumped isotope analysis in carbonates and comparison with ophicalcites in the North-Pyrenean Zone (Urdach and Lherz). G-cubed 18 (2), 631–652. https://doi.org/10.1002/2016GC006690.

Deschamps, F., Godard, M., Guillot, S., Hattori, K., 2013. Geochemistry of subduction zone serpentinites: a review. Lithos 178, 96–127.

Duval, B., Cramez, C., Jackson, M.P.A., 1992. Raft tec-tonics in the Kwanza Basin, Angola: marine and Petro-leum. Geology 9, 389–404. https://doi.org/10.1016/0264-8172(92)90050-O (12).

Eichenseer, H.T., Walgenwitz, F.R., Biondi, P.J., 1999. Stratigraphic control on facies and diagenesis of dolomitized oolitic siliciclastic ramp sequences (Pinda Group, Albian, offshore Angola). Am. Assoc. Pet. Geol. Bull. 83, 1729–1758.

Epin, M.E., Manatschal, G., Sapin, F., Rowan, M.G., 2021. The tectono-magmatic and subsidence evolution during lithospheric breakup in a salt-rich rifted margin: insights from a 3D seismic survey from southern Gabon. Mar. Pet. Geol. 128 https://doi.org/10.1016/j.marpetgeo.2021.105005.

Erratt, D., 1993. Relationships between basement faulting, salt withdrawal and Late Jurassic rifting. In: Parker, J.R. (Ed.), Petroleum Geology of Northwest Europe: Proceedings of the 4th Conference: Geological Society. Petroleum Geology Conference series, London, pp. 1211–1219.

Faryad, S.W., Spišiak, J., Horvath, P., Hovorka, D., Dianiška, I., Jozsa, S., 2005. Petrological and geochemical features of the Meliata mafic rocks from the sutured Triassic oceanic basin, Western Carpathians. Ofioliti 30, 27–35.

Faupl, P., Wagreich, M., 1994. Palaeogeography and geodynamic evolution of the Gosau Group of the Northern Calcareous Alps (Late Cretaceous, Eastern Alps, Austria). Palaeogeogr. Palaeoclimatol. Palaeoecol. 110, 235–254.

Faupl, P., Wagreich, M., 2000. Late Jurassic to Eocene Palaeogeography and Geodynamic Evolution of the Eastern Alps. Mitt. Österr. Geol. Ges. 92, 79–94.

Fernández, O., Habermüller, M., Grasemann, B., 2021. Hooked on salt: Rethinking Alpine tectonics in Hallstatt (Eastern Alps, Austria). Geology 49 (3), 325–329.

Fodor, L., Oravecz, E., Less, G., KövéS., 2023. CEEG 2023 Pre- and post-conference field trip guide. Acta Mineralogica-Petrographica. Field Guide Series 34, 66 pp.

Frank, W., Schlager, W., 2006. Jurassic strike slip versus subduction in the Eastern Alps. Int J Earth Sci (Geol Rundsch) 95, 431–450. https://doi.org/10.1007/s00531-005-0045-7.

Frisch, W., Gawlick, H.J., 2003. The nappe structure of the central Northern Calcareous Alps and its disintegration during Miocene tectonic intrusion - a contribution to understanding the orogenic evolution of the Eastern Alps. Int. J. Earth Sci. 92 (5), 712–727. https://doi.org/10.1007/s00531-003-0357-4.

Froitzheim, N., Plašienka, D., Schuster, R., 2008. Alpine tectonics of the Alps and the Western Carpathians. In: McCann, T. (Ed.), The Geology of Central Europe, vol. 2, 1031144/CEV2P.6. Mesozoic and Cenozoic.

Galbrun, B., Boulila, S., Krystyn, L., Richoz, S., Gardin, S., Bartolini, A., Maslo, M., 2020. "Short" or "long" Rhaetian? Astronomical calibration of Austrian key sections. Glob. Planet. Chang. 192, 103253. https://doi.org/10.1016/j.gloplacha.2020.103253.

Gawlick, H.J., Königshof, P., 1993. Diagenesis, Very Low Grade and Low-Grade Metamorphism in the Southern Salzburg Area - Paleotemperatures Based on Conodont Colour Alteration Index (CAI) Data - (Northern Calcareous Alps, Austria). Jahrb. Geol. Bundesanst. 136 (1), 39–48.

Gawlick, H.J., Missoni, S., 2015. Middle Triassic radiolarite pebbles in the Middle Jurassic Hallstatt Melange of the Eastern Alps: implications for Triassic-Jurassic geodynamic and paleogeographic reconstructions of the western Tethyan realm. Facies 61, 13. https://doi.org/10.1007/s10347-015-0439-3.

Gawlick, H.J., Missoni, S., 2019. Middle-Late Jurassic sedimentary mélange formation related to ophiolite obduction in the Alpine-Carpathian-Dinaridic Mountain Range. Gondwana Res. 74, 144–172. https://doi.org/10.1016/j.gr.2019.03.003.

Gawlick, H.J., Krystyn, L., Lein, R., 1994. Conodont colour alteration indices: Palaeotemperatures and metamorphism in the Northern Calcareous Alps—a general view. Geol. Rundsch. 83, 660–664.

Gawlick, H.J., Missoni, S., Schlagintweit, F., Suzuki, H., Frisch, W., Krystyn, L., Blau, J., Lein, R., 2009. Jurassic Tectonostratigraphy of the Austroalpine Domain. J. Alpine Geol. 50, 1–152.

Ge, Z., Gawthorphe, R.L., Rotevatn, A., Zijerveld, L., Jackson, C.A.-L., Oluboyo, A., 2020. Minibasin depocentre migration during diachronous walt welding, offshore Angola. Basin Res. 32, 875–893.

Gouiza, M., Hall, J., Welford, J.K., 2017. Tectono-stratigraphic evolution and crustal architecture of the Orphan Basin during North Atlantic rifting. Int. J. Earth Sci. 106, 917–937.

Grad, M., Tiira, T., ESC Working Group, 2009. The Moho depth map of the European Plate. Geophys. J. Int. 176, 279–292. https://doi.org/10.1111/j.1365-246X.2008.03919.x.

Granado, P., Urgeles, R., Sàbat, F., Albert-Villanueva, E., Roca, E., Muñoz, J.A., Mazzuca, N., Gambini, R., 2016a. Geodynamical framework and hydrocarbon plays of a salt giant: the NW Mediterranean Basin. Pet. Geosci. 22 (4), 309–321.

Granado, P., Thöny, W., Carrera, N., Gratzer, O., Strauss, P., Muñoz, J.A., 2016b. Basement-involved reactivation in foreland fold-and-thrust belts: the Alpine-Carpathian Junction (Austria). Geol. Mag. 153 (5–6), 1110–1135. https://doi.org/10.1017/S0016756816000066.

Granado, P., Roca, E., Strauss, P., Pelz, K., Muñoz, J.A., 2019. Structural styles in fold-and-thrust belts involving early salt structures: the Northern Calcareous Alps (Austria). Geology 47 (1), 51–54. https://doi.org/10.1130/G45281.1.

Granado, P., Ruh, J.B., Santolaria, P., Strauss, P., Muñoz, J.A., 2021. Stretching and contraction of extensional basins with pre-rift salt: a numerical modeling approach. Front. Earth Sci. 9, 648937 https://doi.org/10.3389/feart.2021.648937.

Granado, P., Santolaria, P., Muñoz, J.A., 2023. (In Press). Interplay of downbuilding and gliding in salt-bearing rifted margins: insights from analogue modelling and natural case studies. Submitted to AAPG Bull. https://doi.org/10.1306/08072221203.

Haas, J., Kovàcs, S., Krystyn, L., Lein, R., 1995. Significance of Late Permian–Triassic facies zones in terrane reconstructions in the Alpine–North Pannonian domain. Tectonophysics 242, 19–40. https://doi.org/10.1016/0040-1951(94)00157-5.

Habler, G., Thöni, W., 2001. Preservation of Permo-Triassic low-pressure assemblages in the cretaceous high-pressure metamorphic Saualpe crystalline basement (Eastern Alps, Austria). J. Metamorph. Geol. 19, 679–697.
Hahn, F.F., 1912. Versuch zu einer Gliederung der austroalpinen Masse westlich der österreichischen Traun. Verh. k.k. geol. Reichsanst., 1912/15, 337-344. Wien.
Hahn, F.F., 1913. Grundzüge des Baues der nördlichen Kalkalpen zwischen Inn und Enns. Teil I und II. Mitt. Geol. Ges. Wien 6 (1913), 238–357 u. 374-501, Wien.
Hantschel, T., Kauerauf, A.I., 2009. Fundamentals of Basin and Petroleum Systems Modeling. Berlin, Heidelberg, Springer Berlin Heidelberg. https://doi.org/10.1007/978-3-540-72318-9.
Hardebol, N.J., Callot, J.P., Bertotti, G., Faure, J.L., 2009. Burial and temperature evolution in thrust belt systems: sedimentary and thrust sheet loading in the SE Canadian Cordillera. Tectonics 28. https://doi.org/10.1029/2008TC002335. TC3003.
Hassaan, M., Faleide, J.I., Gabrielsen, R.H., Tsikalas, F., 2021. Effects of basement structures and Carboniferous basin configuration on evaporite distribution and the development of salt structures in Nordkapp Basin, Barents Sea—Part I. Basin Res. 33 (4), 2474–2499. https://doi.org/10.1111/bre.12565.
Hornung, T., Brandner, R., 2005. Biochronostratigraphy of the Reingraben Turnover (Hallstatt Facies Belt): local black shale events controlled by regional tectonics, climatic change and plate tectonics. Facies 51, 475–494.
Hossack, J.R., 1979. The use of balanced cross-sections in the calculation of orogenic contraction: a review. J. Geol. Soc. 136 (6), 705–711. https://doi.org/10.1144/gsjgs.136.6.0705.
Hossack, J.R., 1995. Geometric rules of section balancing for saltstructures. In: Jackson, M.P.A., Roberts, D.G., Snelson, S. (Eds.), SaltTectonics: A Global Perspective, American Association of PetroleumGeologists Memoir, 65, pp. 29–40.
Huang, Q., Neubauer, F., Liu, Y., Genser, J., Guan, Q., Chang, R., Yuan, S., Yu, S., 2022. (2022). Permian-Triassic granites of the Schladming Complex (Austroalpine basement): Implications for subduction of the Paleo-Tethys Ocean in the Eastern Alps. Gondwana Res. https://doi.org/10.1016/j.gr.2022.05.006.
Hubbard, R.J., 1988. Age and significance of sequence boundaries on Jurassic and Early Cretaceous rifted continental margins. Am. Assoc. Pet. Geol. Bull. 72, 49–72.
Huismans, R., Beaumont, C., 2011. Depth-dependent extension, two-stage breakup and cratonic underplating at rifted margins. Nature 4 7 3, 74–79. https://doi.org/10.1038/nature09988.
Jackson, C.A.-L., Elliott, G.M., Royce-Rogers, E., Gawthorpe, R.L., Aas, T.E., 2018. Salt thickness and composition influence rift structural style, northern North Sea, offshore Norway. Basin Res. 31, 514–538. https://doi.org/10.1111/bre.12332.
Jammes, S., Manatschal, G., Lavier, L., Masini, E., 2009. Tectonosedimentary evolution related to extreme crustal thinning ahead of a propagating ocean: example of the western Pyrenees. Tectonics 28 (4). https://doi.org/10.1029/2008TC002406 (2009).
Jeanniot, L., Kusznir, N., Mohn, G., Manatschal, G., Cowie, L., 2016. Constraining lithosphere deformation modes during continental breakup for the Iberia–Newfoundland conjugate rifted margins. Tectonophysics 680, 28–49. https://doi.org/10.1016/j.tecto.2016.05.006.
Joffe, A., Jackson, C.-L., Pichel, L.M., 2023. Syn-depositional halokinesis in the Zechstein Supergroup (Lopingian) controls Triassic minibasin genesis and location. Basin Res. 35, 784–801. https://doi.org/10.1111/bre.12735.
Karlo, J.F., van Buchem, F.S.P., Moen, J., Milroy, K., 2014. Triassic-age salt tectonics of the Central North Sea. Interpretation 2 (4). https://doi.org/10.1190/INT-2014-0032.1. SM19–SM28.
Knoll, T., Huet, B., Schuster, R., Mali, H., Ntaflos, T., Hauzenberger, C., 2023. Lithium pegmatite of anatectic origin-A case study from the Austroalpine Unit Pegmatite Province (eastern European Alps): geological data and geochemical model. Ore Geol. Rev. 154, 105298. https://doi.org/10.1016/j.oregeorev.2023.105298.
Kohút, M., Hofmann, M., Havrila, M., Linnemann, U., Havrila, J., 2017. Tracking an upper limit of the “Carnian Crisis” and/or Carnian stage in the Western Carpathians (Slovakia). Int J Earth Sci (Geol Rundsch) 107, 321–335. https://doi.org/10.1007/s00531-017-1491-8.
Koyi, H., Jenyon, M.K., Petersen, K., 1993. The effect of basement faulting on diapirism. J. Pet. Geol. 16, 285–312. https://doi.org/10.1111/j.1747-5457.1993.tb00339.x.
Kozur, H., 1991. The evolution of the Meliata-Hallstatt Ocean and its significance for the early evolution of the Eastern Alps and Western Carpathians. Palaeogeogr. Palaeoclimatol. Palaeoecol. 87, 109–135.
Kozur, H., Mostler, H., 1991. Erster paläontologischer Nachweis von Meliaticum und Süd-Rudabanyaicum in den Nördlichen Kalkalpen (Österreich) und ihre Beziehungen zu den Abfolgen in den Westkarpaten. Geologisch-Paläontologische Mitteilungen Innsbruck 18, S.87–129.
Krainer, K., 1993. Late- and Post-Variscan sediments in the Eastern and Southern Alps. In: Raumer, J.F., Neubauer, F. (Eds.), Pre-Mesozoic Geology in the Alps. Springer, Berlin, pp. 537–564.
Krainer, K., Stingl, V., 1986. Alluviale Schuttfächersedimente im Ostalpinen Perm am Beispiel der Präbichlschichten an der Typuslokalität bei Eisenerz/Steiermark (Österreich). Mitteilungen der österreichischen Geologischen Gesellschaft 78, 231–249.
Kralik, M., Krumm, W., Schramm, J.-M., 1987. Low grade and very low grade metamorphism in the Northern Calcareous Alps and in the Greywacke Zone: illite crystallinity data and isotopic ages. In: Flügel, H.W., Faupl, P. (Eds.), Geodynamics of the Estern Alps, pp. 164–178 (Deuticke) Wien.
Krenmayr, H.G., 1999. The Nierental Formation of the Upper Gosau Group (Upper Cretaceous- Lower Paleocene, Northern Calcareous Alps) in Berchtesgaden: Definition, Facies and Environment. Jahrb. Geol. Bundesanst. 141 (4). S.409–447.
Kreuss, O., 2014. Geofast - Zusammenstellung ausgewählter Archivunterlagen der Geologischen Bundesanstalt 1:50.000–100 Hieflau: Stand 2014, Ausgabe 2014/09.
Kristan, E., 1958. Geologie der Hohen Wand und des Miesenbachtales (Niederösterreich). Jahrb. Geol. Bundesanst. 101. S.249-291.
Krystyn, L., 1973. Zur Ammoniten- und Conodonten-Stratigraphie der Hallstätter Obertrias (Salzkammergut, Österreich). In: Verhandlungen der Geologischen Bundesanstalt, pp. 113–153.
Krystyn, L., Lein, R., 1996. Triassische Becken- und Plattformsedimente der östlichen Kalkalpen. Berichte der Geologischen Bundesanstalt 33.
Krystyn, L., Lein, R., Richoz, S., 2008. Der Gamsstein: Werden und Vergehen einer Wettersteinkalk-Plattform. PANGEO 2008. Fieldtrip Guide. J. Alpine Geol. 49, 157–172.
Kukla, P.A., Strozyk, F., Mohriak, W.U., 2018. South Atlantic salt basins – witnesses of complex passive margin evolution. Gondwana Res. 53, 41–57.
Kunz, B.E., Manzotti, P., von Niederhäusern, B., Engi, M., Darling, J.R., Giuntoli, F., Lanari, P., 2018. Permian high-temperature metamorphism in the Western Alps (NW Italy). Int. J. Earth Sci. 107 (1), 203–229.
Kupper, D.H., Hossack, J.R., 1981. Discussion on the use of balanced cross-sections in the calculation of orogenic contraction: a review. J. Geol. Soc. 138 (1), 107–108. https://doi.org/10.1144/gsjgs.138.1.0107.
Lafay, R., Deschamps, F., Schwartz, S., Guillot, S., Godard, M., Debret, B., Nicollet, C., 2013. High-pressure serpentinites, a trap-and-release system controlled by metamorphic conditions: example from the Piedmont zone of the western Alps. Chem. Geol. 343, 38–54.
Lavier, L., Manatschal, G., 2006. A mechanism to thin the continental lithosphere at magma-poor margins. Nature 440, 324–328. https://doi.org/10.1038/nature04608.
Lein, R., 1987. Evolution of the Northern Calcareous Alps during Triassic times. In: Flügel, H., Faupl, P. (Eds.), Geodynamics of the Eastern Alps. Wien Deuticke, pp. 85–102.
Lein, R., Krystyn, L., Richoz, S., Lieberman, H., 2012. Middle Triassic platform/basin transition along the Alpine passive continental margin facing the Tethys Ocean – the Gamsstein: the rise and fall of a Wetterstein Limestone Platform (Styria, Austria). J. Alpine Geol. 54, 471.
Leitner, C., Spötl, C., 2017. The Eastern Alps: multistage development of extremely deformed evaporites. In: By Soto, J.I., Finch, J.F., Tari, G. (Eds.), Permo-Triassic Salt Provinces of Europe, North Africa and the Atlantic Margins. Tectonics and Hydrocarbon Potential. Elsevier, Amsterdam, pp. 467–479. Chapter 21.
Leitner, C., Neubauer, F., Urai, J.L., Schoenherr, J., 2011. Structure and evolution of a rocksalt-mudrock-tectonite: the Haselgebirge in the Northern Calcareous Alps. J. Struct. Geol. 33, 970-984.–498.
Leitner, C., Neubauer, F., Genser, J., Borojevic-Sostaric, S., Rantitsch, G., 2014. 40Ar/39Ar ages of crystallization and recrystallization of rockforming polyhalite in Alpine rocksalt deposits. Geol. Soc. Lond., Spec. Publ. 378, 207–224. https://doi.org/10.1144/SP378.5.
Leitner, C., Weismaier, S., Köster, M.H., Gilg, H.A., Finger, F., Neubauer, F., 2017. Alpine halite-mudstone-polyhalite tectonites: Sedimentology and early diagenesis of evaporites in an ancient rift setting (Haselgebirge Formation, eastern Alps). Geol. Soc. Am. Bull. https://doi.org/10.1130/B31747.1.
Leitner, C., Gross, D., Friedl, G., Genser, J., Neubauer, F., 2020. Sandstone diagenesis in a halite deposit, from surface to high-grade diagenesis (Haselgebirge Formation, Eastern Alps). Sediment. Geol. 399, 105614 https://doi.org/10.1016/j.sedgeo.2020.105614.
Lescoutre, R., Tugend, J., Brune, S., Masini, E., Manatschal, G., 2019. Thermal evolution of symmetric hyperextended magma-poor rift systems: results from numerical modeling and Pyrenean field observations. Geochem. Geophys. Geosyst. 20, 4567–4587. https://doi.org/10.1029/2019GC008600.
Less, Gy, Mello, J., Elečko, M., Kovács, S., Pelikán, P., Pentelényi, L., Peregi, Z.S., Pristraś, J., Radócz, G.Y., Szentpétery, I., Vass, D., Vožár, J., Vozárová, A., 2004. Geological Map of the Gemer-Bükk Area 1: 100000. Geological Institute of Hungary, Budapest.
Linzer, H.G., Ratschbacher, L., Frisch, W., 1995. Transpressional collision structures in the upper crust: the fold-thrust belt of the Northern Calcareous Alps. Tectonophysics 242, 41–61.
Linzer, H.G., Moser, F., Nemes, F., Ratschbacher, L., Sperner, B., 1997. Build-up and dismembering of the eastern Northern Calcareous Alps. Tectonophysics 272, 97–124.
Manatschal, G., Sauter, D., Karpoff, A.M., Masini, E., Mohn, G., Lagabrielle, Y., 2011. The Chenaillet Ophiolite in the French/Italian Alps: an ancient analogue for an Oceanic Core Complex? Lithos 124, 169–184. https://doi.org/10.1016/j.lithos.2010.10.017.
Manatschal, G., Chenin, P., Ghienne, J., Ribes, C., Masini, E., 2022. The syn-rift tectono-stratigraphic record of rifted margins (Part I): insights from the Alpine Tethys. Basin Res. 34, 457–488 (2022).
Manatschal, G., Chenin, P., Ulrich, M., Petri, B., Morin, M., Ballay, M., 2023. Tectono-magmatic evolution during the extensional phase of a Wilson Cycle: a review of the Alpine Tethys case and implications for Atlantic-type margins Ital. J. Geosci. 142, 5–27.
Mandl, G.W., 1984. Zur Trias des Hallstätter Faziesraumes - ein Modell am Beispiel Salzkammergut (Nördliche Kalkalpen, Österreich). In: Mitteilungen der Gesellschaft der Geologie- und Bergbaustudenten in Österreich, 30/31. S.133–176.
Mandl, G.W., 1996. Zur Geologie des Ödenhof-Fensters (Nördliche Kalkalpen, Österreich). Jb. Geol. B.-A. 139 (4), 473–495.
Mandl, G.W., 2000. The Alpine sector of the Tethyan shelf - examples of Triassic to Jurassic sedimentation and deformation from the Northern Calcareous Alps. Mitteilungen der Österreichischen Geologischen Gesellschaft 92, 61–77.
Mandl, G.W., 2016. Das Kalkalpine Stockwerk auf GK50 Blatt 103 Kindberg. In: Arbeitstagung 2015 der Geologischen Bundesanstalt Geologie der Kartenblätter GK50 ÖK 103 Kindberg und ÖK 135 Birkfeld, Mitterdorf im Mürztal 21.–25. September 2015 (2016), pp. 88–101.

Mandl, G.W., 2017. Vom Traunstein zum Dachstein – Geologie im Querschnit. In: Arbeitstagung 2017 - Angewandte Geowissenschaften an der GBA, 19.-22. Juni 2017, Bad Ischl, Hallstatt, Gmunden (2017), S.22–28. https://opac.geologie.ac.at/ais312/dokumente/ATA_2017_022.pdf. Juni 2017, Bad Ischl, Hallstatt, Gmunden (2017), S.22–28.

Mandl, G.W., Ondrejičková, A., 1991. Über eine triadische Tiefwasserfazies (Radiolarite, Tonschiefer) in den Nördlichen Kalkalpen – ein Vorbericht Jahrb. Geol. Bundesanst. 134, 309–318.

Mandl, G.W., Ondrejicková, A., 1993. Radiolarien und Conodonten aus dem Meliatikum im Ostabschnitt der NKA (A). Jb. Geol. B.-A. 136/4, 841–871. Wien.

McKenzie, D.P., 1978. Some remarks on the development of sedimentary basins. Earth Planet. Sci. Lett. 40, 20–32.

McPhee, P.J., van Hinsbergen, D.J.J., Maffione, M., Altıner, D., 2018. Palinspastic reconstruction versus cross-section balancing: how complete is the central Taurides fold-thrust belt (Turkey)? Tectonics 37, 4285–4310. https://doi.org/10.1029/2018TC005152.

Melcher, F., Meisel, T., Puhl, J., Koller, F., 2002. Petrogenesis and geotectonic setting of ultramafic rocks in the Eastern Alps: constraints from geochemistry. Lithos 65 (1–2), 69–112. https://doi.org/10.1016/S0024-4937(02)00161-5.

Mock, R., Sykora, M., Aubrecht, R., Ozvoldova, L., Kronome, B., Reichwalder, P., Jablonsky, J., 1998. Petrology and stratigraphy of the Meliaticum near the Meliata and Jaklovce villages, Slovakia. Slovak Geol. Mag. 4, 223–260.

Moore, V.M., Blanchard, R.H., 2017. Raft-related structures of the Albian Madiela formation, offshore South Gabon. AAPG Search and Discovery Article #51373.

Moser, M., Tanzberger, A., 2015. Mikrofacies und Stratigrafie des Gamssteines (Palfau, Steiermark). Jahrb. Geol. Bundesanst. 155, 235–263.

Mueller, S., Krystyn, L., Kürschner, W.M., 2016. Climate variability during the Carnian Pluvial Phase – a quantitative palynological study of the Carnian sedimentary succession at Lunz am See, Northern Calcareous Alps, Austria. Palaeogeogr. Palaeoclimatol. Palaeoecol. 441, 198–211.

Mutti, M., Weissert, H., 1995. Triassic monsoonal climate and its signature in Ladinian-Carnian carbonate platforms (Southern Alps, Italy). J. Sediment. Res. 65b, 357–367.

Neubauer, F., 1988. Bau und Entwicklungsgeschichte des Rennfeld-Mugel- und des Gleinalmkristallins (Ostalpen). Abhandlungen der Geologischen Bundesanstalt 42, 1–137.

Neubauer, F., Genser, J., Handler, R., 2000. The Eastern Alps: result of a two-stage collision process. Mitt. Österr. Geol. Ges. 92, 117–134.

Neuhuber, S., Wagreich, M., Wendler, I., Spötl, C., 2007. Turonian Oceanic Red Beds in the Eastern Alps: Concepts for palaeoceanographic changes in the Mediterranean Tethys. Palaeogeogr. Palaeoclimatol. Palaeoecol. 251, 222–238.

Ondrejka, M., Uher, P., Putiš, M., et al., 2021. Permian A-type granites of the Western Carpathians and Transdanubian regions: products of the Pangea supercontinent breakup. Int J Earth Sci (Geol Rundsch) 110, 2133–2155. https://doi.org/10.1007/s00531-021-02064-2.

Onuzi, K., Koller, F., Matiasek, E., 2021. Ophiolitic Massives of Voskopoja, Morava, Vithkuq-Rehova (Albania) Geology and Petrology, 224 pp. Vlore, Triptik.

Ostroff, A.G., 1964. Conversion of gypsum to anhydrite in aqueous salt solutions. Geochim. Cosmochim. Acta 28 (9), 1363–1372.

Pérez-Gussinyé, M., Collier, J.S., Armitage, J.J., Hopper, J.R., Ranero, C.R., 2023. (2023) Towards a process-based understanding of rifted continental margins. Nat. Rev Earth Environ 4, 166–184. https://doi.org/10.1038/s43017-022-00380-y.

Péron-Pinvidic, G., Manatschal, G., 2009. The final rifting evolution at deep magma-poor passive margins from Iberia-Newfoundland: a new point of view. Int J Earth Sci (Geol Rundsch) 98, 1581–1597. https://doi.org/10.1007/s00531-008-0337-9.

Péron-Pinvidic, G., Manatschal, G., "IMAGinING RIFTING" Workshop Participants, 2019. Rifted Margins: State of the Art and Future Challenges. Earth Sci, Front. https://doi.org/10.3389/feart.2019.00218.

Petri, B., Mohn, G., Skrzypek, E., Mateeva, T., Galster, F., Manatschal, G., 2017. U–Pb geochronology of the Sondalo gabbroic complex (Central Alps) and its position within the Permian post-Variscan extension. Int. J. Earth Sci. 106 (8), 2873–2893.

Petri, B., Duretz, T., Mohn, G., Schmalholz, S.M., Garner, G.D., Münterner, O., 2019. Thinning mechanisms of heterogeneous continental lithosphere. Earth Planet. Sci. Lett. 512, 147–162.

Picazo, S., Münterner, O., Manatschal, G., Bauville, A., Karner, G., Johnson, C., 2016. Mapping the nature of mantle domains in Western and Central Europe based on clinopyroxene and spinel chemistry: evidence for mantle modification during and extensional cycle. Lithos 266-267, 233–263.

Piller, W.E., Egger, H., Erhart, C.W., Gross, M., Harzhauser, M., Hubmann, B., van Husen, D., Krenmayr, H.G., Krystyn, L., Lein, R., Lukeneder, A., Mandl, G.W., Rögl, F., Roetzel, R., Rupp, C., Schnabel, W., Schönlaub, H.P., Summesberger, H., Wagreich, M., Wessely, G., 2004. Die stratigraphische Tabelle von Österreich 2004 (sedimentäre Schichtfolgen).

Plöchinger, B., 1961. Die Gosaumulde von Grünbach und der Neuen Welt (Niederösterreich). JB. Geol. B. A. 104, 359–441.

Prosser, S., 1993. Rift-related linked depositional systems and their seismic expression. In: Williams, G.D., Dobb, A. (Eds.), Tectonics and Seismic Sequence Stratigraphy. Geological Society Special Publication, pp. 35–66.

Putiš, M., Radvanec, M., Segeev, S., Koller, F., Michálek, M., Snárska, B., Koppa, M., Šarinová, K., Németh, Z., 2011. Metamorphosed succession of cherty shales with basalt and diastrophic breccia in olistolith of the Meliatic Jurassic accretion wedge near Jaklovce (Slovakia), dated on zircon (U-Pb SIMS SHRIMP). Miner. Slov. 48, 135–144.

Putiš, M., Soták, J., Li, Q.-L., Ondrejka, M., Li, X.-H., Hu, Z., Ling, X., Nemec, O., Németh, Z., Ružička, P., 2019a. Origin and Age Determination of the Neotethys Meliata Basin Ophiolite Fragments in the Late Jurassic–Early Cretaceous Accretionary Wedge Mélange (Inner Western Carpathians, Slovakia). Minerals 9. https://doi.org/10.3390/min9110652, 652-.

Putiš, M., Koller, F., Li, X.-H., Qui-Li, L., Larionov, A., Siman, P., Ondrejka, M., Uher, P., Németh, Z., Ružička, P., Nemec, O., 2019b. Geochronology of Permian-Triassic tectono-magmatic events from the Inner Western Carpathian and Austroalpine units. Geol. Carpath. 70. Smolenice, October 9-11.

Puziewicz, J., Matusiak-Małek, M., Nataflos, T., Grégoire, M., Kaczmarek, M.-A., Aulbach, S., Ziobro, M., Kukuła, A., 2020. Three major types of subcontinental lithospheric mantle beneath the Variscan orogen in Europe. Lithos 362–363, 105467. https://doi.org/10.1016/j.lithos.2020.105467.

Quesnel, B., Boiron, M.-C., Cathelineau, M., Truche, L., Rigaudier, T., Bardoux, G., Agrinier, P., de Saint Blanquat, M., Masini, E., Gaucher, E.C., 2019. Nature and origin of mineralizing fluids in hyperextensional systems: the case of Cretaceous Mg metasomatism in the Pyrenees. Geofluids 2019. https://doi.org/10.1155/2019/7213050. Article ID 7213050, 18 pages, 2019.

Quirk, D.G., Hertle, M., Jeppesen, J.W., Raven, M., Mohriak, W.U., Kann, D.J., Mendes, M.P., 2013. Rifting, subsidence and continental break-up above a mantle plume in the Central South Atlantic. In: Mohriak, W.U., Daforth, A., Post, P.J., Brown, D.E., Tari, G., Nemčok, M., Sinha, S.T. (Eds.), Conjugate Divergent Margins. London, Geological Society, London, Special Publication, 369, pp. 185–214. https://doi.org/10.1144/SP369.20.

Ranero, C., Perez-Gussinye, M., 2010. Sequential faulting explains the asymmetry and extension discrepancy of conjugate margins. Nature 468, 294–299. https://doi.org/10.1038/nature09520.

Rantitsch, G., Bryda, G., Gawlick, H.-J., 2020. Conodont thermometry by Raman spectroscopy on carbonaceous material: a case study from the Northern Calcareous Alps (Mürzalpen Nappe, Eastern Alps). Austrian J. Earth Sci. 113 (2), 201–210. https://doi.org/10.17738/ajes.2020.0012.

Raymond, L.A., 1984. Classification of me'langes. In: Raymond, L.A. (Ed.), Me'langes: Their Nature, Origin, and Significance: Geological Society of America, Boulder, Special Publication 228, pp. 7–20.

Rebay, G., Spalla, M.I., 2001. Emplacement at granulite facies conditions of the Sesia–Lanzo metagabbros: an early record of Permian rifting? Lithos 58, 85–104.

Reston, T.J., Pérez-Gussinyé, M., 2007. Lithospheric extension from rifting to continental breakup at magma-poor margins: rheology, serpentinisation and symmetry. Int J Earth Sci (Geol Rundsch) 96, 1033–1046. https://doi.org/10.1007/s00531-006-0161-z.

Ribes, C., Manatschal, G., Ghienne, J.-F., Karner, G.D., Johnson, C.A., Figueredo, P.H., Incerpi, N.N., Epin, M., 2019a. The syn-rift stratigraphic record across a fossil hyper-extended rifted margin: the example of the northwestern Adriatic margin exposed in the Central Alps. Int. J. Earth Sci. 108, 2071–2095. https://doi.org/10.1007/s00531-019- 01750-6.

Ribes, C., Petri, B., Ghienne, J., Manatschal, G., Galster, F., Karner, G.D., Figueredo, P.H., Johnson, C.A., Karpoff, A., 2019b. Tectono-sedimentary evolution of a fossil ocean-continent transition: Tasna nappe, central Alps (SE Switzerland). Geol. Soc. Am. Bull. 1–20 https://doi.org/10.1130/B35310.1/4863878/b35310.pdf.

Ribes, C., Ghienne, J.-F., Manatschal, G., Dall'Asta, N., Stockli, D.F., Galster, F., Gillard, M., Karner, G.D., 2020. The Grès Singuliers of the Mont Blanc region (France and Switzerland): Stratigraphic response to rifting and crustal necking in the Alpine Tethys. Int. J. Earth Sci. 109, 2325–2352. https://doi.org/10.1007/s0053 1-020-01902-z.

Richoz, S., van de Schootbrugge, B., Pross, J., Püttmann, W., Quan, T.M., Lindström, S., Heunisch, C., Fiebig, J., Maquil, R., Schouten, S., Hauzenberger, C.A., Wignall, P.B., 2012. Hydrogen sulphide poisoning of shallow seas following the end-Triassic extinction. Nat. Geosci. 5 https://doi.org/10.1038/NGEO1539.

Rizzi, M., Thibault, N., Ullmann, C.V., Ruhl, M., Olsen, T.K., Moreau, J., Clémence, M.-E., Mette, W., Korte, C., 2020. Sedimentology and carbon isotope stratigraphy of the Rhaetian Hochalm section (Late Triassic, Austria). Glob. Planet. Chang. 191 https://doi.org/10.1016/j.gloplacha.2020.103210.

Roca, E., Ferrer, O., Rowan, M.G., Muñoz, J.A., Butillé, M., Giles, K.A., Arbués, P., deMatteis, M., 2021. Salt tectonics and controls on halokinetic-sequence development of an exposed deepwater diapir: The Bakio Diapir, Basque-Cantabrian Basin, Pyrenees. Mar. Pet. Geol. 123, 104770 https://doi.org/10.1016/j.marpetgeo.2020.104770.

Roda, M., Zucali, M., Li, Z.-X., Spalia, M.I., Yao, W.V., 2018. Pre-Alpine contrasting tectono-metamorphic evolutions within the Southern Steep Belt, Central Alps. Lithos 310–311, 31–49. https://doi.org/10.1016/j.lithos.2018.03.025.

Rouby, D., Raillard, S., Guillocheau, F., Bouroullec, R., Nalpas, T., 2002. Kinematics of a growth fault/raft system on the West African margin using 3-D restoration. J. Struct. Geol. 24 (4), 783–796. https://doi.org/10.1016/S0191-8141(01)00108-0.

Rowan, M.G., 2014. Passive-margin salt basins: Hyperextension, evaporite deposition, and salt tectonics. Basin Res. 26, 154–182.

Rowan, M.G., Ratliff, R.A., 2012. Cross-section restoration of salt-related deformation: best practices and potential pitfalls. J. Struct. Geol. 41, 24–37. https://doi.org/10.1016/j.jsg.2011.12.012.

Rowan, M.G., Vendeville, B.C., 2006. Foldbelts with early salt withdrawal and diapirism: physical models and examples from the northern Gulf of Mexico and the Flinders Ranges, Australia. Mar. Pet. Geol. 23, 871–891.

Santolaria, P., Granado, P., Wilson, E.P., de Matteis, M., Ferrer, O., Strauss, P., Pelz, K., König, M., Oteleanu, A.E., Roca, E., Muñoz, J.A., 2022. From salt-bearing rifted margins to fold-and-thrust belts. Insights from analog modeling and Northern Calcareous Alps case study. Tectonics 41. https://doi.org/10.1029/2022TC007503 e2022TC007503.

Schauberger, O., 1986. Bau und Bildung der Salzlagerstätten des ostalpinen Salinars. In: Archiv für Lagerstättenforschung der Geologischen Bundesanstalt, Vol. 7, pp. 217–254.

Schlager, W., Schöllnberger, W., 1974. Das Prinzip stratigraphischer Wenden in der Schichtfolge der Nördlicher Kalkalpen. Mitteilungen der Österreichischen Gesellschaft 66 (67), 165–193.
Schmid, S.M., Fügenschuh, B., Kissling, E., Schuster, R., 2004. Tectonic map and overall architecture of the Alpine orogen. Eclogae Geol. Helv. 97, 93–117.
Schmid, S.M., Bernoulli, D., Fügenschuh, B., Matenco, L., Schefer, S., Schuster, R., Ustaszewski, K., 2008. The Alpine-Carpathian-Dinaridic orogenic system: correlation and evolution of tectonic units. Swiss J. Geosci. 101, 139–183.
Schmid, S.M., Fügenschuh, B., Kounov, A., Matenco, L., Nievergelt, P., Oberhänsli, R., Pleuger, J., Schefer, S., Schuster, R., Tomljenovic, K., van Hinsbergen, D.J.J., 2020. Tectonic units of the Alpine collision zone between Eastern Alps and western Turkey. Gondwana Res. 78, 308–374.
Schnabel, W., Fuchs, G., Matura, A., Bryda, G., Egger, J., Krenmayer, H.G., Mandl, G., Nowotny, A., Rotzel, R., Scharbert, S., 2002. Geologische Karte von Niederösterreich 1:200.000 mit Legende und Kurzerläuterung. 3B1, Vienna, Geol. B.A. 2 sheets.
Schollnberger, W.E., 2021. Comment on Strauss et al., 2020: Subsidence analysis of salt tectonics-driven minibasins (Northern Calcareous Alps, Austria). Basin Res. 33 (5), 2545–2548. https://doi.org/10.1111/bre.12549.
Schorn, A., Neubauer, F., Genser, J., Bernroider, M., 2013. The Haselgebirge evaporitic melange in central Northern Calcareous Alps (Austria): part of the Permian to Lower Triassic rift of the Meliata ocean? Tectonophysics 583, 28–48.
Schuster, R., Stüwe, K., 2008. Permian metamorphic event in the Alps. Geology 36 (8), 603–606. https://doi.org/10.1130/G24703A.1.
Schuster, R., Scharbert, S., Abart, R., Frank, W., 2001. Permo-Triassic extension and related HT/LP metamorphism in the Austroalpine-Southalpine realm. Mitteilungen der Geologie und Bergbau Studenten Österreichs 44, 111–141.
Sekiguchi, K., 1984. A method for determining terrestrial heat flow in oil basinal areas. Tectonophysics 103 (1–4), 67–79. https://doi.org/10.1016/0040-1951(84)90075-1.
Spötl, C., Hasenhüttl, C., 1998. Thermal History of an evaporitic Mélange in the Northern Calcareous Alps (Austria): a Reconnaissance Illite 'crystallinity' and Reflectance Study. Geol. Rundsch. 87, 449–460.
Stampfli, G.M., Borel, G.D., 2002. A Plate Tectonic Model for the Paleozoic and Mesozoic Constrained by Dynamic Plate Boundaries and Restored Synthetic Oceanic Isochrons. Earth Planet. Sci. Lett. 196, 17–33. https://doi.org/10.1016/S0012-821X(01)00588-X.
Stampfli, G., Mosar, J., Marquer, D., Marchant, R., Baudin, T., Borel, G., 1998. Subduction and obduction processes in the Swiss Alps. Tectonophysics 296, 159–204.
Stewart, S.A., 2007. Salt tectonics in the North Sea Basin: A structural style template for seismic interpreters. Geol. Soc. Lond., Spec. Publ. 272, 361–396. https://doi.org/10.1144/GSL.SP.2007.272.01.19.
Stewart, S., Coward, M., 1995. Synthesis of salt tectonics in the southern North Sea, UK. Mar. Pet. Geol. 12, 457–475.
Strauss, P., Granado, P., Muñoz, J.A., 2021a. Subsidence analysis of salt tectonics-driven carbonate minibasins (Northern Calcareous Alps, Austria). Basin Res. 33 (2), 968–990. https://doi.org/10.1111/bre.12500.
Strauss, P., Granado, P., Muñoz, J.A., 2021b. Reply to the comment of Schollnberger on 'Subsidence analysis of salt tectonics-driven carbonate minibasins' (Northern Calcareous Alps, Austria). Basin Res. 33 (5), 2636–2642. https://doi.org/10.1111/bre.12577.
Stüwe, K., Schuster, R., 2010. Initiation of subduction in the Alps: continent or ocean? Geology 38 (2), 175–178. https://doi.org/10.1130/G30528.1.
Summesberger, H., 1991. Puchberg am Schneeberg. Geologische Karte 1:50.000. Geologische Bundesanstalt. Wien. https://doi.org/10.1016/j.lithos.2020.105467.
Sun, S.-S., McDonough, W.F., 1989. Chemical and isotopic systematics of oceanic basalts: implications for mantle composition and processes. In: Saunders, A.D., Norry, M.J. (Eds.), Magmatism in the Ocean Basins. Geological Society, London, Special Publications, 42, pp. 313–345.
Sutra, E., Manatschal, G., Mohn, G., Unternehr, P., 2013. Quantification and restoration of extensional deformation along the Western Iberia and Newfoundland rifted margins. Geochem. Geophys. Geosyst. 14, 2575–2597. https://doi.org/10.1002/ggge.20135.
Tavani, S., Bertok, C., Granado, P., Piana, F., Salas, R., Vigna, B., Muñoz, J.A., 2018. The Iberia-Eurasia plate boundary east of the Pyrenees. Earth Sci. Rev. 187, 314–337. https://doi.org/10.1016/j.earscirev.2018.10.008.
Tavani, S., Granado, P., Corradetti, A., Camanni, G., Vignaroli, G., Manatschal, G., Mazzoli, S., Muñoz, J.A., Parente, M., 2021. Rift inheritance controls the switch from thin- to thick-skinned thrusting and basal décollement re-localization at the subduction-to-collision transition. GSA Bull. 133 (9–10), 2157–2170. https://doi.org/10.1130/B35800.1.
Theunissen, T., Huismans, R.S., 2022. Mantle exhumation at magma-poor rifted margins controlled by frictional shear zones. Nat. Commun. 13 https://doi.org/10.1038/s41467-022-29058-1.
Thöni, M., Miller, C., 2000. Permo-Triassic pegmatites in the eo-Alpine eclogite-facies Koralpe complex, Austria: age and magma source constraints from mineral chemical, Rb-Sr and Sm-Nd isotope data. In: Schweizerische Mineralogische und Petrographische Mitteilungen, 80 (2000), S.169–186.
Tollmann, A., 1976a. Analyse Des Klassischen Nordalpinen Mesozoikums. Wien, Deuticke, 580 p.
Tollmann, A., 1976b. Der Bau der Nördlichen Kalkalpen. Wien, Deuticke, 449 p.
Tollmann, A., 1985. Geologie von Österreich, Bd. II: Außerzentralalpiner Anteil. – 710 p. Wien (Deuticke).
Tollmann, A., 1987. Late Jurassic/Neocomian gravitational tectonics in the Northern Calcareous Alps in Austria. In: Flügel, H.W., Faupl, R. (Eds.), Geodynamics of the Eastern Alps. Deuticke, Wien, pp. 112–125.
Tollmann, A., Faupl, P., 1972. Alpiner Verrucano im Semmering- und Wechselgebiet. Verh. Geol. Bundesanst. 1972, 107–118.
Tugend, J., Manatschal, G., Kusznir, N.J., Masini, E., Mohn, G., Thinon, I., 2014. Formation and deformation of hyperextended rift systems: Insights from rift domain mapping in the Bay of Biscay Pyrenees. Tectonics 33, 1239–1276. https://doi.org/10.1002/2014TC003529.
Van Hinsbergen, D.J.J., Torsvik, T.H., Schmid, S.M., Maţenco, L.C., Maffione, M., Vissers, R.L.M., Gürer, D., Spakman, W., 2020. Orogenic architecture of the Mediterranean region and kinematic reconstruction of its tectonic evolution since the Triassic. Gondwana Res. 81, 79–229. https://doi.org/10.1016/j.gr.2019.07.009.
Vidal-Royo, O., Rowan, M.G., Ferrer, O., Fischer, M.P., Fiduk, J.C., Canova, D.P., Hearon, T.E., Giles, K.A., 2021. The transition from salt diapir to weld and thrust: examples from the Northern Flinders Ranges in South Australia. Basin Res. 33, 2675–2705. https://doi.org/10.1111/bre.12579.
Villaseñor, G., Catlos, E.J., Broska, I., Kohút, M., Hraško, L., Aguilera, K., Etzel, T.M., Kyle, J.R., Stockli, D.F., 2021. Evidence for widespread mid-Permian magmatic activity related to rifting following the Variscan orogeny (Western Carpathians). Lithos 390-391. https://doi.org/10.1016/j.lithos.2021.106083.
Von Eynatte, H., Gaupp, R., 1999. Provenance of Cretaceous synorogenic sandstones in the Eastern Alps: constraints from framework petrography, heavy mineral analysis and mineral chemistry. Sediment. Geol. 124 (1–4), 81–111. https://doi.org/10.1016/S0037-0738(98)00122-5.
Wachtel, G., Wessely, G., 1981. Die Tiefbohrung Berndorf 1 in den östlichen Kalkalpen und ihr geologischer Rahmen. Mitt. Österr. Geol. Ges. 74 (75), 137–165.
Wagreich, M., 1995. Subduction tectonic erosion and Late Cretaceous subsidence along the northern Austroalpine margin (Eastern Alps, Austria). Tectonophysics 242 (1–2), 63–78. https://doi.org/10.1016/0040-1951(94)00151-X.
Wagreich, M., Decker, K., 2001. Sedimentary tectonics and subsidence modelling of the Upper cretaceous Gosau basin (Northern Calcareous Alps, Austria). Geol. Rundsch. 90, 714–726.
Wagreich, M., Faupl, P., 1994. Palaeogeography and geodynamic evolution of the Gosau Group of the Northern Calcareous Alps (late cretaceous, Eastern Alps, Austria). Palaeogeogr. Palaeoclimatol. Palaeoecol. 110, 235–254.
Wagreich, M., Krenmayr, H.G., 2005. Upper cretaceous oceanic red beds (CORB) in the Northern Calcareous Alps (Nierental Formation, Austria): slope topography and clastic input as primary controlling factors. Cretac. Res. 26 (1), 57–64.
Wagreich, M., Pavlishina, P., Malata, E., 2006. Biostratigraphy of the lower red shale interval in the Rhenodanubian Flysch Zone of Austria. Cretac. Res. 27, 743–753.
Wagreich, M., Luckeneder, A., Egger, H., 2008. Cretaceous History of AustriaIn: Berichte der Geologischen Bundesanstalt, ISSN 1017–8880, Band 74, 2008. Wien.
Warren, J.K., 2006. Evaporites: Sediments, Resources and Hydrocarbons. Springer, Berlin, 1036p.
Warsitzka, M., Závada, P., Jähne-Klingberg, F., Krzywiec, P., 2021. Contribution of gravity gliding in salt-bearing rift basins – a new experimental setup for simulating salt tectonics under the influence of sub-salt extension and titlting. Solid Earth 12, 1987–2020. https://doi.org/10.5194/se-12-1987-2021.
Wernicke, B., 1985. Uniform-sense normal simple shear of the continental lithosphere. Can. J. Earth Sci. 22, 108–125.
Wessely, G., 2006. Geologie von Niederösterreich. Geologische Bundesanstalt, Wien, p. 416.
Woodward, N.B., Boyer, S.E., Supper, J., 1989. Balanced Geological Cross-Sections: An Essential Technique in Geological Research and Exploration, Vol. 6. American Geophysical Union. Book Series: Short Courses in Geology, Washington, D. C, 138pp.
Ziegler, P.A., Cloetingh, S., 2004. Dynamic processes controlling evolution of rifted basins. Earth Sci. Rev. 64 (1–2), 1–50. https://doi.org/10.1016/S0012-8252(03)00041-2.
Zimmer, W., Wessely, G., 1996. Exploration results in thrust and sub-thrust complexes in the Alps and below the Vienna Basin in Austria. In: Wessely, G., Liebl, W. (Eds.), Oil and Gas in Alpidic thrust belts and basins of Central and Eastern Europe, 5. EAGE Special Publication, pp. 81–107 (1996).